AD-A132 586 INTUMESCENT REACTION MECHANISMS: AN ANALYTIC MODEL(U) 1/2
SOUTHWEST RESEARCH INST SAN ANTONIO TX
C E ANDERSON ET AL. MAY 83 NADC-82211-60
UNCLASSIFIED N62269-81-C-0246 F/G 19/1 NL

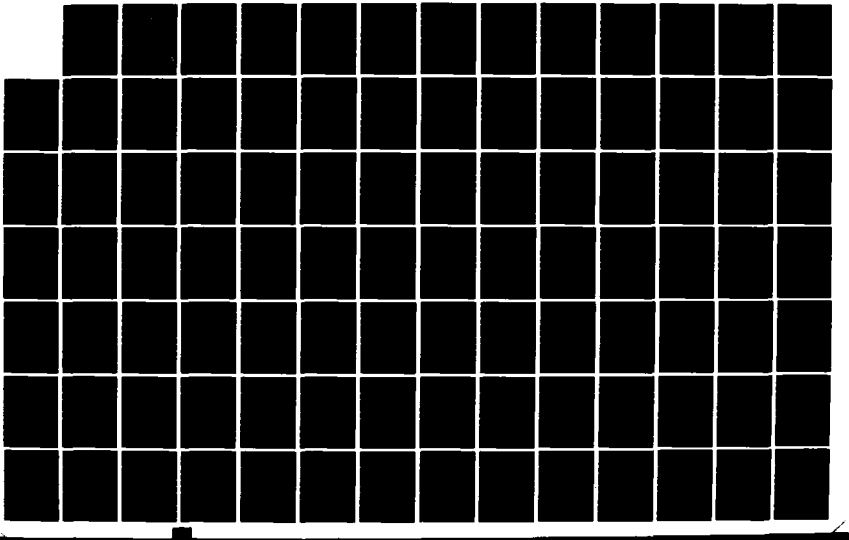

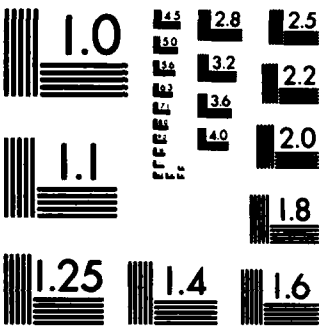

MICROCOPY RESOLUTION TEST CHART
NATIONAL BUREAU OF STANDARDS-1963-A

REPORT NO. NADC-82211-60

INTUMESCENT REACTION MECHANISMS: AN ANALYTIC MODEL

Charles E. Anderson, Jr.
Donna K. Wauters
Southwest Research Institute
6220 Culebra Road
San Antonio, Texas 78284

MAY 1983

FINAL REPORT
N63126-81-WR-21-704
Work Unit CC110

Approved for Public Release; Distribution Unlimited

Prepared for
NAVAL AIR DEVELOPMENT CENTER
Warminster, PA 18974

Unclassified

SECURITY CLASSIFICATION OF THIS PAGE (When Data Entered)

REPORT DOCUMENTATION PAGE		READ INSTRUCTIONS BEFORE COMPLETING FORM
1. REPORT NUMBER NADC-82211-60	2. GOVT ACCESSION NO. AD-A132 586	3. RECIPIENT'S CATALOG NUMBER
4. TITLE (and Subtitle) Intumescent Reaction Mechanisms: An Analytic Model		5. TYPE OF REPORT & PERIOD COVERED Final Report July 1981 to March 1983
		6. PERFORMING ORG. REPORT NUMBER SwRI 6648/1
7. AUTHOR(s) Charles E. Anderson, Jr. Donna K. Wauters		8. CONTRACT OR GRANT NUMBER(s) N62269-81-C-0246
9. PERFORMING ORGANIZATION NAME AND ADDRESS Southwest Research Institute 6220 Culebra Road San Antonio, TX 78284		10. PROGRAM ELEMENT, PROJECT, TASK AREA & WORK UNIT NUMBERS N63126-81-WR-21-704 Work Unit CC110
11. CONTROLLING OFFICE NAME AND ADDRESS Naval Air Development Center Attn: NADC-6062 Warminster, PA 18974		12. REPORT DATE May 1983
		13. NUMBER OF PAGES 130
14. MONITORING AGENCY NAME & ADDRESS(if different from Controlling Office)		15. SECURITY CLASS. (of this report) Unclassified
		15a. DECLASSIFICATION DOWNGRADING SCHEDULE

16. DISTRIBUTION STATEMENT (of this Report)

Approved for Public Release
Distribution Unlimited

17. DISTRIBUTION STATEMENT (of the abstract entered in Block 20, if different from Report)

18. SUPPLEMENTARY NOTES

19. KEY WORDS (Continue on reverse side if necessary and identify by block number)

Intumescence
Intumescent Coatings
Cook-Off

20. ABSTRACT (Continue on reverse side if necessary and identify by block number)

Intumescent coatings are used to protect a substrate, such as warheads, from heat sources, e.g., fires. When subjected to heat, various mechanisms are activated to dissipate the incident heat. Characteristic of intumescent systems is the evolution of gases in a pyrolysis zone which causes the coating to expand or inflate, i.e., intumesce. A char is formed which is generally graphitic and resistant to burning, and which also acts as a further thermal barrier because of its low thermal conductivity. A mathematical

DD FORM 1 JAN 73 1473 EDITION OF 1 NOV 65 IS OBSOLETE

Unclassified

SECURITY CLASSIFICATION OF THIS PAGE (When Data Entered)

20. model has been developed which describes the various physical processes by considering mass and energy control volumes. Expansion is explicitly accounted for by assuming it to be a function of mass loss. Thermodynamic data from thermogravimetric analysis and differential scanning calorimeter characterizes the chemical constituents of the coating. A computer program has been written to solve the system of equations, with appropriate boundary conditions, as a function of time. Experimentally determined parameters such as mass loss as a function of temperature requires a Lagrangian formulation, but the computational grid is rezoned after each time step to re-establish an Eulerian grid for numerical accuracy in the difference equations. Mass loss, temperature, expansion velocities, etc., are computed. The model is exercised to determine the influence of various physical/chemical processes/constituents on the heat transfer to a substrate, and the model's predictions are compared against experimental data. Strengths and weaknesses of the model are delineated.

ACKNOWLEDGEMENT

The authors would like to thank Mr. Dave Pulley of the Naval Air Development Center and Mr. Paul McQuaide of the Pacific Missile Test Center for their interest and support in this research program. We would also like to acknowledge the contributions of Dr. George Lee, Mr. Jerry Dziuk, and Mr. Thomas Lew of Southwest Research Institute for their contributions in TGA and DSC measurements and interpretation.

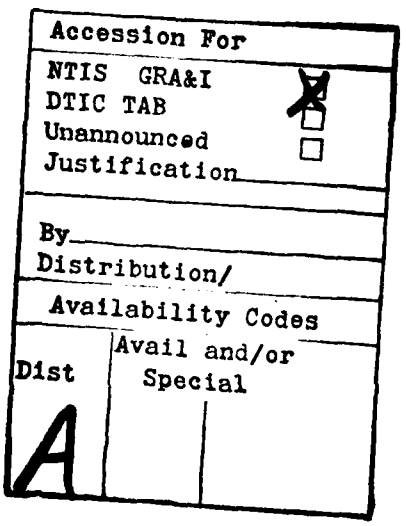

This Page Intentionally Left Blank

TABLE OF CONTENTS

TABLE OF CONTENTS (CONTINUED)

TABLE OF CONTENTS (CONTINUED)

This Page Intentionally Left Blank

LIST OF ILLUSTRATIONS

LIST OF ILLUSTRATIONS (CONTINUED)

LIST OF TABLES

This Page Intentionally Left Blank

1.0 INTRODUCTION

An explosive or propellant, usually confined as in a warhead, undergoes a chemical reaction when exposed to heat. The rate of this reaction is temperature-dependent. The thermal response can be expressed mathematically by:

$$-k \nabla^2 T + \rho C_p \frac{\partial T}{\partial t} = \rho Q n e^{-E/RT} \qquad (1\text{-}1)$$

where the first term on the left is the heat conduction term, the second term is the sensible energy accumulated, and the term on the right is a heat generation term. The symbols, k, ρ, C_p, t, and T, carry their usual connotation of thermal conductivity, density, specific heat, time, and temperature, respectively. The heat generation term also depends upon the heat of decomposition Q, the collision number n, the activation energy E, and the gas constant R. As the explosive heats up, the heat generated continues to increase until detonation. Indeed, for a particular geometry, if a "layer" of explosive reaches a temperature above its critical temperature T_c, even if all other heat sources (such as external fires) are suddenly removed, the explosive will still detonate as the heat generated in the explosive cannot be dissipated by conduction through the shell. Instead, the heat feeds itself, releasing more heat, causing the reaction to release more heat at a faster rate ..... until detonation.

Studies by the Army have shown, for Army munitions, that propellant fires, though extremely hot, are not likely to be a problem because of their short duration (less than 10 seconds). However, longer duration fires, such as those resulting from burning explosive, sequential initiation of different propellant charges, or pool-type fires from fuels (such as JP-4 or JP-5) will lead to cook-off, as it is commonly called.

The United States Navy first became interested in the cook-off problem as a result of two disasterous fires aboard the aircraft carriers USS FORRESTAL (July, 1967) and USS ENTERPRISE (January, 1969). Both were caused by

accidents on the flight deck. Spilled aviation fuel caused the fire to spread rapidly. Weapons lying on the deck and hung under the wings of nearby aircraft soon became enveloped in these fires. Within one to three minutes after the flames first became evident, the weapons began to detonate or launch propulsively. The catastrophic fire aboard the USS FORRESTAL resulted in 72 million dollars of damage to the ship, and the deaths of 133 men. The fire aboard the USS ENTERPRISE, while not as catastrophic, also resulted in loss of life, injury, and ship damage [1].

Another carrier incident involving weapons and fire occurred aboard the USS ORISKANY. This fire, attributed to the lack of environmental sensing fuzes, was not propagated by aircraft fuel but did result in cook-off of numerous flares causing extensive ship damage and loss of life. In September 1970, at Danang Air Base, an accidental fire erupted under an F-4B during aircraft refueling operations. As the fire was being brought under control, a Sparrow warhead cooked-off, killing 3 and injuring 13. In 1973, there were two railroad boxcar fires, one in a railroad yard at Roseville, California, involving 7000 bombs, and another in a remote location in Benson, Arizona. In both fires, bombs detonated causing extensive property damage, and in the Roseville fire, injury also resulted. In November 1975, a collision between the cruiser USS BELKNAP and the aircraft carrier USS JOHN F. KENNEDY occurred. Ruptured fuel lines on the KENNEDY spewed fuel down the stacks and across the deck of the BELKNAP. The resulting fire caused ordnance cook-off [1]. The most recent cook-off occurred aboard the aircraft carrier USS NIMITZ in the spring of 1981 which resulted in the immediate deaths of 14 men and over 60 million dollars of damage.

In 1969, the Weapons Cook-Off Improvement Program was established to accomplish two specific objectives: delay the ordnance reaction for at least five minutes and limit the extent of that reaction to a deflagration (case rupture and burning of explosive). Since then, the five-minute delay has been successfully achieved primarily through the use of ablative and intumescent coatings on the exterior skin of various bombs, rocket launchers, mines,

missiles, etc. Intumescent coatings are the material of choice whenever high insulation efficiency from a limited film thickness is desired [2].

Many thermal materials have been evaluated and several high thermal efficiency intumescent coatings have been found to be viable and are currently used to protect rocket launchers, missiles, and warheads. While chemists have become quite adept at developing intumescent coatings, this is a result of some quantitative physical and chemical understanding, a larger amount of qualitative physical and chemical understanding, experience, trial and error, and "black magic." What is desired is that a more quantitative understanding of the intumescence process be obtained by analyzing typical intumescent reaction mechanisms and developing an appropriate model which predicts heat transfer and accounts for fundamental chemical, thermodynamic, and physical processes such as kinetics and swelling.

This Page Intentionally Left Blank

2.0 THE PHYSICAL PROCESSES AND CHEMISTRY OF INTUMESCENCE

In order for intumescence to occur, several distinct reactions must occur nearly simultaneous, but in the proper sequence. Generally, the composition of an intumescent system consists of the following functional entities:

(1) An inorganic acid or a material yielding acid at temperatures between 100° and 250°C,

(2) A polyhydric material rich in carbon,

(3) An organic amine, amide, or azo compound,

(4) A halogenated material or other suitable material which can decompose and serve as a blowing agent,

(5) A hydrated salt (e.g., borax, sodium silicate, aluminum hydroxide, ammonia phosphate, etc.), and

(6) A binder.

Most formulations contain an example of each, although in some cases, two or more functional groupings are included in a single component.

The state-of-the-art to date in intumescent systems includes several basic categories of material which can be summarized as follows:

(1) Elastomer-based, filled film which contains such intumescent solids as hydrates of boron salts, alkali silicates, and mineral hydrates such as perlite and vermiculite. Elastomeric binders include polyurethanes, silicones, chloroprenes, polysulfide, and mixtures of these with rigid plastics such as phenolics and acetals.

(2) Acetal binders such as melamine, phenol formaldehyde, urea formaldehyde filled with hydrated salts, and intumescent minerals as above.

(3) Analine-bisulfite addition products which intumesce to a char upon heating/burning.

(4) Inorganic coatings filled with intumescent compounds including hydrated salts, minerals, and organic agents which oxidize to a char such as polysachrides (sugars, starches) and certain phenolics.

(5) Intumescent film forming materials such as alkali metal silicate solutions with and without fillers.

(6) Thermoplastic material filled with gas producing compounds which release vaporous gases such as freons, carbon dioxide, and nitrogen during heating and produce an expanding mass of flame inhibited plastic until the expansion is complete and the barrier gases escape. The material may then melt, burn, or char, depending upon composition.

The fire barrier qualities of each of the above must be weighed individually but, in general, the mechanism is quite similar.

A typical intumescing coating, as it is exposed to heat, has the following history [3]. First, the acid salt* must decompose to yield the dehydrating acid. This inorganic acid is capable of esterification of polyols.

---

* The intumescent system investigated in this program is discussed in detail in Section 4.0. Because it contains a hydrated salt, the intumescence occurs by a different reaction mechanism than an acid salt.

That is, the resultant acid removes the water from the carbonaceous polyol at temperatures slightly above the acid release temperature. Amides (or amines) probably catalyze this reaction resulting in its completion at temperatures lower than would be observed in their absence. The acid acts as a dehydration agent leaving a carbonaceous residue.

The "timing" (that is, the temperature sequence of the various components) is very important. The acid-carbonaceous polyol must melt prior to or during esterification so that when the polyol decomposes via hydration (forming a carbon-inorganic residue), the released blowing agent and the evolution of other nonflammable gases cause the carbonizing mass to puff and foam. One of the purposes of the organic amine or amide (such as urea, melamine, dicyandiamide, urea formaldehyde, etc.) is the release of nonflammable gases (CO_2, NH_3, etc.) that physically cause the carbonaceous melt to foam. If a phosphoric acid is used, amides/amines act as dehydrating agents promoting phosphorylation and enhancing the conversion of the carbon in the polyol to char.

In addition to the gases from amides/amines, the conventional intumescent system includes a halogenated organic material or other suitable material. These materials release a large volume of nonflammable gases, forming bubbles which result in the characteristic puff or foam of an intumescent system. While water vapor and carbon oxides also may be released during dehydration and thermal decomposition of the polyol, these gases will function as blowing agents only if they are released at the proper time (i.e., after melt, but before solidification occurs). In order to insure sufficient gas release at the proper point in the reaction, blowing agents with predetermined decomposition temperatures are employed, e.g., chlorine containing paraffins (HCl release over a temperature range of 160° to 350°C) or melamine (release of ammonia, low molecular weight hydrocarbons, and carbon oxides between 300° and 350°C).

As the reaction nears completion, gelation and finally solidification occurs. This solid is in the form of multicellular foam which contributes to

insulation of the substrate. Typically, this char has a volume that is from 5 to 200 times the original volume of the coating.

As can be seen readily from the above discussion, if any one of the reactions does not proceed at the required time, intumescence will not occur. Thus, the temperature at which the specified reactions take place is extremely important.

The binder insures a continuous and uniform structure throughout the coating system and helps to insure a uniform foam structure. It essentially holds the intumescent system plus inert fillers together. It can be a thermoplastic resin, or a convertible resin which hardens by either oxidation or polymerization. The resin film must not be so inflexible that it interferes with intumescence. The binder must also incorporate the expected properties of a coating system:

(1) Stable for long times in its pre-application state (e.g., storage in a can),

(2) Noncorrosive,

(3) Easily applied,

(4) Present an aesthetically pleasing appearance, and

(5) Resistant to soiling, water, UV, etc.

An intumescent coating system must generally be able to provide all the advantages of a conventional paint system plus the added benefits of fire protection.

3.0 ANALYTICAL MODELING

3.1 Introduction

Heat is initially dissipated by absorption into the coating mass which has a given specific heat or heat capacity. As the heat capacity is exceeded during the thermal flux, the components of the filler are then activated by various mechanisms. A hydrated solid will first begin to melt or liquify, dissipating some thermal energy in this process, then it proceeds to distill away increments of the bound water, further dissipating energy as it distills. A state of viscoelasticity is achieved by the molten or liquified hydrate which traps the evolving water vapor and other gases and commences to expand, inflate, grow, i.e., intumesce. This also dissipates thermal energy. Finally, the water or volatiles are gone and the expanding matrix releases the last traces of moisture, becoming a solid anhydrous mass of increased volume.

If the above description occurs in the proper sequence, then the char acts as a thermal barrier because of its low thermal conductivity. The heat transfer to the protected substrate is, thus, significantly retarded. This matrix is also a heat-dissipating medium, especially if the matrix expands to a char along with the intumescent fillers (most intumescing systems have this characterization). The resulting char is graphitic (polyaromatic) and is resistant to burning. Such chars are like coke and charcoal to some degree in that they may glow and slowly oxidize in air, but do not deflagrate easily. As the char glows, it begins to radiate back what can be a significant amount of heat.

An appropriate mathematical model must describe the various processes discussed previously. The ultimate goal of any intumescent system is to protect a substrate, such as the metal skin of a warhead. Indeed, the effectiveness of an intumescing system is based generally on its ability to protect the substrate thermally. Typically, the effectiveness is determined from the temperature-time history of the substrate. Thus, to compare the mathematical

description with experimental data, a one-dimensional heat transfer model has been developed to describe the heat transfer through an intumescing system to a metal substrate.

Figure 3-1 depicts schematically the thermal model developed. Figure 3-1(a) depicts the coating material at time t = 0. At a later time t_1, heat has caused the intumescent system to react, expanding and forming a char, Figure 3-1(b). Eventually, if the heat is applied for enough time, the entire coating will have been transformed into char. The metal substrate is assumed to have an adiabatic back, and the applicable equations are applied to the intumescent material in differential elements dx from x = 0 to the outer surface, $x = x_B(t)$. The continuity and energy equations, listed below, are derived in Appendix A.

3.2 Continuity Equations

$$\frac{d\rho}{dt} + \rho \frac{\partial v}{\partial x} = - \dot{\Gamma}_g \tag{3-1}$$

$$\frac{d\rho_g}{dt} + \rho_g \frac{\partial v}{\partial x} = + \dot{\Gamma}_g \tag{3-2}$$

The density, ρ, represents the "solid" density. As the material expands through intumescence, the total solid mass becomes less because of outgassing of volatile products, $\dot{\Gamma}_g$. The mass lost to outgassing can be computed from laboratory experiments and is a function of the local temperature and the chemical components of the intumescent coating. The gas density, ρ_g, is dependent on the outgassing products. The outgassing activity takes place only in the pyrolysis zone, Figure 3-1, which is expanding at a velocity, v, due to the pressure of the outgassed components on the viscous "semi-solid" bulk. The gradient of the velocity is non-zero only in the pyrolysis zone. It is zero in the char region and in the coating region where $\dot{\Gamma}_g = 0$. This is equivalent to asserting that there is no expansion (or compression) of material outside the pyrolysis region.

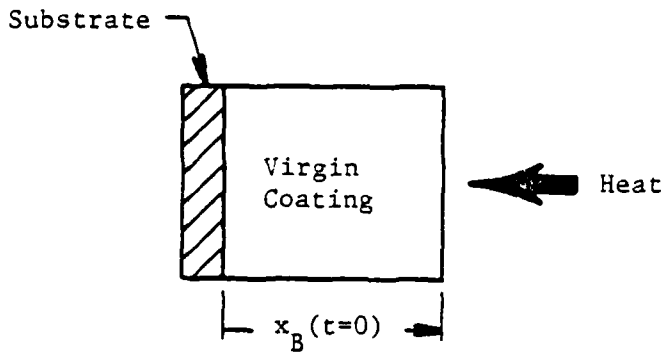

Figure 3-1(a)

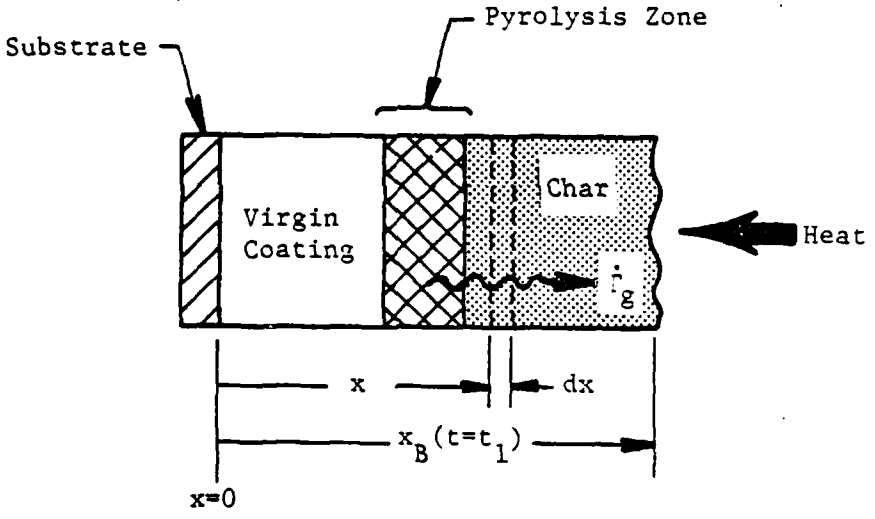

Figure 3-1(b)

Figure 3-1. Schematic Depiction of Model

The $d\rho/dt$ in Equations (3-1) and (3-2) refer to the material derivative:

$$\frac{d\rho}{dt} = \frac{\partial \rho}{\partial t} + v \frac{\partial \rho}{\partial x} \tag{3-3}$$

The reason for this notation will be explained in the discussion of the computational algorithms formulated to obtain numerically the time history (position, density, and temperature) of the intumescent coating and substrate.

3.3 Energy Equation

$$\left[\rho C_p + \rho_g \left(C_p\right)_g\right] \frac{\partial T}{\partial t} =$$

$$\frac{\partial}{\partial x} k \frac{\partial T}{\partial x} - \left(h_g - h\right) \dot{\Gamma}_g - v \left[\rho C_p + \rho_g \left(C_p\right)_g\right] \frac{\partial T}{\partial x} - \rho \dot{q}_{chem} \tag{3-4}$$

In this equation, T is the temperature, k is the thermal conductivity, C_p and $(C_p)_g$ are the solid and gas specific heats, h and h_g are the specific enthalpies of the solid and gas, and $\dot{q}_{chem}$ is the rate of heat per unit mass generated by chemical reactions. The convention has been adopted where a negative $\dot{q}_{chem}$ implies an exothermic chemical reaction. The term on the left-hand side represents the sensible energy accumulated, while the terms on the right-hand side of Equation (3-4) represent, respectively, the net heat conduction in the solid, the heat absorbed by phase changes, the heat absorbed due to the expansion or convective process, and the heat generated by chemical reactions. Notice that the various mechanisms described in subsection 3.1 of this section are described mathematically in Equation (3-4). Heat is conducted into the material which increases in temperature. As the temperature increases, the material melts, liquifies, and outgases, described by the second term on the right-hand side, which absorbs energy. The expansion of the material, the third term, also absorbs energy. The thermal conductivity, k, can change between the virgin and char material, generally decreasing in value, the char

being a better insulator. Additionally, because of the expansion, the heat must be conducted through more material, thus further retarding the heat flow to the substrate.

It has been assumed in the derivation of these equations that the gas temperature and solid, or bulk temperature, are identical at the same position, x. This is not an unreasonable assumption since the phase transitions occur at constant temperature. Also, if the gas generated in the interior moves "slow enough" to the surface, it will have essentially the same temperature as the bulk material. Additionally, the gas velocity has been assumed to be equivalent to the bulk velocity, again a reasonable assumption since it is the gas that pushes against the "soft and pliable" viscous material causing it to intumesce. Equation (3-4) can be slightly simplified by neglecting the $\rho_g (C_p)_g$ terms since the solid density is approximately a thousand times larger than that of the evolved gases, while the solid and gaseous specific heats are the same order of magnitude.

3.4 Expansion Factor

One additional equation is required to relate the velocity to other parameters. Normally, a momentum balance, similar to the mass and energy conservation equations, would be performed to obtain the relationship between the pressure generated by the volatile products, the bulk viscosity of the semi-fluid solid, and the velocity. But the pressure field and viscosity, which would be strong functions of temperature, are not easily attainable experimentally.

An alternate approach has been adopted analogous to an approach taken by Clark, et al. [4]. A characteristic of an intumescent system is that it expands when subjected to sufficient heat. Expansion factors of 5 to 10 are common, but paints have been formulated with factors as high as 50 to 60 times their original thickness. It is not unreasonable to associate the amount of expansion with the mass loss. That is, it is the outgassing of pyrolyzed

material that generates the pressure which drives the expansion. Hence, an expansion factor, E_f, is defined to be proportional to the quantity of outgassed material:

$$E_f \propto \frac{m_o - m}{m_o - m_c} \tag{3-5}$$

where m_o is the original mass, m_c is the final or char mass, and m is the current mass. The proportionality is chosen such that Expression (3-5) has the correct limits:

$$E_f = 1 + \left[\left(E_f\right)_{max} - 1 \right] \left[\frac{m_o - m}{m_o - m_c} \right]^n \tag{3-6}$$

The maximum expansion factor is given by $(E_f)_{max}$. For example, it is the 5 to 10 just mentioned.

The movement of a "particle" can be written in terms of its original coordinate position:

$$y = \int_o^x E_f[m(z)]\, dz \tag{3-7}$$

where y is the coordinate the expanding (or intumescing) particle has moved to, its original location being the coordinate x. It can be seen, by examining Equation (3-6), that if the paint at a particular location has not begun to outgas (i.e., intumesce), then $m = m_o$ and the local expansion factor is 1.0 [$E_f(m_o) = 1.0$]. Equation (3-7) then implies, as it should, that the particle has not moved to a new location, i.e., $y = x$. When the paint has intumesced fully, the density is equal to the char density, $m = m_c$, and $E_f(m_c) = (E_f)_{max}$. Examination of Equation (3-7) shows that the position of a particle is not only dependent upon what is occurring locally, but also depends upon the history of interior points of the paint. As a "point" intumesces, the expansion

factor associated with that "point" changes continuously from 1.0 to $(E_f)_{max}$. The ultimate position of a particle A is the integral effect of all the particles interior to particle A.

The exponent, n, in Equation (3-6) simply describes the dependence of $E_f(m)$ on the change in mass from m_o. If the expansion occurs very early in the outgassing stage, that is, small changes from the original mass result in a significant portion of the expansion, then the exponent lies between 0 and 1. If the expansion occurs only after significant outgassing, i.e., large changes from the initial paint mass occur before significant expansion ensues, then the exponent n is greater than 1. An exponent of 1 implies a linear relationship between the outgassing products and the expansion. Figure 3-2 plots the scaled expansion factor versus the scaled mass for various values of the exponent n. The features just described can be observed by examining this graph. For example, for an exponent of 10, when the local density of the paint has undergone 75 percent of its change from m_o to m_c, the material has expanded 24 percent of its maximum value.

The particle velocity, v, can be found by differentiating Equation (3-7) with respect to time:

$$v(x,t) = \frac{dy}{dt} = \int_o^x \frac{d\left(E_f[m(z)]\right)}{dm} \frac{dm}{dt}\, dz \qquad (3\text{-}8)$$

After performing the derivative with respect to m in Equation (3-8) and rearranging terms, Equation (3-8) becomes:

$$v(x,t) = \int_o^x \frac{-n}{m_o - m}\left[E_f(m) - 1\right] \frac{dm}{dt}\, dz \qquad (3\text{-}9)$$

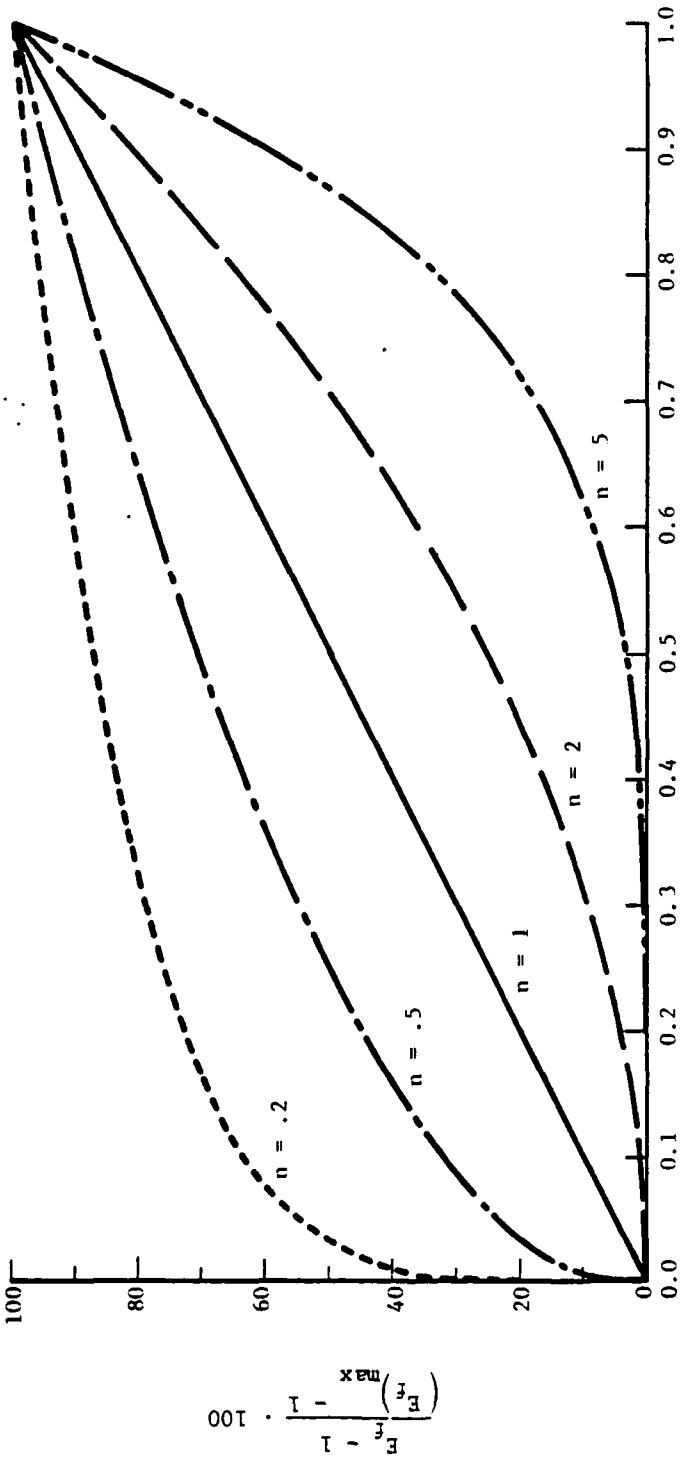

Figure 3-2. Exponential Dependence on Local Expansion Factor

Equation (3-9) shows that the velocity at a point, x, depends upon the accumulative effect of what is occurring interior to that point. Even if the local change in the coating mass (due to outgassing) is zero, the velocity can have a non-zero value because of changes in the mass at interior points.

3.5 Boundary Conditions

The boundary conditions for the energy equation, Equation (3-4), are straightforward. The condition at the outer boundary is the requirement that the heat flux be continuous at $x = x_B$, from which the surface temperature can be determined:

$$k \left.\frac{\partial T}{\partial x}\right|_{x = x_B^-} = h\left(T_F - T_S\right) + \varepsilon_S \sigma \left(\varepsilon_F T_F^4 - T_S^4\right) \qquad (3\text{-}10)$$

where h is the convective heat transfer coefficient, ε_S is the surface emissivity, ε_F is the flame emissivity, σ is the Stefan-Boltzmann constant, T_F is the effective flame temperature, and T_S is the surface temperature of the coating, i.e.,:

$$T_S = T\left(x_B, t\right) \qquad (3\text{-}11)$$

The symbol $x = x_B^-$ indicates that the temperature gradient is computed into the coating material.

The boundary condition at the interface of the coating and substrate, $x = 0$, also requires that the heat flux be continuous at the interface. However, because of the large value of the thermal conductivity for the substrate (a steel plate) and the relative "thinness" of the plate (1.6 mm), essentially no temperature gradient exists through the thickness of the plate. Assuming an adiabatic back to the substrate (i.e., no heat losses from the back of the plate), all heat crossing the boundary at $x = 0$ goes into heating the substrate:

$$\rho_p \left(C_p\right)_p \tau_p \frac{dT_p}{dt} = k \left.\frac{\partial T}{\partial x}\right|_{x = 0^+} \tag{3-12}$$

The subscript p refers to substrate (plate) properties, with ρ, C_p, τ, and T referring to the density, specific heat, thickness, and temperature of the plate, respectively. This condition determines the plate temperature, which is also the temperature at the interface of the coating and plate:

$$T_p = T(0,t) \tag{3-13}$$

The boundary condition on Equation (3-1) is determined as follows. At time zero, the density at $x = x_B$ is the initial density, ρ_o:

$$\rho\left(x_B, 0\right) = \rho_o \tag{3-14}$$

The surface temperature, for very early times, can be estimated by solving the heat equation for transient heat flow in a semi-infinite solid exposed to a constant heat flux, $\dot{q}_o$. The surface temperature, as a function of time, t, can be computed from:

$$T_{surface} = T_o + \frac{2\,\dot{q}\,\sqrt{\alpha t/\pi}}{k} \tag{3-15}$$

where T_o is the initial surface temperature, and α and k are the thermal diffusivity and thermal conductivity of the coating material. For an incident heat flux typical of aviation fuel fires, 2.7 cal/cm^2-s (10 BTU/ft^2-s), the time for the surface to reach 800°C (using typical values for α and k, and an initial surface temperature of 25°C) is computed from Equation (3-15) to be of the order of one second. Most intumescent systems have finished all activity by 800°C. It has just been shown that the surface temperature surpasses very rapidly the temperature required to outgas. Thus, at time 0^+, the surface density becomes the char density, ρ_c:

$$\rho\left(x_B, 0^+\right) = \rho_c \tag{3-16}$$

What must be prescribed now is the form of $\dot{\Gamma}_g$, which is a function of temperature. This couples Equations (3-1) and (3-4). $\dot{\Gamma}_g$ is obtained from experimental data and this procedure is discussed in Section 5.0. With $\dot{\Gamma}_g$ a prescribed function of temperature, we then have the unknowns, ρ, T, and v, and Equations (3-1), (3-4), and (3-9) with appropriate boundary and initial conditions.

This Page Intentionally Left Blank

4.0 INTUMESCENT PAINT FORMULATION

4.1 Formulation

The intumescent paint formulation examined for this study was developed by NASA Ames Research Center (Formulation EX-1C-82), and is one that the U. S. Navy has found to be effective. It consists of two parts, A and B, which are combined just before application. The formulation consists of three major components: the intumescent filler — borax; the binder — an epoxy; and a fiber — glass. Since epoxies tend to be very hard and brittle, polysulfide has been added to make the binder more flexible. Hydrated salts such as sodium tetraborate decahydrate, or borax, function by a different reaction mechanism than the one described in Section 2.0. First, they decompose endothermically. This process absorbs a large quantity of heat and effectively prevents the transfer of energy through the coating. The second process involves transpirational cooling by the water vapor produced from the decomposition as it leaves the coating surface. The sublimation of water molecules cools the upper layers of the coating by convection and reduces the thermal transport of energy through the boundary layer region immediately above the surface. The third process involves the formation of a viscous material. Because of the blowing action of the water, the molten material is transformed into an expanded char which solidifies and provides thermal insulation [5].

The formulations for Part A and Part B are given in Table 4-1, along with their respective concentration by mass of the various constituents for Part A, Part B, and Part A+B. Table 4-2 lists the percentage by weight of each of the constituents. It is these numbers which will be used later in the modeling to combine the constituents.

Table 4-1. Intumescent Paint Formulation (Masses)
NASA Formulation EX-1C-82

Component	Density (g/cm^3)	Concentrations [By Mass (g)] A	B	(A+B)*
Polysulfide	1.270	45.10	—	45.10
DMP-30	0.973	6.50	—	6.50
EPON 828	1.170	—	46.00	46.00
Borax	1.730	63.20	45.00	108.20
Glass	2.500	0.32	0.25	0.57
	TOTAL	115.12	91.25	206.37

* A and B mixed at a ratio (by mass) of 1.26 to 1.

Table 4-2. Intumescent Paint Formulation
(Percentage Concentration)
NASA Formulation EX-1C-82

Component	Concentrations (% By Weight) A	B	(A+B)*
Polysulfide	39.18		21.85
DMP-30	5.64		3.15
EPON 828		50.41	22.29
Borax	54.90	49.32	52.43
Glass	0.28	0.27	0.28
Part A			55.78
Part B			44.22

* A and B mixed at a ratio (by mass) of 1.26 to 1.

4.2 Density Determination

4.2.1 Initial, Bulk Density

The bulk density of the coating system can be computed from the densities of the constituents. The total mass of the coating system can be obtained by summing the mass contributions of each of the constituents:

$$M_{total} = M_{borax} + M_{DMP-30} + M_{polysulfide} + M_{EPON} + M_{glass} \qquad (4-1)$$

The bulk density, $\bar{\rho}$, is defined by:

$$\bar{\rho}\, V = \sum_{j=1}^{J} X_j\, M_{total} \qquad (4-2)$$

where V is the total volume of the coating system and X_j is the percentage of total mass of the j^{th} constituent. For example:

$$X_{borax}\, M_{total} = M_{borax} \qquad (4-3)$$

Assuming the total volume is the sum of the volumes of the constituents (generally a valid assumption except for solutions):

$$X_j\, M_{total} = \rho_j\, V_j = \rho_j\, X_j\, V \qquad (4-4)$$

and hence:

$$\bar{\rho} = \sum_{j=1}^{J} X_j\, \rho_j \qquad (4-5)$$

Equation (4-5) can then be used to compute the bulk density.

As already stated, the intumescent paint formulation consists of two parts, A and B, which are combined just before application. Using the densities and percentage by weight from Tables 4-1 and 4-2, respectively, the theoretical bulk densities of Part A, Part B, and Part A+B have been computed, Table 4-3.

Table 4-3. Theoretical Density Determinations

	g/cm^3
Part A	1.509
Part B	1.450
Part A+B	1.483

A bulk density for Part A+B was determined by two methods. The first method involved the preparation of two sample plates. The plates were weighed before and after coating, the thickness of the plate and plate plus coating measured, and the cross-sectional areas of the coatings determined. The density determined by this manner was approximately 1.0 g/cm^3, substantially less than the theoretical value of 1.483 g/cm^3. Examination of the process of mixing Parts A and B and application to the plates indicates that air gets trapped in the volume. After the coating has dried, "air bubbles" can be identified. The more viscous the formulation during mixing and application, the more air that can get trapped. The trapped air manifests itself in an increased thickness of the coating, thereby reducing the experimentally determined bulk density. There is no effective control (except experience) of how much air is entrapped (with subsequent increased thickness). When the densities for the first two plates came out to approximately 1.0 g/cm^3, a third

plate was prepared. Great care was taken to avoid air entrapment, but observations during application indicated the "air pockets" were still unavoidable. A value of 1.22 g/cm^3 was determined for this third plate.

The second method was a specific gravity measurement of an uncured Part A+B sample, which yielded a density of 1.49 g/cm^3, in very good agreement with the theoretical limit. Bulk densities for Part A and Part B were also determined through specific gravity measurements and found to be 1.32 and 1.31 g/cm^3, respectively. Again, entrapped air increased the volume of these samples.

The mass of the applied coating is important since enthalpy, specific heat, etc., are given in units of energy per gram of material. An effective thickness, which would be the thickness if no air were entrapped in the applied coating, will be used for modeling purposes.

4.2.2 Final, Char Density

The final density is related to the total mass lost and the expansion of the coating. The initial mass, m_o, and the final mass, m_f, are given by:

$$m_o = \int_o^{X_o} \rho_o \, dx = \rho_o \, X_o \qquad (4\text{-}6)$$

$$m_f = \int_o^{X_f} \rho_c \, dx = \rho_c \, X_f \qquad (4\text{-}7)$$

where X_o is the original thickness and X_f is the final, or expanded, thickness of the coating:

$$X_f = \left(E_f\right)_{max} X_o \tag{4-8}$$

Conservation of mass requires:

$$m_o = m_f + m_{lost} \tag{4-9}$$

or, rearranging terms:

$$m_{lost} = m_o \left(1 - \frac{m_f}{m_o}\right) \tag{4-10}$$

But Equation (4-9), making use of Equations (4-6) and (4-7), can also be written as:

$$\rho_o X_o = \rho_c X_f + m_{lost} \tag{4-11}$$

Thus:

$$\rho_o X_o = \rho_c \left(E_f\right)_{max} X_o + m_o \left(1 - \frac{m_f}{m_o}\right) \tag{4-12}$$

Equation (4-12) can be solved for the char density:

$$\rho_c = \frac{\rho_o \left(m_f/m_o\right)}{\left(E_f\right)_{max}} \tag{4-13}$$

As will be seen in the next section, the quantity (m_f/m_o) is determined from thermogravimetric analyses. The amount of expansion, $(E_f)_{max}$, is determined experimentally from measurements of the thickness of the coating material before and after intumescence.

This Page Intentionally Left Blank

5.0 TGA DATA — MASS LOSS

5.1 Introduction

Thermogravimetric analysis (TGA) measures and records the mass of a sample versus temperature. A known mass, typically a few milligrams, is placed on an accurate balance. The sample is heated at a prescribed rate (e.g., 20°C/min) and the sample mass is recorded as a function of temperature. Generally, the rate of mass loss as a function of temperature is also recorded at the same time.

The TGA data for the various constituents need to be put into a form which can be easily handled by the numerical analysis scheme. Two procedures will be presented, fitting to Arrehnius' equation and Fourier series representation. The Fourier series representation was finally chosen as the best procedure for reasons to be discussed below.

5.2 Curve Fitting

5.2.1 Arrehnius' Equation to Represent Rate of Mass Loss

It is well known that the rate of many chemical reactions is strongly dependent upon the temperature, and Arrehnius found that this rate, r, could be expressed as:

$$r = Be^{-E/RT} \qquad (5\text{-}1)$$

where B is the frequency factor, E is the activation energy, R is the gas constant, and T is the absolute temperature.

The problem with Equation (5-1) is that it does not go to zero when the reactants have been completely used. In the particular case of a reactant being one of the constituents of an intumescent coating formulation, then

eventually all the "volatiles" will be outgassed. Equation (5-1) can be modified to make it go to zero by multiplying by a term that looks like:

$$\left(\frac{m - m_r}{m_i}\right)^b \tag{5-2}$$

where m is the current mass, m_i is the initial mass, and m_r is the residual mass. The exponent b allows for nonlinearities.

The rate of mass loss then can be expressed as:

$$\frac{d\left(m/m_i\right)}{dT} = Be^{-E/RT}\left(\frac{m - m_r}{m_i}\right)^b \tag{5-3}$$

where B, E/R, and b have to be determined by curve fits to the data. One method for fitting Equation (5-3) to the data is to first take the natural logarithm:

$$\ln\left[\frac{d\left(m/m_i\right)}{dT}\right] = \ln B - \frac{E}{RT} + b \ln\left(\frac{m - m_r}{m_i}\right) \tag{5-4}$$

Next, consider the change in the above expression as sequential data points are analyzed:

$$\Delta \ln\left[\frac{d\left(m/m_i\right)}{dT}\right] = -\frac{E}{R}\Delta\left(\frac{1}{T}\right) + b\,\Delta\left[\ln\left(\frac{m - m_r}{m_i}\right)\right] \tag{5-5}$$

Note that ln B is a constant so that the change in ln B is zero. By considering adjacent data points from the TGA curve, the change in the natural log of

$$\frac{d\left(m/m_i\right)}{dT},$$

the change in the inverse temperature, and the change in the natural log of the mass can all be computed. By plotting:

$$\frac{\Delta \ln\left[d\left(m/m_i\right)/dT\right]}{\Delta\ (1/T)} \text{ versus } \frac{\Delta\left[\ln\left(\left(m - m_r\right)/m_i\right)\right]}{\Delta\ (1/T)} \tag{5-6}$$

then the slope of the straight line is the exponent b, and the intercept is -E/R. Once b and -E/R are determined, Equation (5-4) can be used to determine the frequency factor, B.

An alternate method for determining the three unknown coefficients is to perform a least squares curve fit of Equation (5-4), which has the form:

$$y = a - \frac{c}{T} + bz \tag{5-7}$$

where:

$$y = \ln\left[\frac{d\left(m/m_i\right)}{dT}\right] \tag{5-8}$$

$$a = \ln B \tag{5-9}$$

$$c = E/R \tag{5-10}$$

and:

$$z = \ln\left(\frac{m - m_r}{m_i}\right) \tag{5-11}$$

where the constants a, c, and b are to be determined.

One last comment before further discussion of these two curve fit procedures. The constituents of the paint formulation are compounds with various

types of chemical bonds. These different bonds are broken at different temperatures. That is, more energy (as indicated by a higher temperature) is required to break some bonds relative to others. Thus, we can expect that the curve fits must be applied only over certain regions of the TGA data, and that different activation energies, frequency factors, etc., will be obtained for each region. These parameters will be unique to the particular reaction taking place.

The procedure indicated by Equation (5-5) was used to analyze the TGA data. However, it produced unsatisfactory results. This can be understood by looking at the circled portion of the TGA curve in Figure 5-1. Expression (5-2) is only important as $m \rightarrow m_r$. Otherwise, the exponential in Equation (5-3) dominates. The precision and accuracy at which data can be interpolated is at best 0.025 on the ordinate, and 2.5°C on the abscissa, which thus limits the number of data points for curve fitting. This precision is just not sufficient to allow "good" curve fits.

The procedure indicated by Equation (5-7) was partially successful, but the constants determined by the curve fits are extremely sensitive to the value used for the initial mass, m_i, for the onset of a reaction and the final or residual mass, m_r, at the termination of the reaction. As will be discussed below, the temperature range over which the various reactions take place must be determined graphically. In the procedure described below, we used the original mass, m_o, as our reference point.

By plotting $\ln[d(m/m_o)/dT]$ versus $1/T$ (the natural logarithm is automatically taken by plotting on semi-log paper), the temperature range over which a particular reaction takes place can be ascertained. An example is shown in Figure 5-2 for polysulfide, where two regions are depicted by the symbols △ and □. In fact, least-squares curve fits to the linear portions give the slope, E/R, and the intercept, B, to the expression:

$$\frac{d\left(m/m_o\right)}{dT} = Be^{-E/RT} \qquad (5\text{-}12)$$

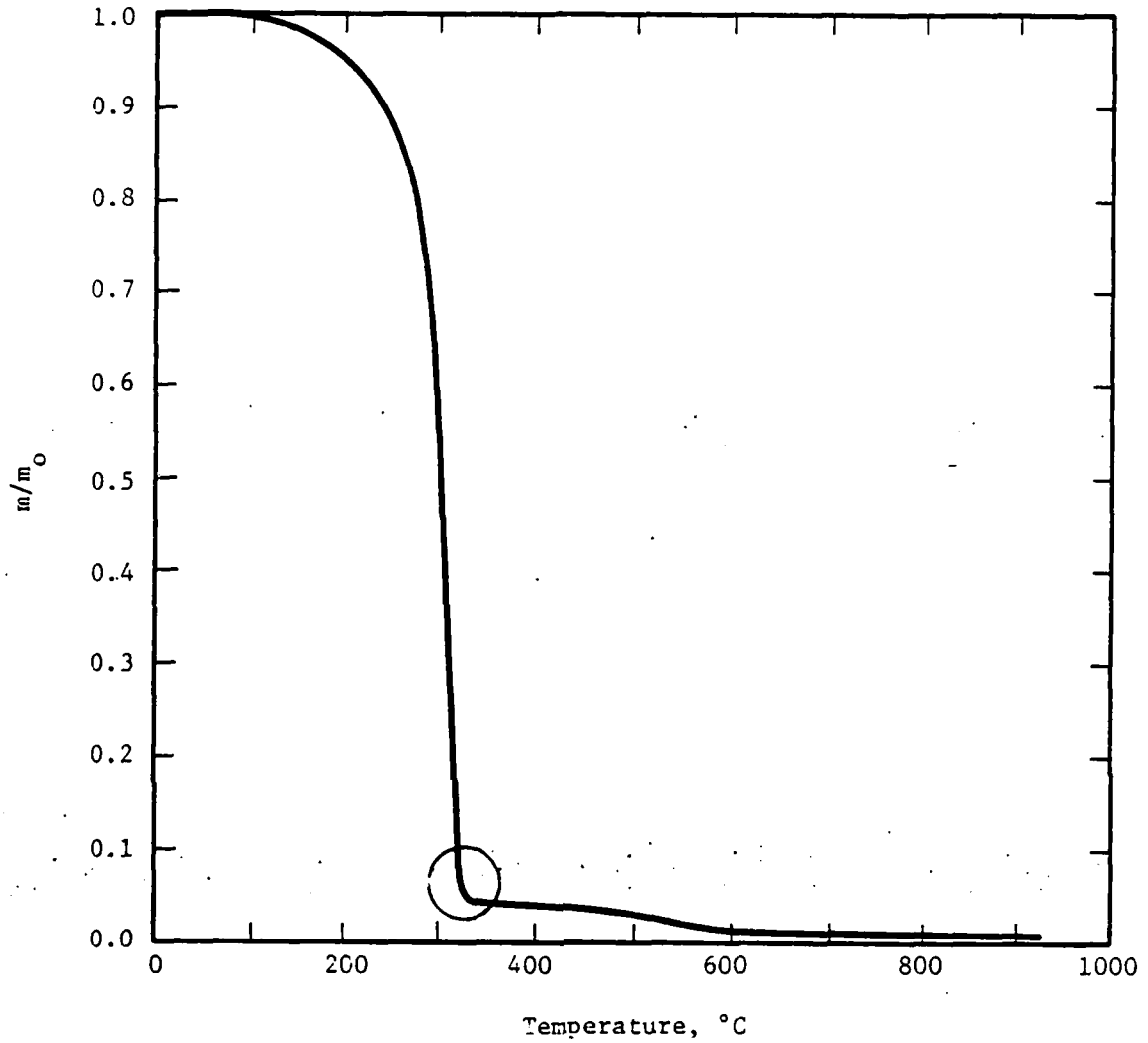

Figure 5-1. TGA: Polysulfide

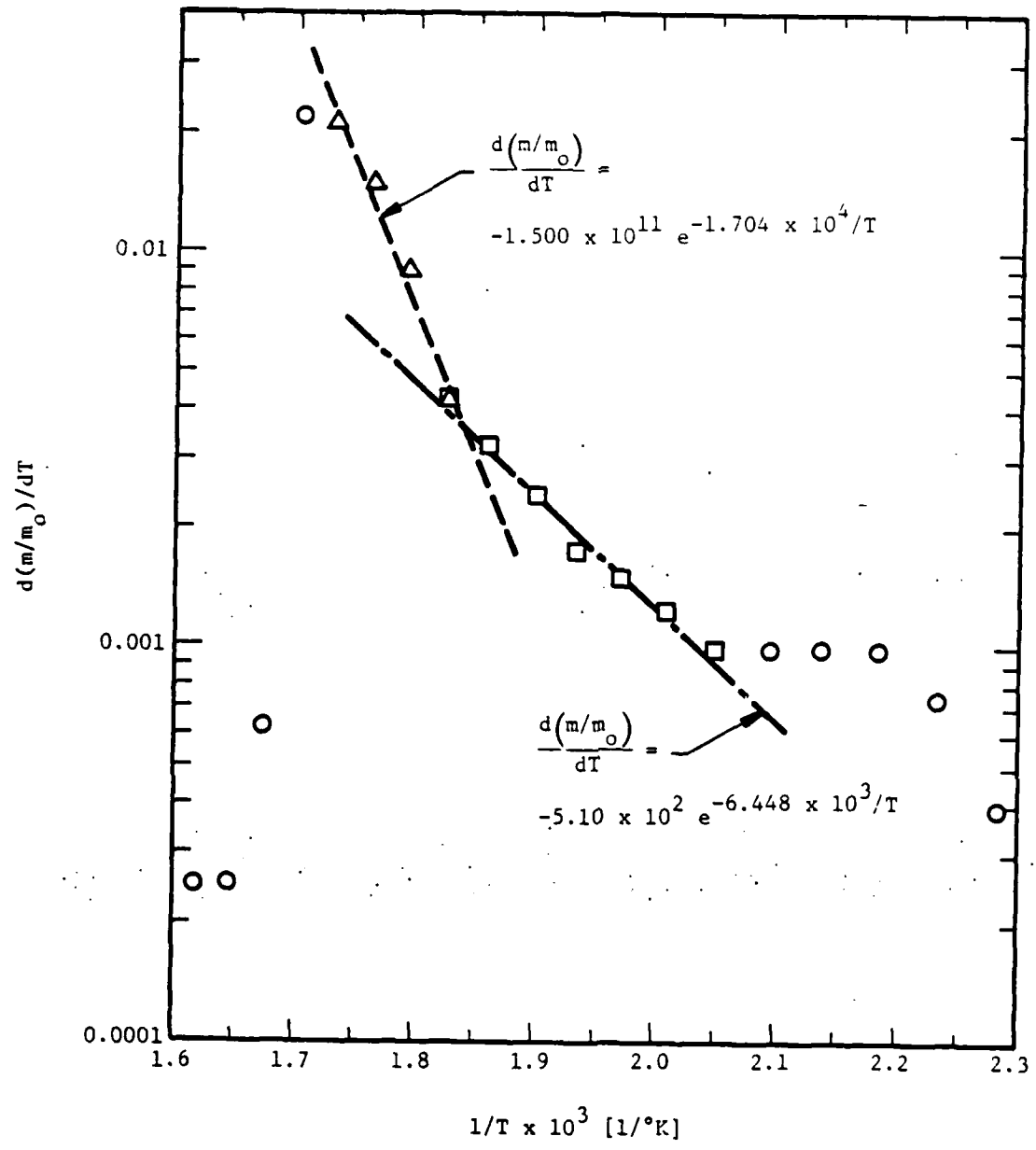

Figure 5-2. Plot of $d(m/m_o)/dT$ Versus 1/T (Polysulfide)

where m_o is the original mass of the intumescent system. The only caution with using Equation (5-12) is that $d(m/m_o)/dT$ must be set to zero when the mass reaches the residual mass for that particular reaction.

Summarizing, the Arrehnius equation is quite adequate for describing the mass loss of those components which undergo a significant mass loss at primarily one temperature, e.g., polysulfide, DMP-30, and the EPON resin. Polysulfide could be represented by Equation (5-12) by dividing the data into five temperature regions. However, this procedure becomes more difficult when a TGA curve is much more complicated. The composite formulation (A+B) required 15 temperature intervals [and 15 equations of the form of Equation (5-12)] to describe the TGA data. The data have to be plotted to determine all the different temperature regions for the purpose of curve fitting. In the case of Part A+B, to obtain a good curve fit, the physical significance of activation energy has been lost (some regions have a positive exponent). Thus, this procedure is not too attractive if a number of TGA data curves are to be analyzed.

5.2.2 Fourier Series Representation

a. Methodology

Because of the aforementioned difficulties of using the Arrehnius equation, we have turned to a Fourier series representation to describe the mass loss as a function of temperature. As will be shown, a Fourier series representation has some very nice features for handling and combining the data.

The mass loss as a function of temperature can be written as a sum of cosine terms times their respective Fourier coefficients:

$$f(T) \equiv \frac{d\left(m/m_o\right)}{dT} = \frac{a_o}{2} + \sum_{n=1}^{\infty} a_n \cos\left(\frac{n \pi T}{T_{max}}\right) \qquad (5\text{-}13)$$

where T_{max} is the temperature interval of interest. The Fourier coefficients are given by:

$$a_n = \frac{2}{T_{max}} \int_0^{T_{max}} f(T) \cos\left(\frac{n \pi T}{T_{max}}\right) dT \qquad n = 0, 1, 2, 3 \ldots \qquad (5\text{-}14)$$

The Fourier coefficients can be found from the experimental data by numerically performing the integration using the trapezoidal rule:

$$a_n = \frac{2}{T_{max}} \sum_{j=0}^{j_{max}-1} \frac{1}{2} \left[f\left(T_j\right) \cos\left(\frac{n \pi T_j}{T_{max}}\right) + f\left(T_{j+1}\right) \cos\left(\frac{n \pi T_{j+1}}{T_{max}}\right) \right] \left(T_{j+1} - T_j\right) \qquad (5\text{-}15)$$

where $T_{jmax} = T_{max}$. The $f(T_j)$'s are the mass loss as a function of temperature and can be read right from the TGA data. It was found that keeping 30 terms of the Fourier series (31 coefficients counting a_o) described the experimental TGA curve quite nicely. Tables 5-1 and 5-2 list the Fourier coefficients for the active components of the intumescent formulation.

The a_o term represents the average mass loss over the entire temperature range. The total mass loss between any two temperatures, T_1 and T_2, is found by integrating Equation (5-13):

$$\left(\frac{m}{m_o}\right)_{\substack{\text{lost} \\ T_1 \to T_2}} = \int_{T_1}^{T_2} \left[\frac{a_o}{2} + \sum_{n=1}^{30} a_n \cos\left(\frac{n \pi T}{T_{max}}\right) \right] dT \qquad (5\text{-}16)$$

Table 5-1. Coefficients for Fourier Series Representation of Mass Loss Versus Temperature

$a_n \times 10^4$ [Equation (5-13) With T_{max} = 830°C]

n	Polysulfide	DMP-30	EPON Resin	Borax
0	-23.837200	-23.851600	-23.8121000	-7.947930
1	-10.201400	-15.803700	- 8.0017800	-6.200150
2	13.292900	- 1.518170	16.1376000	-3.056320
3	20.331300	10.953300	18.1010000	-0.770384
4	5.625640	18.957100	- 0.0527777	0.421483
5	-14.034000	17.616600	-15.7047000	1.076450
6	-16.288300	5.643540	-12.5818000	1.812130
7	1.117050	- 6.697220	4.9775600	2.229640
8	15.545200	-14.096400	14.7672000	2.172330
9	10.359100	-14.225300	5.2917300	1.829370
10	- 6.147620	- 6.852190	- 8.3865000	1.235300
11	-14.613400	3.278050	- 9.4520600	0.659015
12	- 5.645370	9.687940	- 0.0238021	0.391571
13	9.514870	11.073600	7.7369200	0.678590
14	12.167500	6.136110	5.6203100	1.238240
15	0.457644	- 1.730880	- 3.0595700	1.705800
16	-10.492600	- 7.176350	- 6.8591900	1.956020
17	- 8.483380	- 7.788330	- 1.6365800	1.914740
18	3.139390	- 4.523490	4.6420500	1.667770
19	10.039000	1.554480	4.4529700	1.243320
20	4.351090	5.750160	- 0.9230400	0.668549
21	- 5.796920	5.758830	- 4.6691000	-0.156630
22	- 8.005040	2.933670	- 2.2591100	-1.164170
23	- 0.605511	- 1.176090	2.8329100	-1.997790
24	6.916620	- 4.526830	3.7055700	-2.408130
25	5.661040	- 4.444060	- 0.2895870	-2.319620
26	- 2.151600	- 1.856220	- 3.3918300	-1.902730
27	- 6.608690	1.365300	- 1.7943500	-1.356190
28	- 2.850380	3.396200	1.9160100	-0.886634
29	3.727200	3.188520	2.7002200	-0.533482
30	5.069970	1.078080	- 0.1179260	-0.149958

Table 5-2. Coefficients for Fourier Series Representation of Mass Loss Versus Temperature

$a_n \times 10^4$ [Equation (5-13) With T_{max} = 830°C]

n	Part A	Part B	Part A + B
0	-15.084400	-15.2637000	-15.8770000
1	- 7.643500	- 5.7946500	- 3.3232700
2	3.218150	7.3794600	2.6975300
3	8.231690	7.8223500	3.1181500
4	3.923760	0.7606680	1.7166100
5	- 2.115430	- 4.1354100	- 1.4819600
6	- 2.478680	- 2.9925600	- 2.0689700
7	1.303550	2.9898400	2.8357900
8	5.974840	5.9568400	2.9845200
9	3.998670	1.9698300	1.3247800
10	- 1.438150	- 3.3808300	0.3722910
11	- 6.151490	- 4.6454300	- 2.7066400
12	- 3.785520	- 1.1002200	- 0.7185560
13	1.970420	2.9765600	1.0548600
14	4.887970	1.9932400	1.4344500
15	2.820540	- 1.5676600	0.5010040
16	- 1.930820	- 1.6635700	0.2879580
17	- 3.135440	0.6137730	- 0.3001990
18	- 1.071900	1.5838800	1.0024100
19	2.455260	0.5327720	1.6266700
20	1.968220	- 1.6746400	1.1428100
21	- 1.253590	- 2.4188700	- 0.6697590
22	- 3.860280	- 0.5342380	- 1.1008800
23	- 2.742830	1.1583100	- 0.5433120
24	0.529961	0.9595690	- 0.5706260
25	2.202990	0.1457600	0.0991600
26	1.571850	0.0311966	- 0.2825600
27	- 0.643321	1.0346300	- 0.9209250
28	- 0.918350	1.8587800	- 0.1361500
29	0.429189	0.8723340	0.3600440
30	2.225970	- 0.7435300	0.1014060

$$\left(\frac{m}{m_o}\right)_{\substack{\text{lost} \\ T_1 \rightarrow T_2}} = \frac{a_o\left(T_2 - T_1\right)}{2} + \frac{T_{max}}{\pi}\sum_{n=1}^{30}\frac{a_n}{n}\left[\sin\left(\frac{n\,\pi\,T_2}{T_{max}}\right) - \sin\left(\frac{n\,\pi\,T_1}{T_{max}}\right)\right] \quad (5\text{-}17)$$

The total mass loss from T = 0 to a temperature T is obtained directly from Equation (5-16) by letting $T_1 = 0$ and $T_2 \rightarrow T$:

$$\left(\frac{m}{m_o}\right)_{\substack{\text{lost} \\ 0 \rightarrow T}} = \frac{a_o\,T}{2} + \frac{T_{max}}{\pi}\sum_{n=1}^{30}\frac{a_n}{n}\sin\left(\frac{n\,\pi\,T}{T_{max}}\right) \quad (5\text{-}18)$$

or the mass remaining at the temperature T is:

$$\left(\frac{m}{m_o}\right)_T = 1 - \left(\frac{m}{m_o}\right)_{\substack{\text{lost} \\ 0 \rightarrow T}} \quad (5\text{-}19)$$

Figures 5-3 and 5-4 depict m/m_o versus the temperature for the Fourier series representation and the experimental data for each of the constituents of the formulation. As can be seen, the Fourier series representations provide excellent reproductions of the TGA data. Figures 5-5 and 5-6 depict $d(m/m_o)/dT$ versus temperature [from Equation (5-13)] for each of the constituents of the formulation. As will be explained in Section 5.3, these data are used for computing $\dot{\Gamma}_g$ [Equations (3-1) and (3-4)]. It is interesting to note, from Figure 5-5, that even though the magnitude of $d(m/m_o)/dT$ for borax is substantially smaller than the other three components, borax is considered to be the "blowing agent." The borax curve is repeated, with a different ordinate scale in Figure 5-6. It is also worthwhile to note that a substantial amount of activity is still occurring in Part A+B, the actual intumescent formulation, for temperatures in excess of 400 to 500°C. This activity is not present in any of the other figures and is probably the consequence of the chemical bonding between the two elements of the epoxy binder.

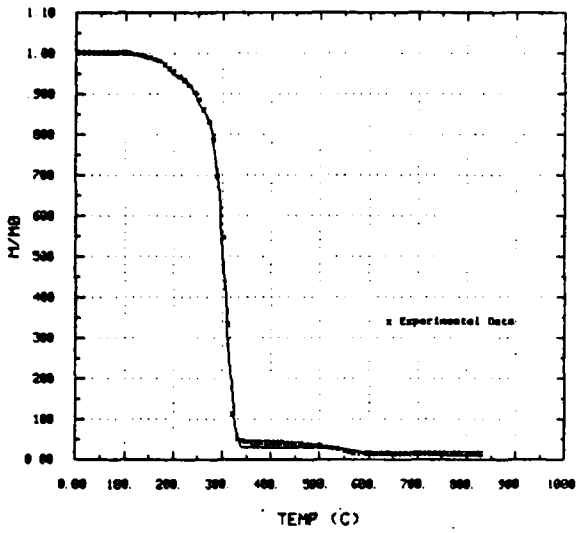

(a) Polysulfide

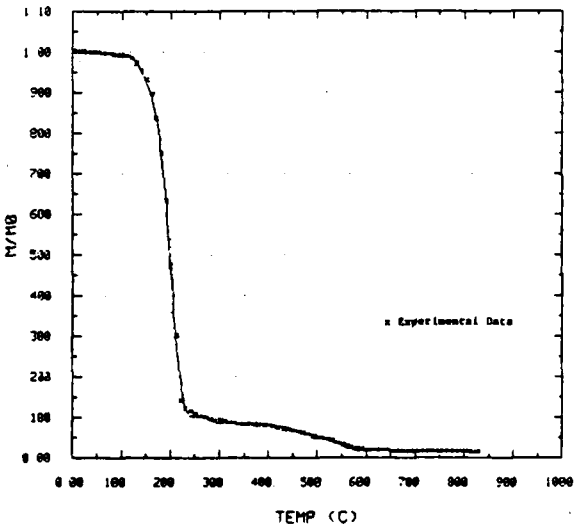

(b) DMP-30

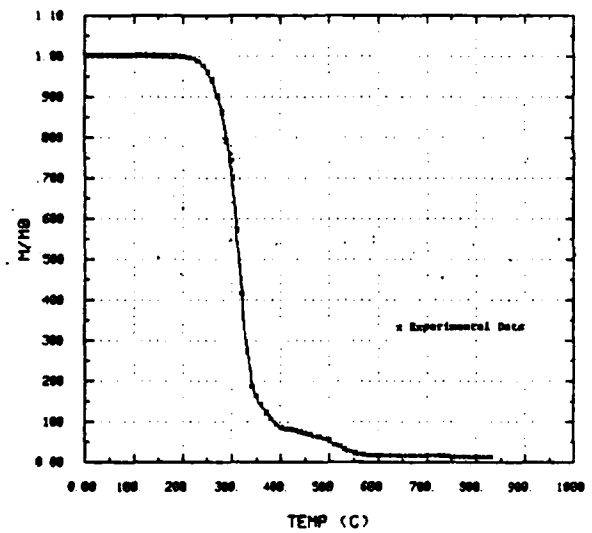

(c) EPON 828 Resin

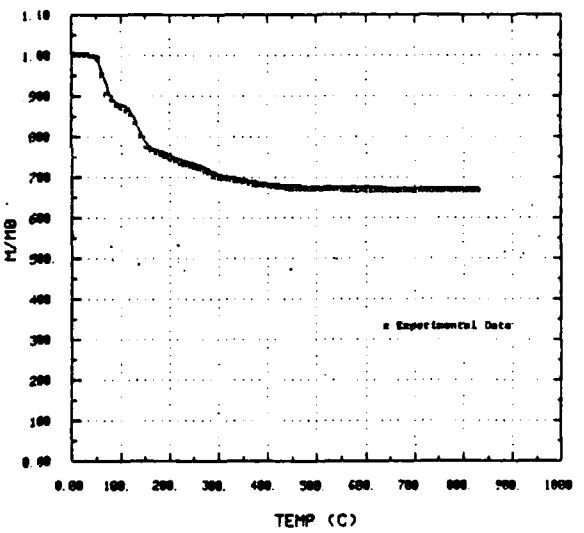

(d) Borax

Figure 5-3. Fourier Series Representation of TGA Data for Polysulfide, DMP-30, EPON Resin, and Borax

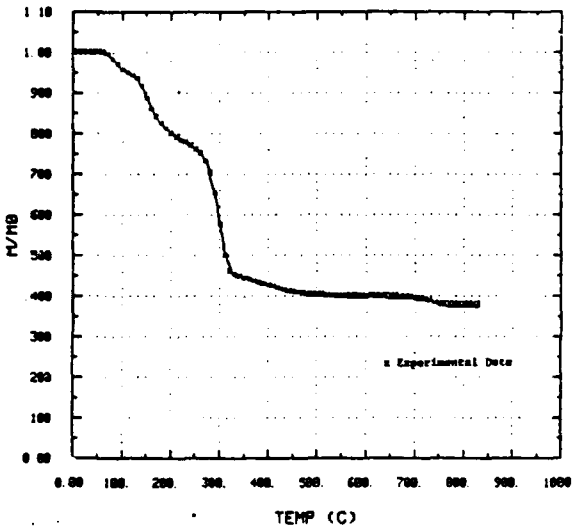

(a) Part A

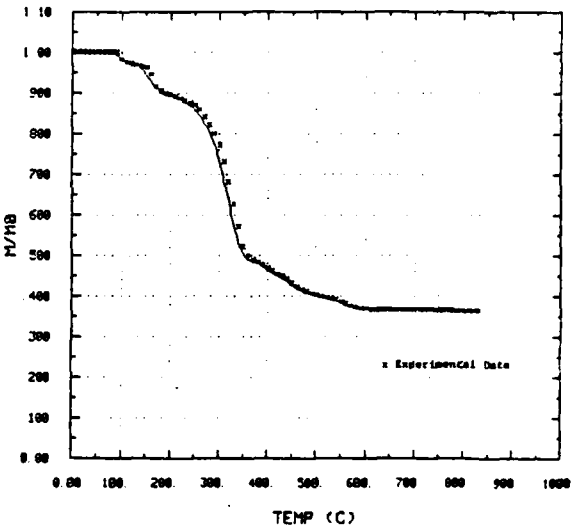

(b) Part B

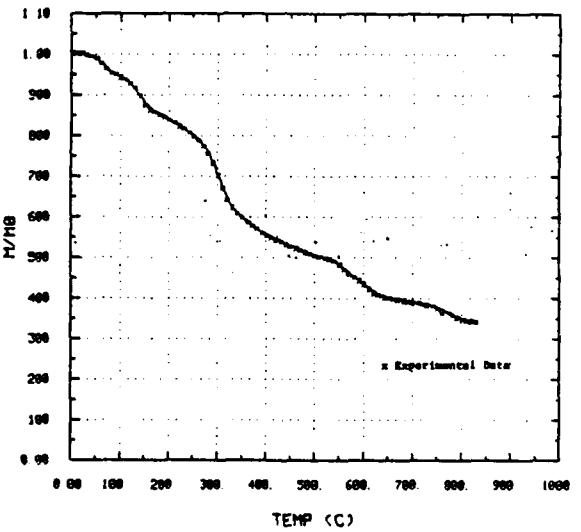

(c) Part A+B

Figure 5-4. Fourier Series Representation of TGA Data for Part A, Part B, and Part A+B

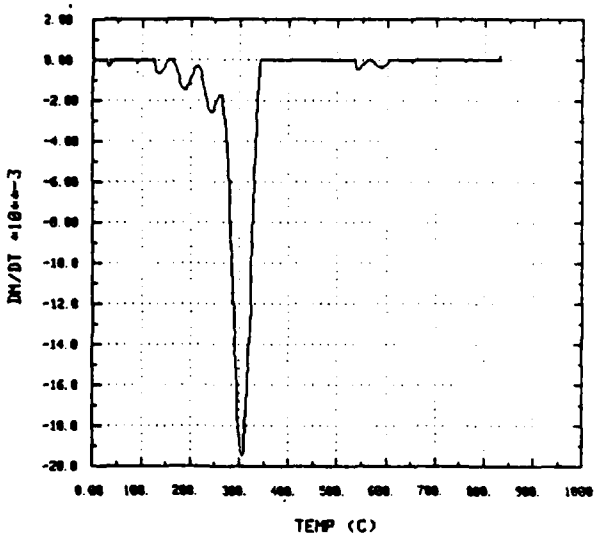

(a) Polysulfide

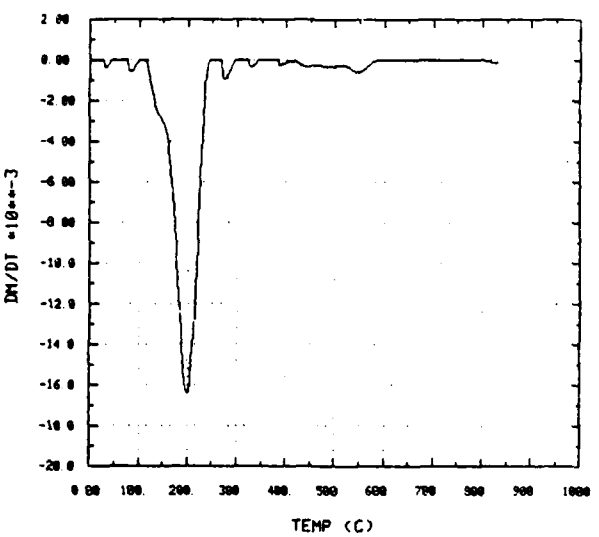

(b) DMP-30

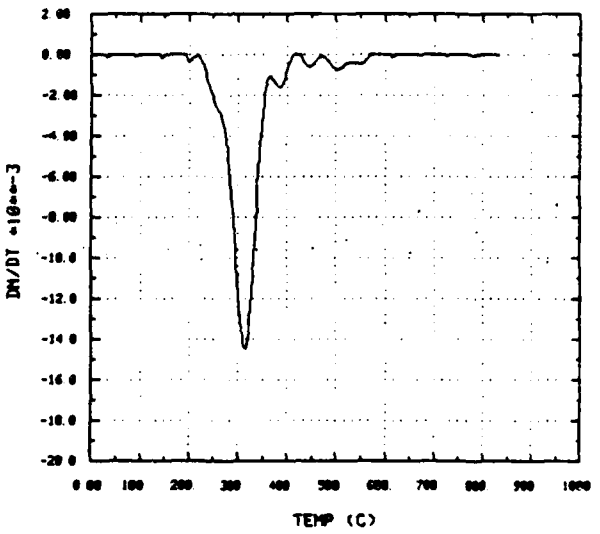

(c) EPON 828 Resin

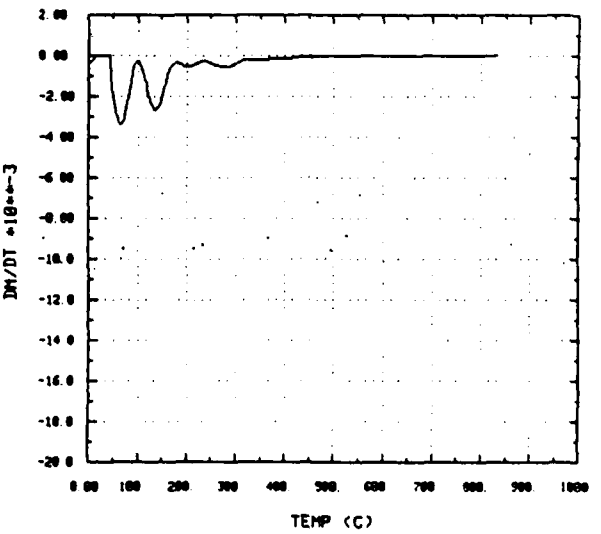

(d) Borax

Figure 5-5. Fourier Series Representation of $d(m/m_o)/dT$ for Polysulfide, DMP-30, EPON Resin, and Borax

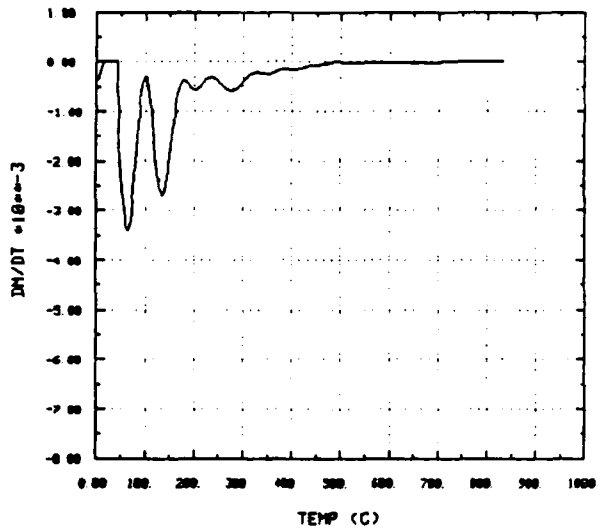

(a) Borax

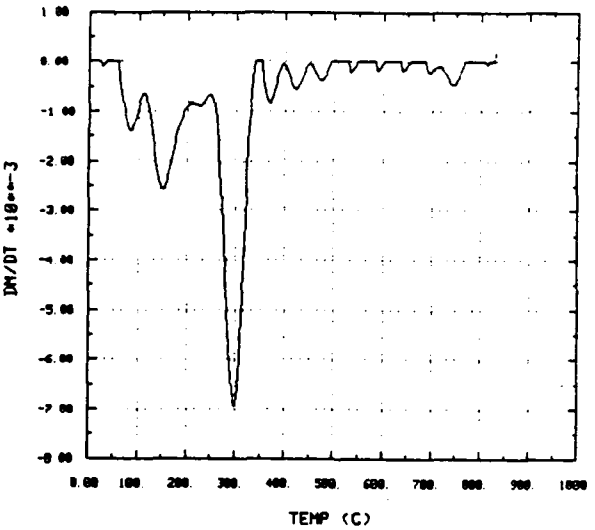

(b) Part A

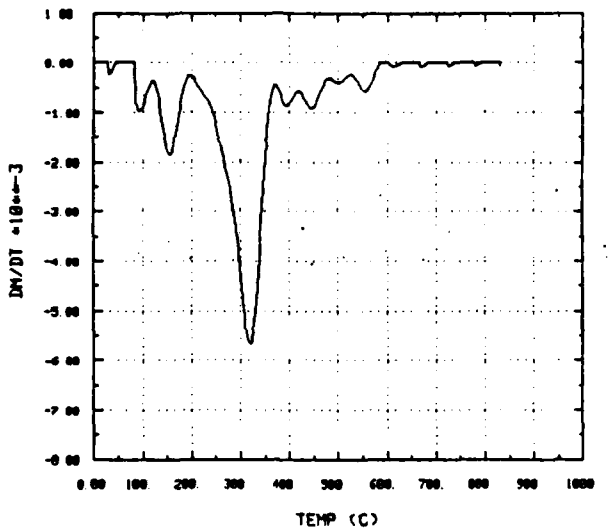

(c) Part B

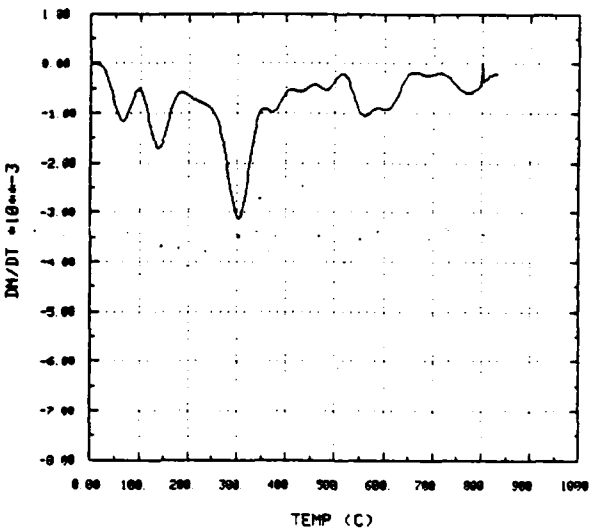

(d) Part A+B

Figure 5-6. Fourier Series Representation of $d(m/m_o)/dT$ for Borax, Part A, Part B, and Part A+B

b. Mixing and Local Concentrations

The different constituents can be mixed by simply summing the Fourier coefficients times their respective relative initial concentrations by weight, X_j:

$$\left[\frac{d\left(m/m_o\right)}{dT}\right]_{composite} = \sum_{j=1}^{J}\left[\frac{d\left(m/m_o\right)}{dT}\right]_j X_j =$$

$$\sum_{j=1}^{J}\left[\frac{a_o X_j}{2} + \sum_{n=1}^{\infty} a_n X_j \cos\left(\frac{n \pi T}{T_{max}}\right)\right] \qquad (5\text{-}20)$$

and:

$$\left[\left(\frac{m}{m_o}\right)_{\substack{lost \\ 0 \rightarrow T}}\right]_{composite} = \sum_{j=1}^{J}\left[\left(\frac{m}{m_o}\right)_{\substack{lost \\ 0 \rightarrow T}}\right]_j X_j =$$

$$\sum_{j=1}^{J}\left[\frac{a_o T X_j}{2} + \frac{T_{max}}{\pi}\sum_{n=1}^{30}\frac{a_n X_j}{n}\sin\left(\frac{n \pi T}{T_{max}}\right)\right] \qquad (5\text{-}21)$$

The mass versus temperature curve can now be computed for the mixture using Equations (5-19) and (5-21). This procedure has been followed to form the (m/m_o) versus temperature curves for Part A, Part B, and Part A+B. Figure 5-7 compares the simple "mixing theory" for Part A and Part B. The relative concentrations of the individual constituents are given in Table 4-2. Overall, the agreement is quite good. The $d(m/m_o)/dT$ versus temperature curves corresponding to the curves in Figure 5-7 are shown in Figure 5-8.

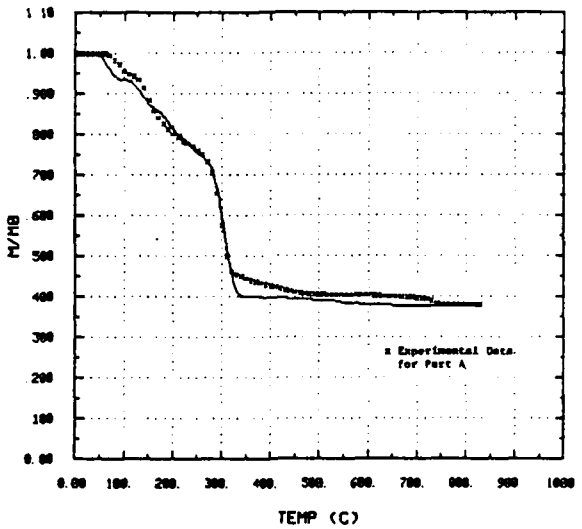

(a) Part A

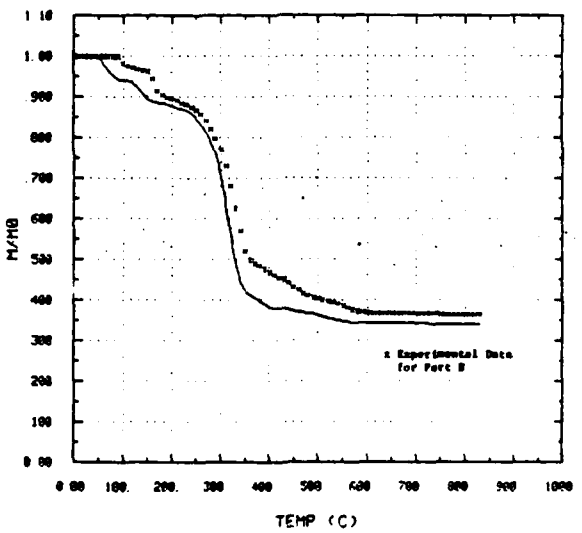

(b) Part B

Figure 5-7. Summation of the Various Constituents, by Concentration, to Form Part A and Part B Mass Loss Versus Temperature Curves

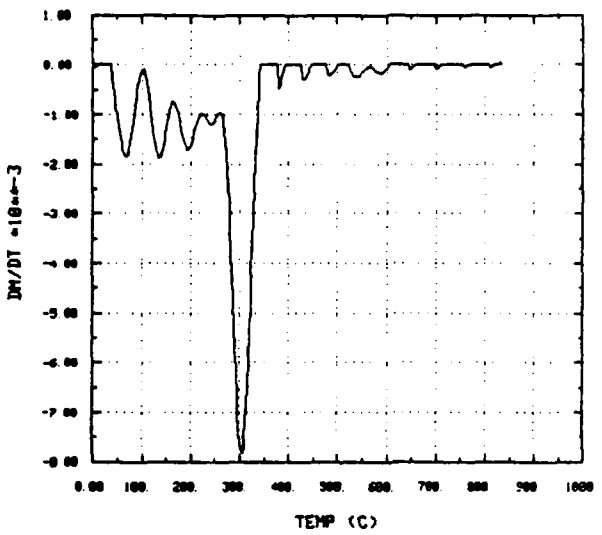

(a) Part A

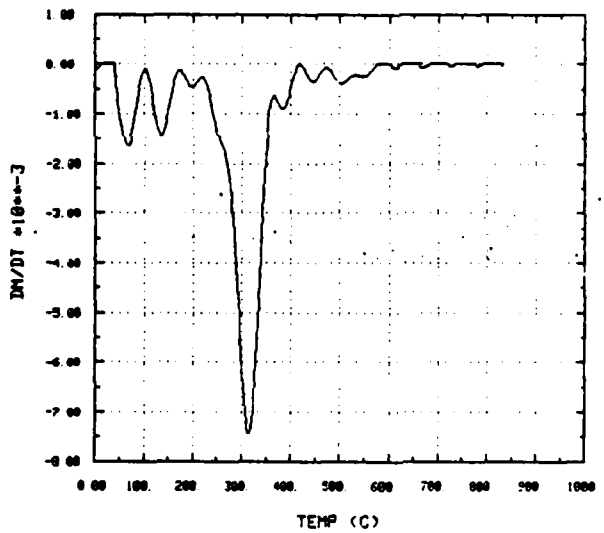

(b) Part B

Figure 5-8. Summation of the Various Constituents, by Concentration, to Form Part A and Part B $d(m/m_o)/dT$ Versus Temperature Curves

Likewise, the entire formulation, Part A+B, can be approximated as a sum of its parts, Figure 5-9. The agreement between the simple mixing theory and the data is not as good as for Part A or Part B. However, considering that no chemical bonding has been accounted for, which particularly occurs when the two components of the epoxy are mixed together, the overall trend of the experimental data is given quite nicely by the simple mixing theory. Figure 5-10 depicts the curves for the corresponding rate of mass loss versus temperature. What remains to be determined is if the model's heat transfer predictions differ significantly for Part A+B compared to Part A+B from the mixing theory.

The relative concentration of a particular constituent is temperature dependent, and thus must be computed at each temperature. Since there exists a temperature gradient through the intumescent coating, the concentration of the various constituents is a function of depth into the insulating system. The local constituent concentration, c_j, is computed from:

$$c_j(T) = \frac{m_j}{\sum_{j=1}^{J} m_j} = \frac{\left(m/m_o\right)_j \left(m_o\right)_j}{\sum_{j=1}^{J} \left(m/m_o\right)_j \left(m_o\right)_j} \qquad (5\text{-}22)$$

where $(m/m_o)_j$ is the local residual mass remaining of constituent j. The original mass of the j^{th} constituent is given by the total mass, m_o, times its original concentration, X_j:

$$\left(m_o\right)_j = m_o X_j \qquad (5\text{-}23)$$

Thus, the local constituent concentration is given by:

$$c_j(T) = \frac{\left(m/m_o\right)_j X_j}{\sum_j \left(m/m_o\right)_j X_j} \qquad (5\text{-}24)$$

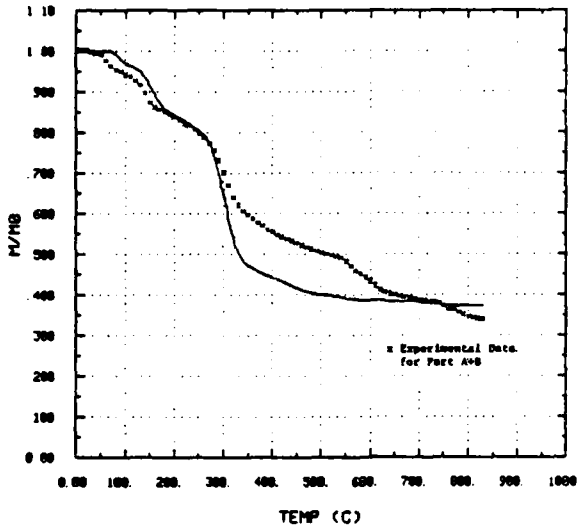

(a) (Part A) · X_A + (Part B) · X_B → Part A+B

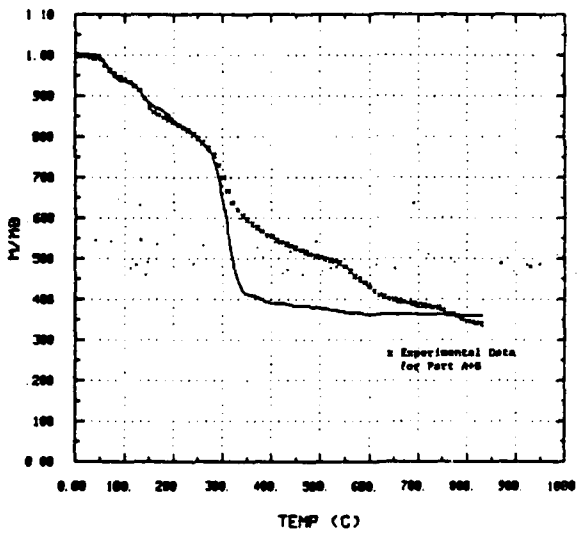

(b) Summation of Constituents (Borax, etc.) by Concentration to Form Part A+B

Figure 5-9. Summation of the Components, by Concentration, to Form Part A+B Mass Loss Versus Temperature Curves

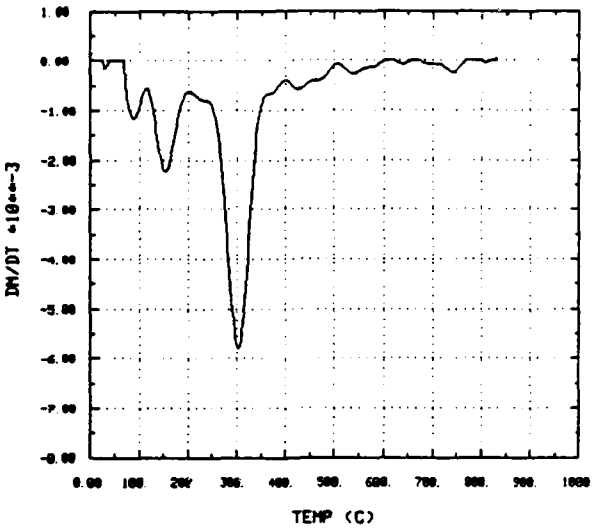

(a) (Part A) · X_A + (Part B) · X_B → Part A+B

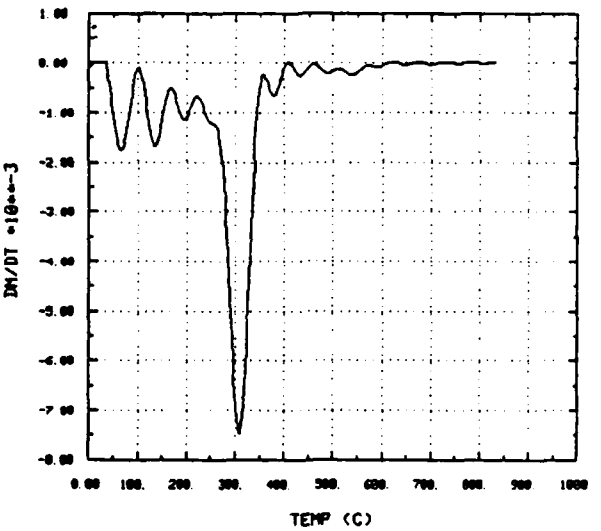

(b) Summation of Constituents (Borax, etc.) by Concentration to Form Part A+B

Figure 5-10. Summation of the Components, by Concentration, to Form Part A+B $d(m/m_o)/dT$ Versus Temperature Curves

It becomes evident that c_j is a function of the temperature since $(m/m_o)_j$ is temperature dependent. Note that $(m/m_o)_j$ is straightforward to compute from Equation (5-19).

5.3 Interpretation of Data for Analytic Model

The quantity $\dot{\Gamma}_g$ in Equation (3-1) has units of mass per unit volume per unit time. We must perform the appropriate conversions on the TGA data to transform the data into a form compatible with the definition of $\dot{\Gamma}_g$. The change in mass with respect to time can be written as:

$$\frac{dm}{dt} = \frac{dm}{dT}\,\frac{dT}{dt} = m_o\,\frac{d\left(m/m_o\right)}{dT}\,\frac{dT}{dt} \qquad (5\text{-}25)$$

The sweep rate of the temperature, dT/dt, is selected by a switch on the instrument. For the TGA runs we have analyzed, a sweep rate of 20°C per minute was used, thus dT/dt = 1/3 °C/s, but in general, for small increments of temperature and time:

$$\frac{dT}{dt} = \frac{\Delta T}{\Delta t} \qquad (5\text{-}26)$$

The change in density of the coating is due to mass loss and the expansion of the coating. The expansion of the coating is essentially one-dimensional, so a differential volume element, ΔV, is related to its initial volume $(\Delta V)_o$ by:

$$\Delta V = A\,(\Delta x) = A\,E_f\,(\Delta x)_o = E_f\,(\Delta V)_o \qquad (5\text{-}27)$$

where A is the cross-sectional area, E_f is the expansion factor, and $(\Delta x)_o$ is the original thickness of the element.

The mass lost by outgassing is given by:

$$m_{lost} = \int_{o}^{t} \dot{\Gamma}_g(\tau)\ [\Delta V(\tau)]\ d\tau \qquad (5\text{-}28)$$

The time rate of change of the mass loss is then given by:

$$\frac{dm}{dt} = \dot{\Gamma}_g\ (\Delta V) = \dot{\Gamma}_g\ E_f\ (\Delta V)_o \qquad (5\text{-}29)$$

Thus, equating Equations (5-25) and (5-29), using Equation (5-26), and using $m_o = \rho_o\ (\Delta V)_o$, yields the rate of material lost due to outgassing per unit volume:

$$\dot{\Gamma}_g = \frac{\Delta T\ \rho_o}{\Delta t\ E_f}\ \frac{d\left(m/m_o\right)}{dT} \qquad (5\text{-}30)$$

where $d(m/m_o)/dT$ is given by Equation (5-20).

This Page Intentionally Left Blank

6.0 DSC DATA

6.1 Introduction

A differential scanning calorimeter (DSC) measures and records the energy necessary to maintain thermal equilibrium between a test sample and a chosen reference. The sample of known mass (generally a few milligrams) is heated at a constant temperature rate (typically 20°C/min) and the rate at which energy is absorbed (endothermic) or emitted (exothermic) is recorded versus temperature. Specific heats are thus proportional to the deviation of the sample thermogram from the baseline. A phase change (solid to liquid, liquid to vapor, or solid to vapor) is represented by a peak. The area of the peak is proportional to the heat of fusion, vaporization, or sublimation. The DSC curve for the intumescent formulation (Part A+B) is shown in Figure 6-1.

To quantify the data from the instrument, three standards were run (indium, tin, and zinc) which have sharp endothermic reactions of 156.6°C, 231.9°C, and 419.4°C, respectively, with enthalpy changes of 0.9657, 1.154, and 1.7226 cal/g. Since the masses, m (mg), of each of the samples were known, and the areas, A ($in.^2$), of the endothermic peaks were measured carefully by a planimeter, three calibration constants, e_c, were obtained using:

$$e_c = \frac{\Delta H \cdot m}{A \cdot B \cdot \Delta q_r} \qquad (6\text{-}1)$$

where ΔH is the enthalpy change (mcal/g), B is the time base setting (sec/in.), and Δq_r is the y-axis range setting of the instrument (mcal/sec/in.). The three calibration constants were then combined into an overall calibration constant, E, as a function of temperature by fitting the e_c's to a parabolic curve:

$$E = 2.024 \times 10^{-6} T^2 + 1.714 \times 10^{-3} T + 0.6476 \qquad (6\text{-}2)$$

where T is in degrees Celsius.

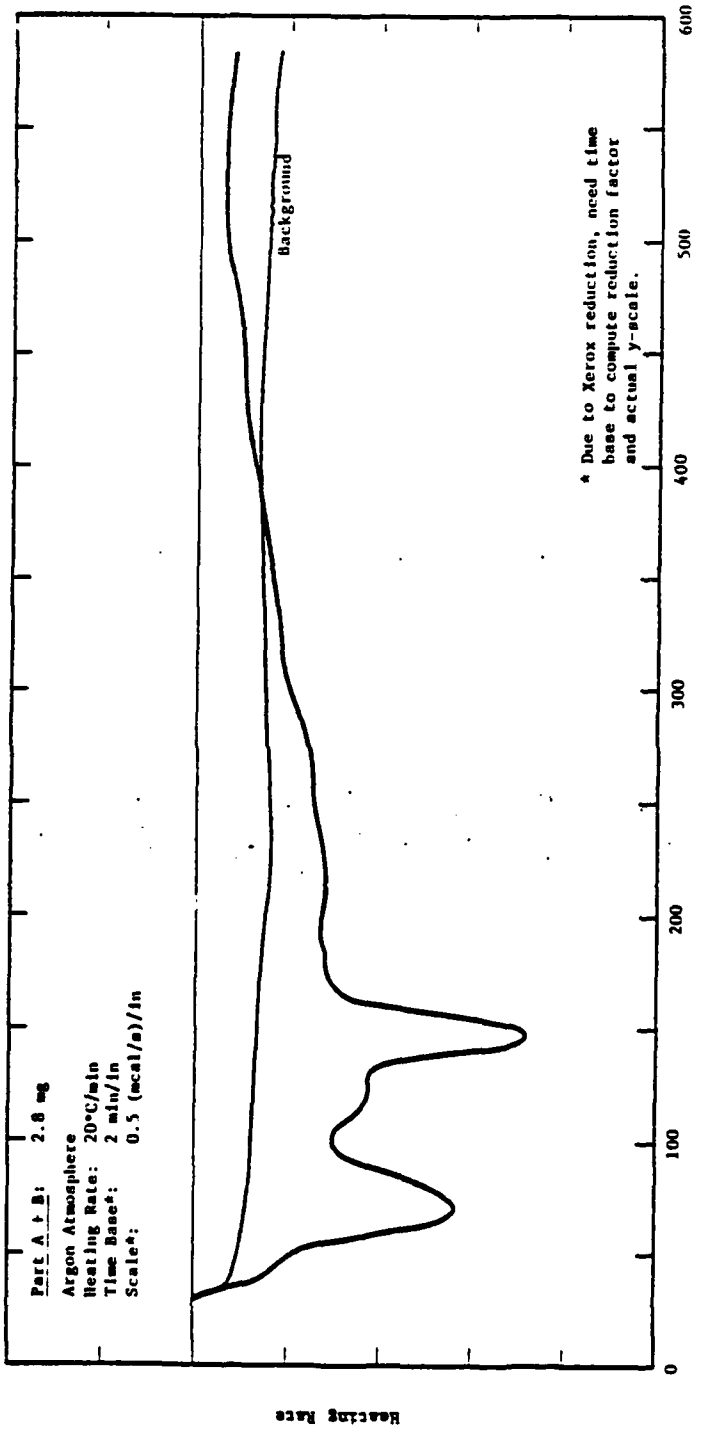

Figure 6-1. Part A+B: DSC With Argon Atmosphere

We note here that it is important that the sample should be tested in an inert atmosphere, such as argon, to avoid exothermic reactions resulting from the oxidation of long-chain polymers.

6.2 Enthalpy Changes

Enthalpy changes, Δh (cal/g), were computed from:

$$\Delta h = \frac{A}{\Delta m}\left(B \cdot E \cdot \Delta q_r\right) \tag{6-3}$$

where A is the area of the peak ($in.^2$) [measured carefully by using a planimeter], B is the time base setting (sec/in.), E is from Equation (6-2), and Δq_r is the y-axis range (mcal/sec-in.). The change in sample mass, Δm (mg), is computed from the TGA data. [Note that it has been assumed, and not unreasonably, that the enthalpy change is associated with a phase change of solid or liquid to a gas so that there is mass loss. This assumption is consistent with the TGA data. Solid-to-liquid phase changes could be accounted for, but examination of TGA data generally shows mass loss during a phase transition. This assumption will be discussed further in the section on reproduction of the DSC data.] The enthalpies are tabulated in Table 6-1.

6.3 Specific Heats

Specific heats, C_p (cal/g-°C), were determined from:

$$C_p = \left(\frac{E \cdot \Delta q_r}{H}\right)\frac{\Delta Y}{m} \tag{6-4}$$

where H is the heating rate (deg/sec), ΔY is the difference in y-axis deflection between the sample and reference background curves at the temperature of interest (in.), m (mg) is the same mass [which is a function of temperature and is obtained from the TGA data], Δq_r is the y-axis range (mcal/sec-in.), and E is from Equation (6-2). Tables 6-2 and 6-3 tabulate the specific heats

Table 6-1. Enthalpy Changes

Temperature (°C)	Enthalpy Change (cal/g)						
	Polysulfide	DMP-30	EPON Resin	Borax	Part A	Part B	Part A + B
53 - 90							444.8
55 - 80				307.9			
65 - 106						1778.0	
68 - 96					1029.00		
132 - 162						972.0	
132 - 162							559.4
135 - 165					452.60		
135 - 175				1140.0			
158 - 222		80.93					
250 - 315			53.29				
268 - 320					48.39		
278 - 330	89.56						

Table 6-2. Specific Heats of Individual Constituents

Temperature (°C)	Specific Heat (cal/g-°C)				
	Polysulfide	DMP-30	EPON Resin	Borax	Glass Fiber
50	0.330	0.347	0.266	0.122	0.04
75	0.352	0.372	0.284	0.227	0.03
100	0.384	0.386	0.302	0.339	0.01
125	0.417	0.454	0.335	0.459	0.03
150	0.447	0.602	0.342	0.534	0.05
175	0.501	0.376	0.364	0.597	0.06
200	0.564	0.362	0.387	0.677	0.09
225	0.660	0.487	0.413	0.656	0.10
250	0.681	0.180	0.526	0.703	0.10
275	1.130	0.180	0.347	0.588	0.08
300	0.763	0.180	0.347	0.508	0.09
325	5.070	0.180	0.347	0.385	0.22
350	6.360	0.180	0.347	0.368	0.14
375	7.030	0.180	0.347	0.326	0.11
400	8.350	0.180	0.347	0.230	0.11
425	9.820	0.180	0.347	0.121	0.17
450	11.800	0.180	0.347	0.121	0.25
475	15.100	0.180	0.347	0.121	0.12
500	19.700	0.180	0.347	0.121	0.14
525	28.600	0.180	0.347	0.121	0.17
550	50.300	0.180	0.347	0.121	0.12
575	79.300	0.180	0.347	0.121	0.14
600	79.300	0.180	0.347	0.121	0.12

Table 6-3. Specific Heat of Mixed Components

Temperature (°C)	Specific Heat (cal/gm-°C)		
	Part A	Part B	Part A + B
50	0.244	0.328	0.260
75	0.310	0.369	0.347
100	0.395	0.447	0.418
125	0.499	0.543	0.677
150	0.596	0.600	0.452
175	0.684	0.614	0.445
200	0.627	0.641	0.430
225	0.681	0.724	0.410
250	0.711	0.780	0.385
275	0.679	0.698	0.380
300	0.778	0.399	0.257
325	0.841	0.524	0.181
350	0.812	0.614	0.169
375	0.830	0.609	0.169
400	0.818	0.664	0.169
425	0.829	0.726	0.169
450	0.937	0.627	0.169
475	0.851	0.623	0.169
500	0.836	0.603	0.169
525	0.783	0.501	0.169
550	0.658	0.460	0.169
575	0.515	0.249	0.169
600	0.515	0.249	0.169

as a function of temperature. If an exothermic reaction takes place, then the procedure adopted was to keep a constant specific heat and balance the energy by a chemical reaction term, discussed in the next subsection.

6.4 Heat Generation Term

After analyzing the DSC data, we concluded that some exothermic reactions were taking place at elevated temperatures. To properly account for exothermic chemical reactions, an extra term had to be included in the energy equation. This term was $(-\rho\ \dot{q}_{chem})$, where $\dot{q}_{chem}$ is the rate of heat generated per unit mass by chemical reactions (e.g., cal/gm-s). The convention has been used were a negative $\dot{q}_{chem}$ implies heat generation.

For those materials where the DSC curve goes above the background, an energy balance was used to compute $\dot{q}_{chem}$:

$$\dot{q}_{chem} + C_p \frac{\Delta T}{\Delta t} = \left(\frac{E \cdot \Delta q_r}{H}\right) \frac{\Delta Y}{m} \frac{\Delta T}{\Delta t} \qquad (6\text{-}5)$$

where $\Delta T/\Delta t$ is the heating rate (e.g., 1/3 °C/s), H is the heating rate (deg/sec) [note that $H = \Delta T/\Delta t$), E is the cell calibration coefficient, Δq_r is the y-axis range, ΔY is the difference in y-axis deflection between the sample and reference background, and m is the residual sample mass (obtained from the TGA curve). The specific heat, C_p, was assumed to be constant for all temperatures once the DSC curve crossed above the background. The $\dot{q}_{chem}$'s, as a function of temperature, are given as Tables 6-4 and 6-5 for each of the components and the mixtures.

6.5 Comments on the Accuracy of Tabular Values

Specific heats and $\dot{q}_{chem}$ values for some of the constituents (polysulfide, DMP-30, and EPON Resin 828) are quite suspect at elevated temperatures. For temperatures higher than 300 to 400°C, the remaining mass of material is

Table 6-4. Exothermic Heat Generation of Individual Constituents

Temperature (°C)	$\dot{q}_{chem}$ (cal/g-s)				
	Polysulfide	DMP-30	EPON Resin	Borax	Glass Fiber
50	0.000	0.0000	0.0000	0.0000	0.00
75	0.000	0.0000	0.0000	0.0000	0.00
100	0.000	0.0000	0.0000	0.0000	0.00
125	0.000	0.0000	0.0000	0.0000	0.00
150	0.000	0.0000	0.0000	0.0000	0.00
175	0.000	0.0000	0.0000	0.0000	0.00
200	0.000	0.0000	0.0000	0.0000	0.00
225	0.000	0.0000	0.0000	0.0000	0.00
250	0.000	0.0000	0.0000	0.0000	0.00
275	0.000	-0.0600	0.0000	0.0000	0.00
300	0.000	-0.0600	- 0.0867	0.0000	0.00
325	0.000	-0.1487	- 0.3243	0.0000	0.00
350	0.000	-0.0600	0.0240	0.0000	0.00
375	0.000	-0.0600	0.1093	0.0000	0.00
400	0.000	0.1283	- 0.1157	0.0000	0.00
425	0.000	0.1577	- 0.4757	0.0000	0.00
450	0.000	0.1940	- 1.5790	-0.0190	0.00
475	0.000	-0.0600	- 3.6490	-0.0850	0.00
500	0.000	-0.8333	- 4.9490	-0.0403	0.00
525	0.000	-1.4970	- 9.4160	-0.0698	0.00
550	0.000	-1.4970	-11.2500	-0.1227	0.00
575	0.000	-1.4970	-10.1800	-0.1263	0.00
600	0.000	-1.4970	-10.1800	-0.1527	0.00

Table 6-5. Exothermic Heat Generation of Mixed Components

Temperature (°C)	$\dot{q}_{chem}$ (cal/gm-s)		
	Part A	Part B	Part A + B
50	0.000	0.000	0.0000
75	0.000	0.000	0.0000
100	0.000	0.000	0.0000
125	0.000	0.000	0.0000
150	0.000	0.000	0.0000
175	0.000	0.000	0.0000
200	0.000	0.000	0.0000
225	0.000	0.000	0.0000
250	0.000	0.000	0.0000
275	0.000	0.000	0.0000
300	0.000	0.000	0.0000
325	0.000	0.000	0.0000
350	0.000	0.000	0.0000
375	0.000	0.000	-0.0415
400	0.000	0.000	-0.0724
425	0.000	0.000	-0.1607
450	0.000	0.000	-0.2120
475	0.000	0.000	-0.2770
500	0.000	0.000	-0.3773
525	0.000	0.000	-0.4363
550	0.000	0.000	-0.4663
575	0.000	0.000	-0.5097
600	0.000	0.000	-0.5097

less than a few percent of the initial mass. With such a small residual mass, the computed C_p's and $\dot{q}_{chem}$'s are extremely sensitive to the stability and accuracy of the DSC apparatus. The measured differences between the sample run and the reference background are probably in the "noise" range of the particular instrument used. There exists a much higher confidence in the computed C_p's and $\dot{q}_{chem}$'s for those substances where the residual mass is at least 30 percent of the initial mass.

7.0 COMPUTATIONAL ALGORITHMS

7.1 Discretizing the Differential Equations

To solve numerically the differential equations which apply at all locations within the intumescent coating, the coating material is divided into increments, Figure 7-1. Because the model is one-dimensional, each increment can be represented by a grid point. The differential equations are then written as difference equations and applied at each of the grid points. Thus, each of the variables, e.g., T, ρ, and v, is computed at each of the grid points. The scheme we have chosen is to let the variable be representative of the region (zone) to the right of the grid line. For example, the values for temperature and density for the cross-hatched zone in Figure 7-1 are given by T_k and ρ_k where the subscript k refers to the k^{th} grid point. Thus, T_k and ρ_k

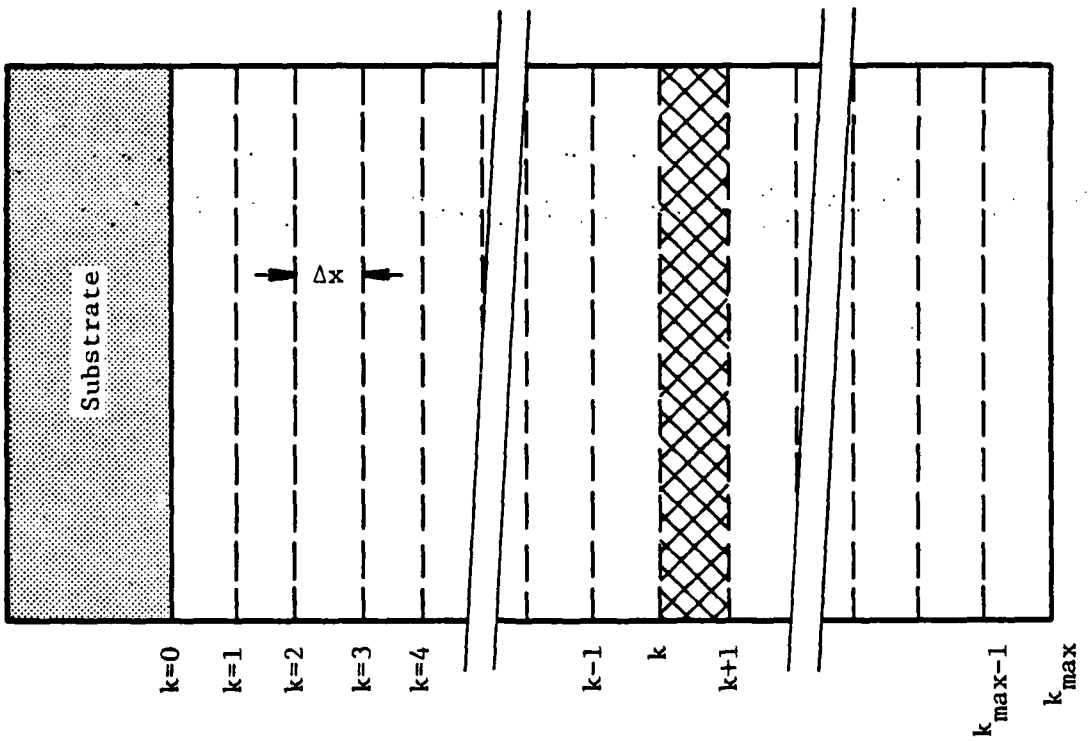

Figure 7-1. Computational Mesh

are the temperature and density for the region between $k \cdot \Delta x \leq x < (k+1) \cdot \Delta x$, where k runs from zero to kmax. With this convention, it is easily seen that the values for T_{kmax} and ρ_{kmax} represent boundary conditions since no intumescent material lies to the right of the kmax grid point.

The overall approach is to move forward in time by computing all the variables at a new time step in terms of known values from the previous time step, and values already computed at the current time step. This explicit formulation, as it is called, is straightforward, but the time step must be within certain bounds for the numerical procedure to remain stable.

A unique feature is the manner in which the equations are solved. The energy equation is solved in an Eulerian (fixed) coordinate system to determine the temperature field in order to compute the mass loss (which is temperature dependent). After computing the mass loss, the energy equation is corrected (by subtracting the convective term and updating the pyrolysis term), and then the continuity and energy equations are solved in a Lagrangian (material) coordinate system. The Lagrangian coordinate system is the "natural" coordinate system because the TGA data are Lagrangian in nature (since the intumescent system expands during outgassing). However, a Lagrangian coordinate system was not adopted for the overall computational approach because the accuracy of the computational scheme would decrease with increasing spatial increments. A velocity is associated with each grid point, and the grid expands according to the velocity field and the time increment (e.g., $\Delta x_{move} = v \cdot \Delta t$). The expanded grid is then rezoned back to its original mesh. Because the coating system expands, the total thickness of the computational mesh grows larger. New zones are added when appropriate.

7.2 Logic Flow

The logic flow is presented now to give the reader an overall view of the structure of the numerical algorithms. Descriptions of the numerical representations of the equations are given in detail in Appendix B.

The procedure to compute the temperature, velocity, and density at the grid points is:

(1) Compute the temperature at all grid points by integrating Equation (3-4).

(2) From the temperatures, compute the mass loss in each zone, i.e., outgassing, Equation (5-30).

(3) From the mass loss, compute the velocity at all grid points, Equation (3-8).

(4) Compute the density at all grid points by integrating Equation (3-1) — the decrease in bulk density at each point is the result of losing mass and expansion.

(5) Compute the expansion of the grid.

(6) Rezone the grid points back to their original locations — add grid points as necessary to account for expansion.

This process is repeated for each time step until program termination. Logic flow diagrams depicting the logic flow of the numerical procedure are given in Appendix B.

This Page Intentionally Left Blank

8.0 MODEL CALCULATIONS

Numerical solutions have been obtained for the analytic model presented in the previous sections. The results of the different problems or parametric studies will be presented in the following subsections.

8.1 Reproduction of DSC Data

With the information from the tables entered into the computer program, a computer run was made to simulate a DSC test. Many things must work correctly, in concert, for the computational model to reproduce the actual DSC experimental curve, including the mass loss, search subroutines, enthalpy changes, specific heat, chemical energy generation, and expansion of the intumescent coating. The total remaining mass is important because of the specific heat and chemical energy generation terms. Likewise, the rate-of-mass loss is important since the total heat absorbed during a phase transition is the enthalpy change times the mass loss. The expansion of the coating must occur correctly or else the computed densities will be in error, and when integrated over the thickness of the expanded coating, will result in an incorrect total remaining mass.

Figure 8-1 reproduces the data from the DSC experiment for Part A+B. Also plotted are the predictions from the analytic model. The curves agree extremely well in regions where there are no phase changes. The two enthalpy peaks are present in the computational predictions, but do not exactly reproduce the data. The model assumption that the total enthalpy change was due to a phase change involving mass loss, must be violated to some extent. It would be extremely difficult to differentiate the quantity of heat going into solid-to-liquid phase changes versus solid-to-gas or liquid-to-gas (with a corresponding mass loss). However, the areas of the two peaks have been reproduced, which implies that the total heat balance has been faithfully replicated. Thus, the fact that the enthalpy peaks have not been exactly reproduced is not of great concern. Therefore, since the current model correctly

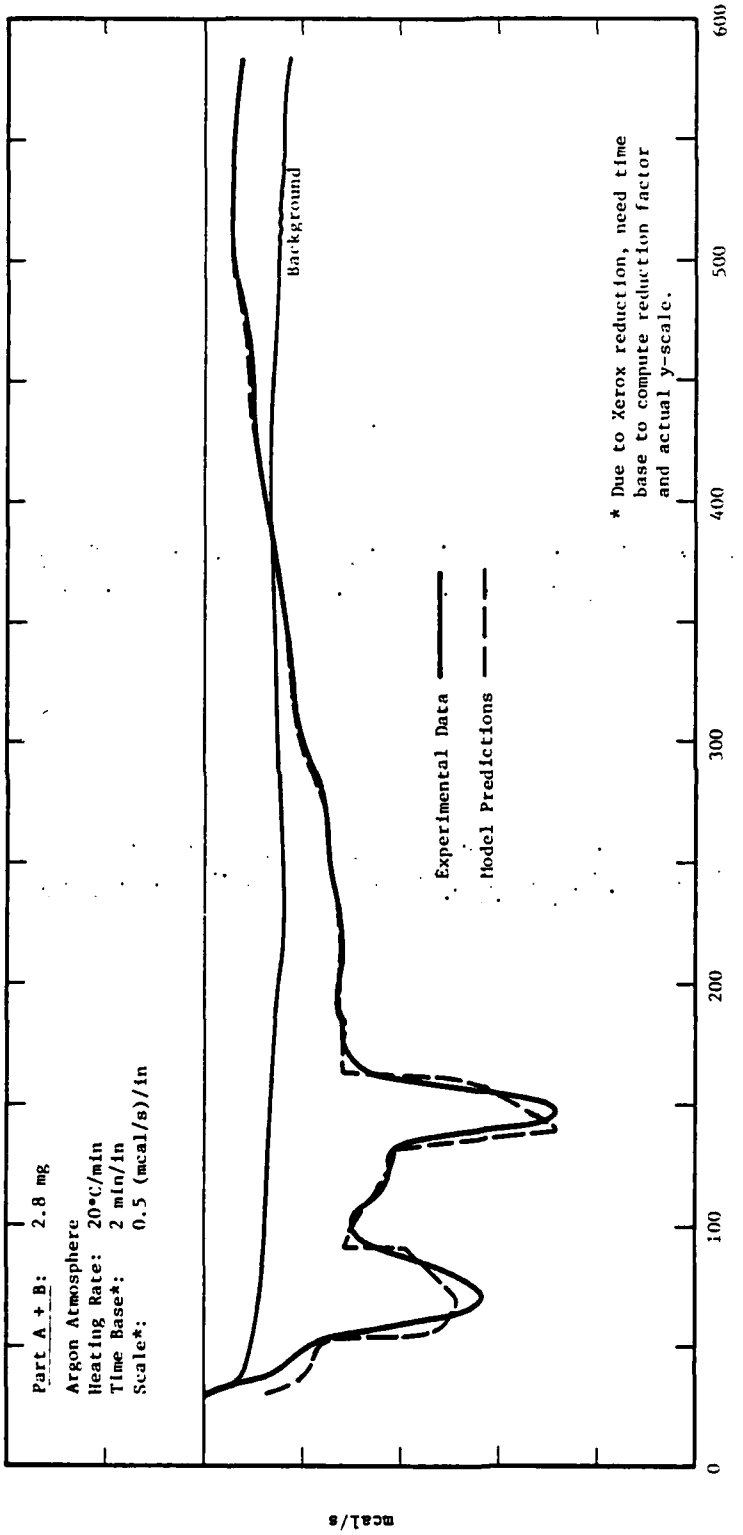

Figure 8-1. Model Comparison With Experimental DSC Data

predicts the overall features of the phase transition, it is felt that the present modeling assumptions are adequate. Solid-to-liquid phase changes could be incorporated into the model at a later date if desired.

8.2 Composite DSC Data

Section 5.2.2(b) showed the results of mass loss versus temperature using the assumption that the sum of the constituents might approximately equal the whole, i.e., the actual formulation of Part A+B (Figure 5-9). The same can be done from an energy absorption/generation standpoint.

The DSC data in Figure 8-1 can be displayed in an alternate form by dividing the energy absorbed/generated by the instantaneous mass per unit length (from the TGA data). This rate at which energy is absorbed or generated per gram of coating material (per square centimeter of surface area) can then be displayed versus temperature. The solid curve in Figure 8-2 is the curve for Part A+B. A hypothetical DSC experiment was then performed with the computer model using the concentrations from Table 4-2 to mix Part A with Part B, and mix the constituents (polysulfide, borax, etc.) to form Part A+B. These results are also shown in Figure 8-2. The densities of the composite formulations were determined from Equation (4-5). It is important, for modeling considerations, that the total mass of the system be represented accurately. Thermodynamic quantities such as specific heat are given in units, for example, of calories per degree Celcius per gram. If an alternate procedure is used to compute the composite density, then the coating thickness may have to be adjusted to insure that the coating mass is modeled correctly.

The mixing of the constituents follow the Part A+B curve much better than the mixing of Part A with Part B. Part A plus Part B has substantially larger endothermic reactions at approximately 75°C and 150°C. Evidently, the mixing of components into Part A and into Part B is slightly exothermic — with the application of heat, the breaking of chemical bonds absorbs significantly more energy.

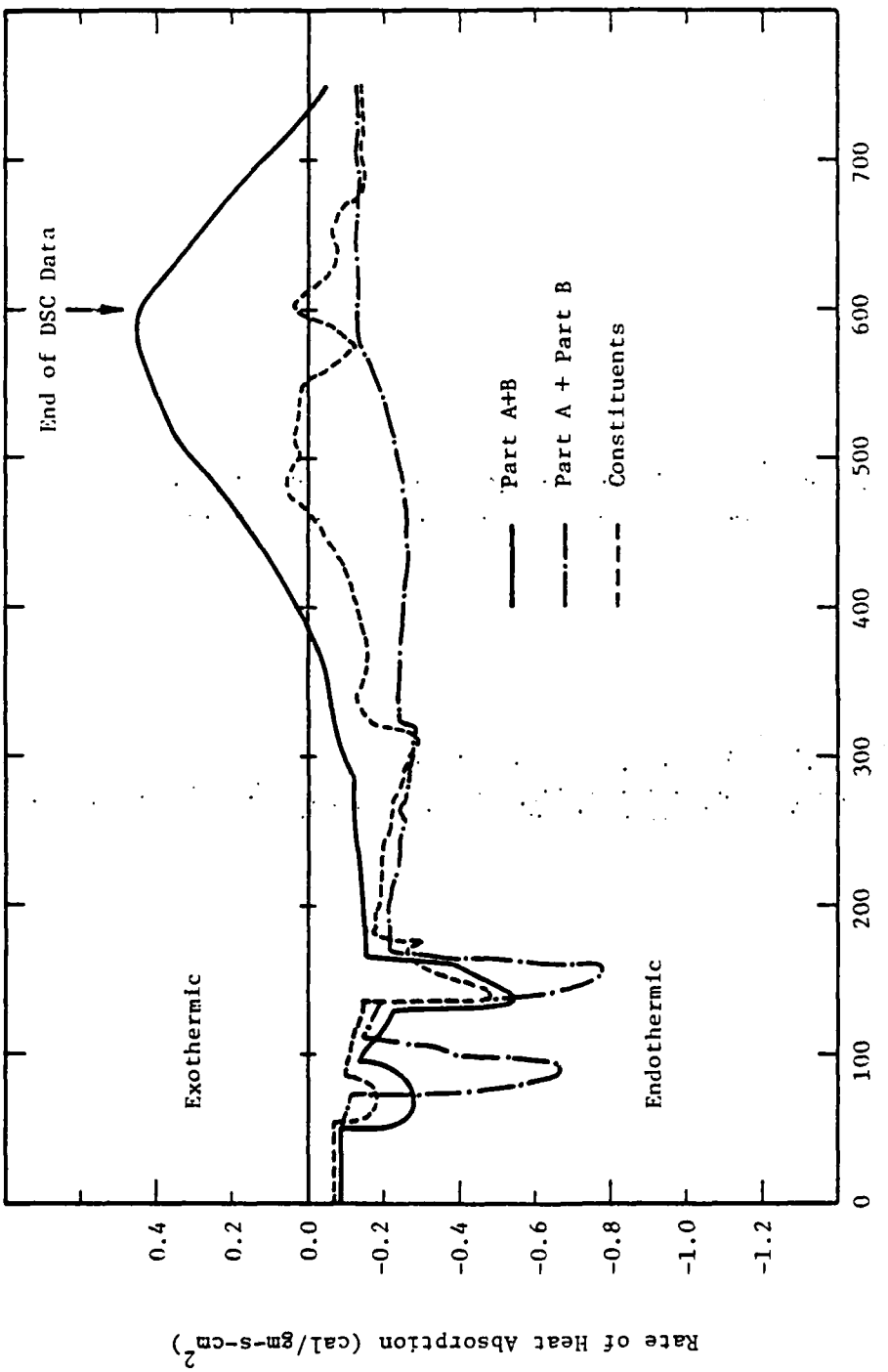

Figure 8-2. Comparison of Rate of Heat Absorption Versus Temperature

Part A+B become exothermic at temperatures in excess of 385°C. However, the unit used to perform the DSC experiment was limited to temperatures less than approximately 600°C. All heat capacities were extrapolated for temperatures in excess of 600°C by assuming the specific heat a constant for higher temperatures. If a sample was exothermic at 600°C, then the exothermic reaction was set to zero at 750°C. From a computational viewpoint, this implies that the exothermic heat generation goes to zero linearly with temperatures from 600°C to 750°C [see Equation (B-52)]. The "jitter" in the curve for the constituents in the temperature range 475°C to 650°C can be attributed to the accuracy of some of the specific heat and $\dot{q}_{chem}$ values, Tables 6-2 and 6-4. Because the mass of a sample becomes very small (e.g., polysulfide) for temperatures in excess of 450°C, small errors in subtracting the DSC data from the background can result in significant changes in calculated specific heats and $\dot{q}_{chem}$'s. The jitter is probably an indication of the stability (accuracy) of the DSC apparatus in running a sample and background at different times.

It is evident from Figure 8-2 that the actual mixing of the components, with the resulting formulation of chemical bonds, has a significant influence on the rate of energy absorption. We can expect different temperature-time histories of the substrate when the model is exercised using the thermodynamic data for Part A+B versus the thermodynamic data for the components that make up Part A+B.

8.3 Coated Substrate

A steel sample plate (approximately 7.6 cm x 7.6 cm x 0.0813 cm) was coated with 0.0965 cm of intumescent formulation. It was then inserted in the furnace test facility at the Naval Air Development Center. The temperature of the substrate, determined by a thermocouple, was monitored versus time. The expanded coating was measured after the test and an expansion factor of 4.47 was determined.

The computer model was set up with five zones initially, each zone being 0.0193 cm thick for a total thickness of 0.0965 cm. A flame temperature of 1227°K (1750°F) and a convective heat transfer coefficient of 2.81×10^{-4} cal/cm^2-s-°C were used. The flame emissivity was assumed to be 1.0, and the surface emissivity 0.8. With these parameters, the initial incident heat flux was 2.68 cal/cm^2-s (9.89 BTU/ft^2-s) with radiation providing 90 percent of the heat flux. This heat flux approximately reproduces the conditions of the test chamber.

The first parameter investigated was the effect of the exponent in the expansion factor [Equation (3-6)]. For values of n less than 1.0, the expansion occurs early in the outgassing stage. For values of n greater than 1.0, the expansion occurs only after significant outgassing (Figure 3-2). As can be seen in Figure 8-3, the time at which the expansion begins has a rather dramatic effect on the temperature of the substrate.

The next parameter investigated was the exponent, q, in the assumed transition law for the thermal conductivity [Equation (B-54)]. (The values chosen for thermal conductivities were: virgin state, $k_o = 5.5 \times 10^{-3}$ cal/cm-s-°C, and char state, $k_c = 2.0 \times 10^{-3}$ cal/cm-s-°C.) The larger the exponent, the faster k_o approaches k_c for a given density, the logic being that the char may be essentially formed during the early stages of mass loss. Figure 8-4 presents the effects of the exponent in the thermal conductivity law for the case of n = 0.6 from Figure 8-3. Except for early times where the substrate heats more slowly for larger values of q, the curves are essentially identical. Thus, the effect of the exponent q is to delay heating of the substrate for early times by retarding the heat flow with a smaller thermal conductivity.

Figure 8-5 presents the influence of the maximum expansion of the coating system on the thermal response of the plate. With the assumption that the char thermal conductivity is relatively independent of density (the density decreases with expansion), the thickness of the char layer has a dramatic

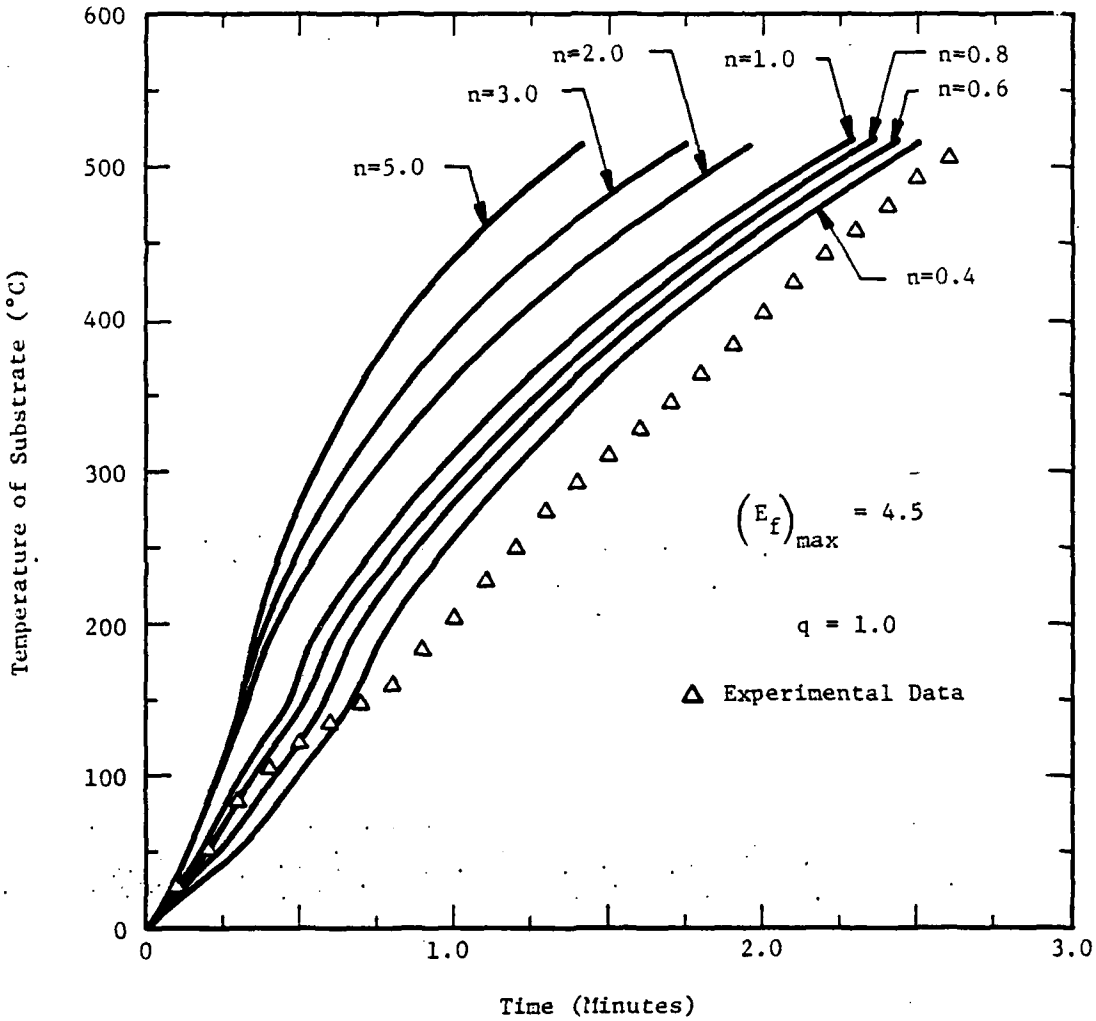

Figure 8-3. Effect of Exponential in Expansion Law on Substrate Temperature History

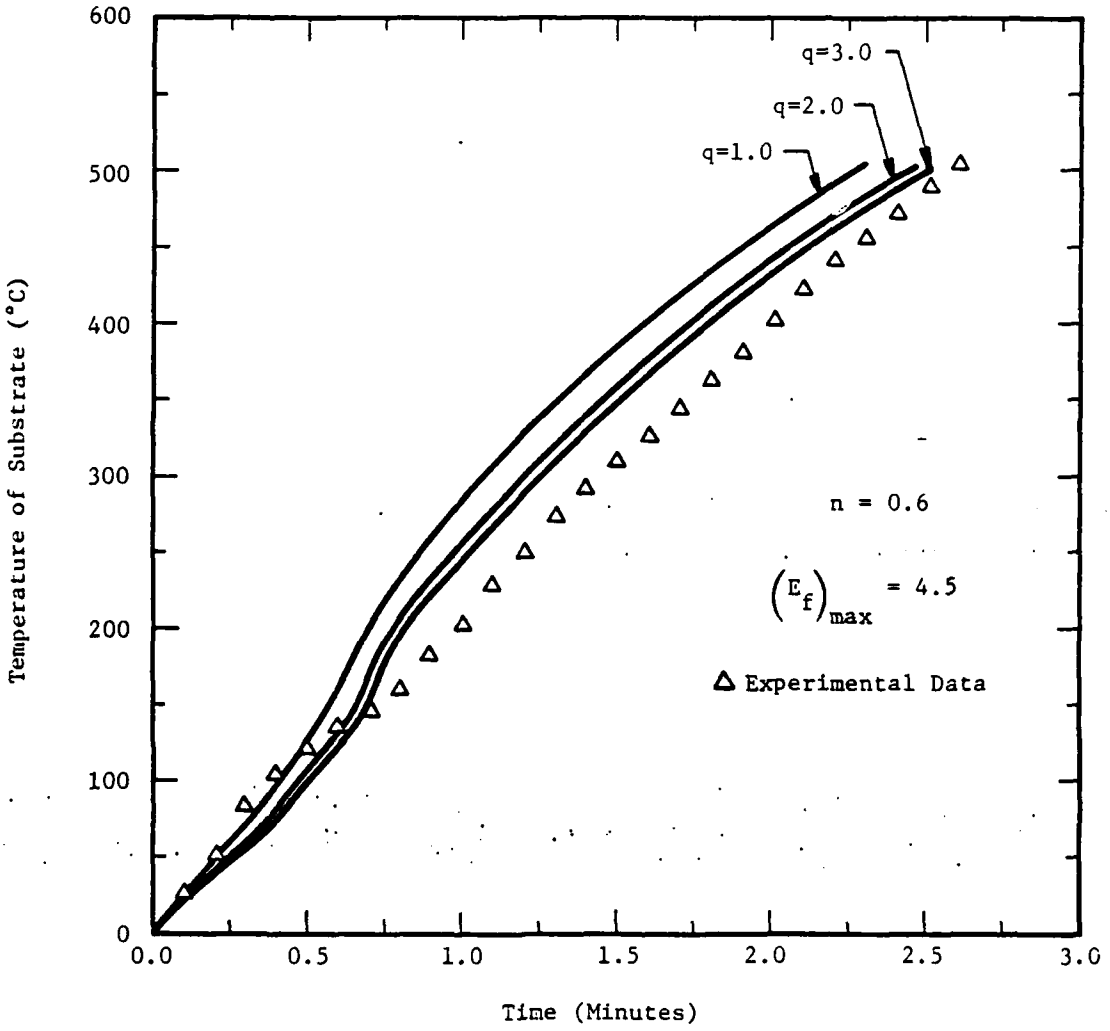

Figure 8-4. Effect of Exponential in Thermal Conductivity Expression on Substrate Temperature History

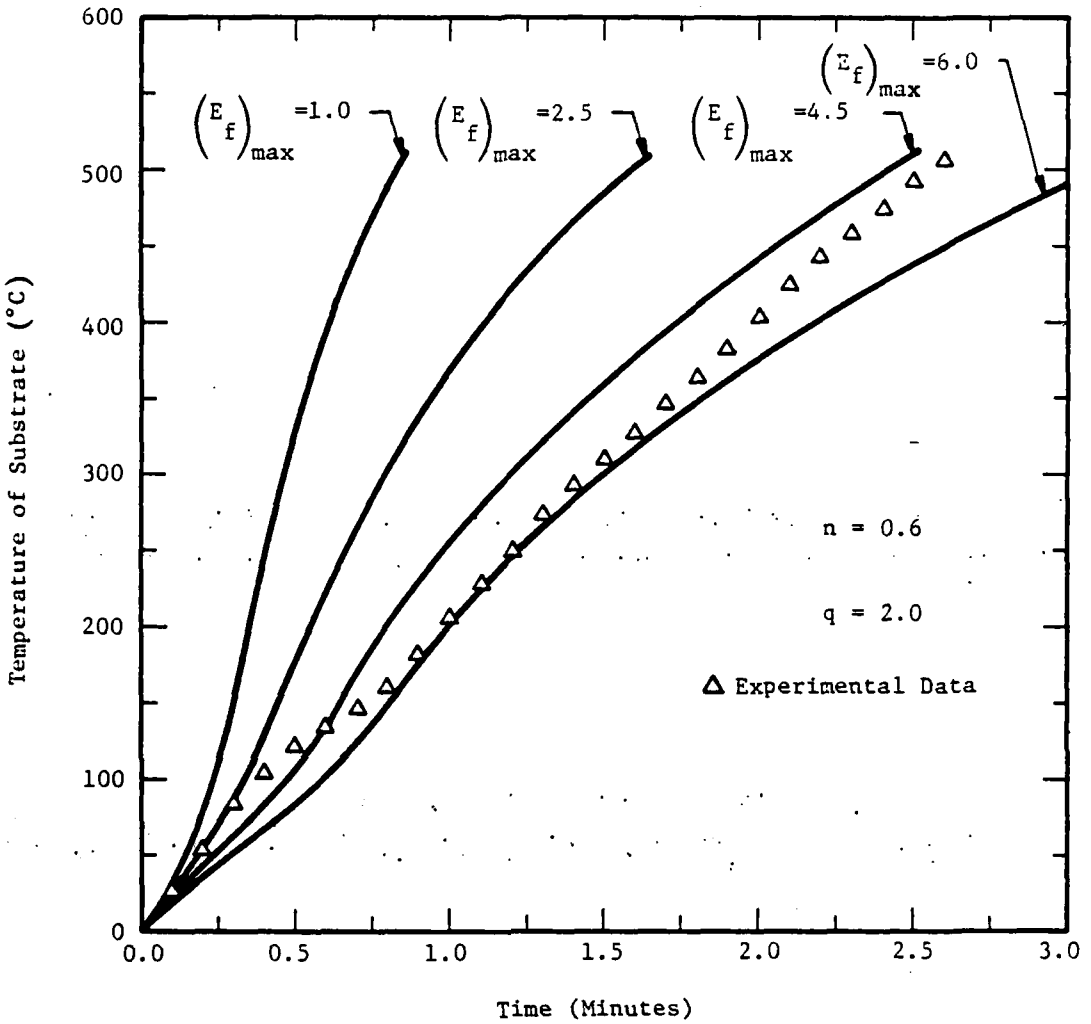

Figure 8-5. Dependence of Maximum Expansion of Coating on Substrate Temperature History

influence on the substrate's thermal response. It is interesting to note here that the measured expansion was found to be 4.47 times its original thickness. A thick sample of the coating (1.0 cm) was placed on a substrate and exposed to a heat source until it had completely intumesced. This coating expanded to 2.6 cm. The next section will briefly discuss this observation.

Plotted in each of the figures are the experimental data for the plate test. The model predictions do not exactly replicate the experimental data. Model assumptions and deficiencies are discussed in the next section, but some observations and conclusions can be drawn from the model's predictions nevertheless.

The experimental data begins rising rather quickly, but the slope decreases for 100°C < T < 155°C, after which the rate of heating increases but is less than the initial heating rate. The model predicts this "bend" in the data, after which the heating rate becomes steeper. This bend in the data and model predictions occurs when the temperature of the coating in contact with the substrate reaches the second endothermic peak shown in the DSC data (see Figure 8-1). Note that if the heat flux to the substrate is sufficiently large, Figures 8-3 and 8-5, the energy absorbed by the endothermic reaction is relatively insignificant with respect to the total heat reaching the substrate and the bend does not appear. The first endothermic peak, because it is smaller and because the thermal conductivity of the virgin material is larger than that of the char, is more difficult to see in the model's predictions but it is discernible. The resolution of the experimental data is not adequate to discern this first endothermic peak. However, possibly for reasons discussed in the next section, the model does not retard the incoming heat flux sufficiently to reproduce the extent of the bending evident in the experimental data.

From Figure 8-3, it is evident that the model does indicate, for better agreement with experimental data, that the expansion should occur early in the mass loss process (n < 1). This is in excellent agreement, from a chemistry

point of view, that the blowing agent results from the hydrating of water from borax. Examination of TGA and DSC data shows that this occurs in the early stages of the mass loss.

Figure 8-5 might, at first glance, seem to indicate that the largest expansion factor [$(E_f)_{max} = 6.0$] yields closer agreement with the experimental data. However, for n = 0.6, it underpredicts the initial heating rate and then has "too much" curvature (i.e., is insulating too well) at late times.

The rate of heating of the substrate for temperatures greater than 175°C is approximately replicated by the model, Figure 8-6, for any of the curves where $(E_f)_{max} = 4.5$ and $n \leq 0$. Very minor differences exist in the curves in Figure 8-3 for n = 0 or Figure 8-4 (q = 1, 2, or 3) for temperatures greater than 175°C. This implies that the heat flow is being controlled by the charred region of the coating. The curve in Figure 8-6 was obtained by shifting the model predictions in time to match the experimental data. This would indicate that late time heat flow is being treated properly. The model predicts a little more curvature than the experimental data, but then the model has assumed the rear surface of the substrate is perfectly insulated. Any heat loss from the back surface of the experimental plate, even though it may be well-insulated, would tend to "straighten" the experimental data curve.

In summary, the model appears to predict very early heating rates and the very late time heating rates reasonably accurately when the expansion process occurs early in the mass loss process ($0.6 < n < 0.8$), for a maximum expansion factor of approximately 4.5. The model computes a heating rate a little too high in the intermediate times, but does predict a relatively sharp increase in the heating rate at approximately 155°C. For best overall agreement, the model calculations indicate that $(E_f)_{max}$ should be approximately 4.5, in excellent agreement with the experimentally determined expansion factor of 4.47.

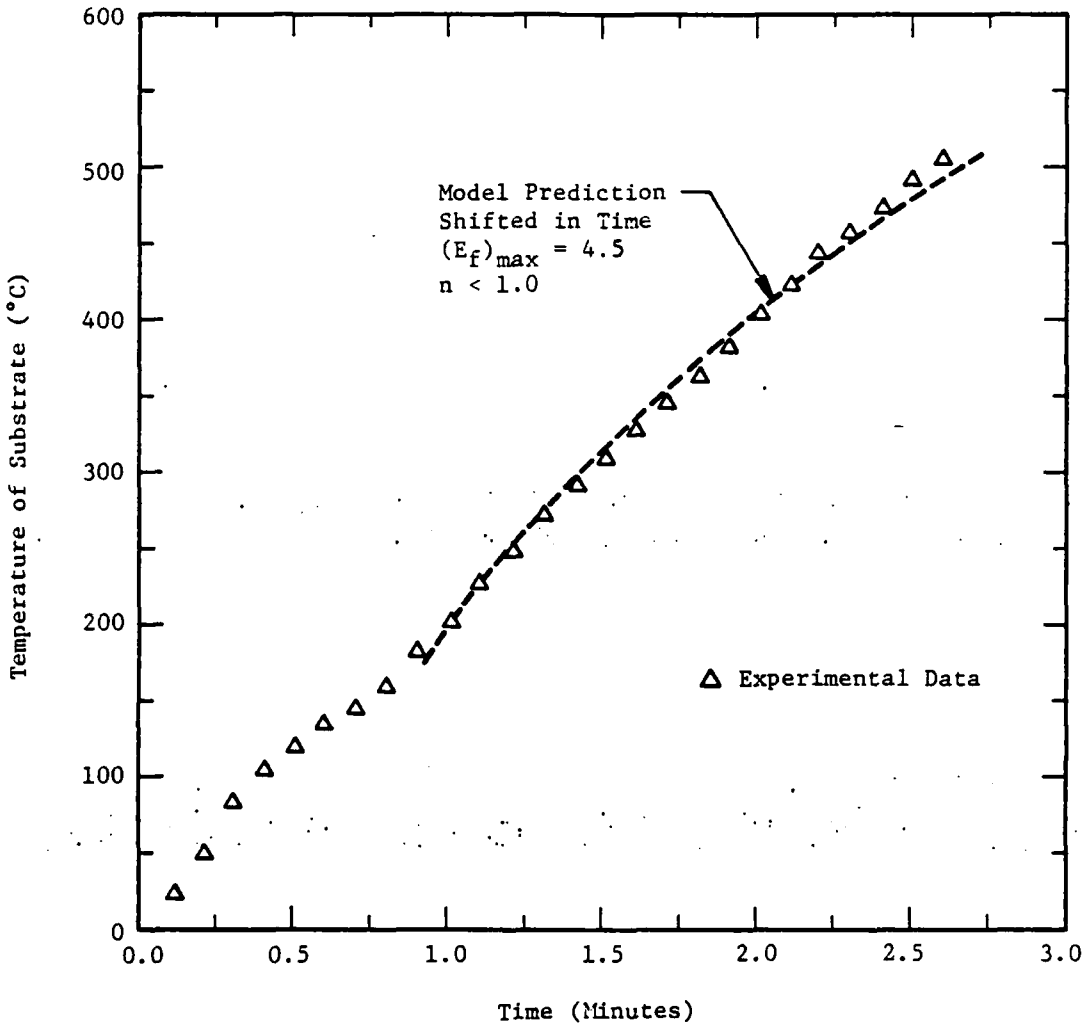

Figure 8-6. Comparison of Late Time Heating Rate of Substrate With Model Predcitions

9.0 CONCLUSIONS

A thermodynamic heat transfer model has been formulated for intumescent systems. This model includes mass loss and expansion of the coating in computing the temperature history of a metal substrate. It should be pointed out that the temperature-time history of the substrate is a function of the heat flux applied at the surface of the coating and the chemistry and physics within the intumescing material. Experimental data exists only for the substrate. To compare the model's predictions with experimental data requires the application of a heat flux at the boundary and computing the heat transfer to the substrate. For the computer calculations presented in the previous section, approximately 18,000 time increments (cycles) were required for each computer solution. If the physics is not modeled correctly, substantial errors can be expected since an error would be "propagated" from the surface to the substrate, accumulating in time. The effects of several parameters have been shown. These parameters are describing, in a sense, something about the physics and chemistry of the intumescing and heat transfer processes.

There exist uncertainties in the thermal conductivities of the virgin and char states, though the model computations would seem to indicate that we have reasonable estimates. The actual transition of k_v to k_c has been assumed to be a function of the density change. Figure 8-4 showed that there is some dependence in the heating rate for different values of the exponent in Equation (B-54), but alternate forms of "transition" functions could be explored.

Thermodynamic data are known only to 600°C, whereas, the mass loss data are known as a function of temperature to 830°C. But, the temperatures present in the fire environment will cause the intumescent material to reach temperatures in excess of 900°C to 1000°C. Data should be obtained for these higher temperatures.

The major assumption in the model is the assumed form of the expansion law. Currently, the expansion law states that the expansion depends only upon

the change in mass relative to the total change, or in a more general sense, is dependent only on the mass loss:

$$E_f = E_f\left(\frac{\Delta m}{m_o}\right)$$

More generally, the expansion factor probably is a function of not only the mass loss, but the rate of mass loss, and the temperature:

$$E_f = E_f\left(\frac{\Delta m}{m_o},\ \dot{m},\ T\right)$$

Since the foaming and intumescence of the coating depends upon the generation of gases to push the material out, it stands to reason that the rate of vapor or gas generation would control the expansion process. Also, the material must be fluid enough (or soft enough) to be pushed or expanded, which results in the temperature dependence. The dependence of the model on alternate forms of the expansion factor should be investigated. Alternate, and perhaps more realistic forms, for the expansion law could account for the discrepancy in the model's predictions and the experimental data. For example, it has already been indicated from exercising the model that the expansion should occur early in the mass loss process. Perhaps the expansion should all occur over a narrow temperature range (which would correspond to a small portion of the mass loss curve). Experimental observations have shown that very thick coatings do not expand to the same extent as thinner applications. A temperature and rate of mass loss dependence would imply that the temperature gradient within the intumescing material could be important in the expansion process.

An analytic model for heat transfer through an intumescing system has been presented. It has been shown that it can predict features observable in experiments, and explain the physical/chemical processes causing these features. The model has some shortcomings, but areas of improvement have been

delineated. As the model continues to develop, it will quantify our understanding of certain features of intumescing systems, and perhaps become a useful, predictive tool for formulating new or improved intumescent coatings.

This Page Intentionally Left Blank

10.0 REFERENCES

1. McQuaide, P. B., "The History and Goals of the Weapon Cook-Off Improvement Program," Pacific Missile Test Center, Point Mugu, California, May 1980.

2. Pulley, D. F., "Intumescent Coatings," Symposium on Corrosion Control by Coatings, Lehigh University, Bethlehem, Pennsylvania, November 15, 1978.

3. Vandersall, H. L., "Intumescent Coating Systems, Their Development and Chemistry," Journal of Fire and Flammability, Volume 2, April 1971, pp. 97-140.

4. Clarke, K. J., Shimizu, A. B., Suchsland, K. E., and Moyer, C. B., "Analytical Modeling of Intumescent Coating Thermal Protection System in a JP-5 Fuel Fire Environment," Aerotherm Final Report No. 74-101, Aerotherm Division, Acurex Corporation, Mountain View, California, June 1974.

5. Pulley, D. F., "Intumescent Coatings," in Encyclopedia of Materials Science and Engineering, Michael Bever, Editor-in-Chief, Pergamon Press Limited, Oxford, England, (To Be Published).

AD-A132 586 INTUMESCENT REACTION MECHANISMS: AN ANALYTIC MODEL(U) 2/2
SOUTHWEST RESEARCH INST SAN ANTONIO TX
C E ANDERSON ET AL. MAY 83 NADC-82211-60
UNCLASSIFIED N62269-81-C-0246 F/G 19/1 NL

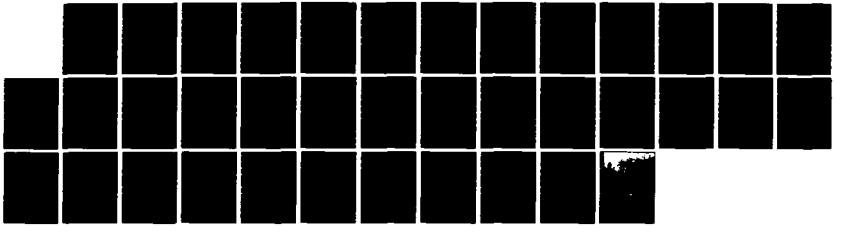

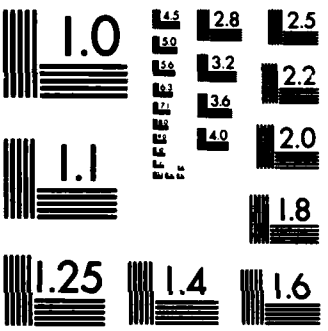

This Page Intentionally Left Blank

APPENDIX A

DERIVATION OF CONTINUITY AND ENERGY EQUATIONS

This Page Intentionally Left Blank

A.1 Continuity Equations

The density of the intumescent system decreases due to expansion and the loss of mass from pyrolysis. Figure A-1 depicts a region with thickness δx and cross-sectional area A. Let the mass in the region be characterized by a mass density, ρ. The rate of change of solid (bulk) mass contained in the region, $\partial(\rho\ \delta x\ A)/\partial t$, must equal the net mass flow across the boundaries of the closed region. The mass flow into the region is given by $\rho(x,t)\cdot v(x,t)\cdot A$ where $\rho(x,t)$ is the bulk density and $v(x,t)$ is its velocity at the coordinate position, x. The mass flow out of the region is given by $-\rho(x+\delta x,t)\cdot v(x+\delta x,t)\cdot A$ where the minus sign denotes mass leaving the region. Note that the density and velocity are computed at the coordinate position of the second boundary, $x+\delta x$. If the temperature is high enough, pyrolysis occurs and gas is generated. This gas generation is at the expense of the mass in the bulk material and is designated by $-\dot{\Gamma}_g\ [T(x)]\ \delta x\ A$. $\dot{\Gamma}_g\ \delta x\ A$ is the rate, then, at which gaseous mass is generated, and it is shown to be an explicit function of the temperature, T.

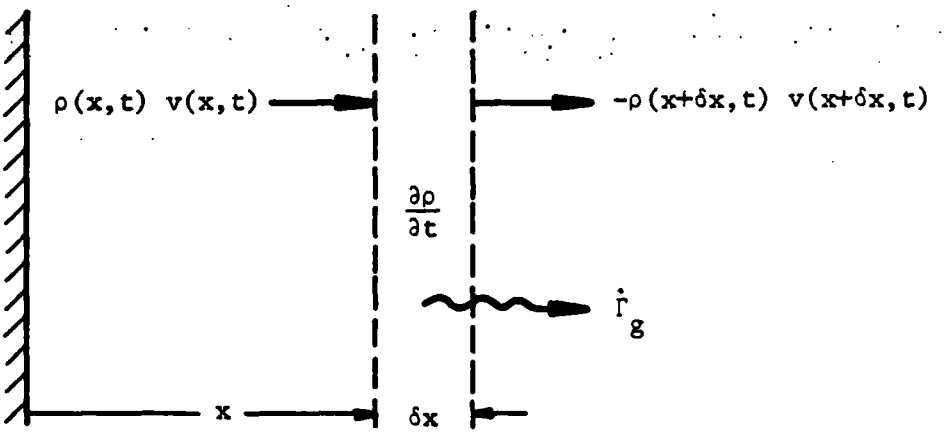

Figure A-1. Mass Conservation

Thus, conservation of mass implies:

$$\frac{\partial}{\partial t} (\rho \, \delta x \, A) = \rho(x,t) \, v(x,t) \, A -$$

$$\rho(x+\delta x,t) \, v(x+\delta x,t) \, A - \dot{\Gamma}_g \, [T(x)] \, \delta x \, A \qquad \text{(A-1)}$$

The second term on the right-hand side of Equation (A-1) can be expanded:

$$\rho(x+\delta x) \, v(x+\delta x) \, A =$$

$$\left[\rho(x,t) + \frac{\partial \rho(x,t)}{\partial x} \delta x + \ldots\right] \left[v(x,t) + \frac{\partial v(x,t)}{\partial x} \delta x + \ldots\right] A =$$

$$\rho(x,t) \, v(x,t) \, A + \rho(x,t) \frac{\partial v(x,t)}{\partial x} \delta x \, A +$$

$$v(x,t) \frac{\partial \rho(x,t)}{\partial x} \delta x \, A + 0\left[(\delta x)^2\right] \qquad \text{(A-2)}$$

Thus, Equation (A-1) becomes, as the infinitesimal element $\delta x \to 0$:

$$\frac{\partial \rho}{\partial t} + v \frac{\partial \rho}{\partial x} + \rho \frac{\partial v}{\partial x} = - \dot{\Gamma}_g \, [T(x)] \qquad \text{(A-3)}$$

A similar equation can be written for the change in the mass of the gas due to outgassing during pyrolysis:

$$\frac{\partial \rho_g}{\partial t} + v \frac{\partial \rho_g}{\partial x} + \rho_g \frac{\partial v}{\partial x} = + \dot{\Gamma}_g \, [T(x)] \qquad \text{(A-4)}$$

where the subscript g denotes gas. The action of pyrolysis is the source for changing the gas density. It was assumed in the derivation of Equation (A-4) that the gas velocity, v_g, is equivalent to the bulk velocity, v. It is the gas which "pushes" against the molten and/or pliable viscous material causing the coating to intumesce. Thus, it is reasonable that the two velocities are

approximately equal. It is true that the gas eventually diffuses to the surface as the expanding coating begins to harden and form the char residue, but little error should be incurred by the approximation of the two velocities being equal.

A.2 Energy Equation

The energy equation is derived similarly to the continuity equations. Figure A-2 depicts a fixed region. The rate of change of energy within the region equals the net energy flow into the region. The change in energy is given by $\partial(\rho h\ \delta x\ A)/\partial t$, where h is the specific enthalpy. This change in energy results from heat conduction, and the mass flow of energy (both bulk and gaseous material) across the boundaries:

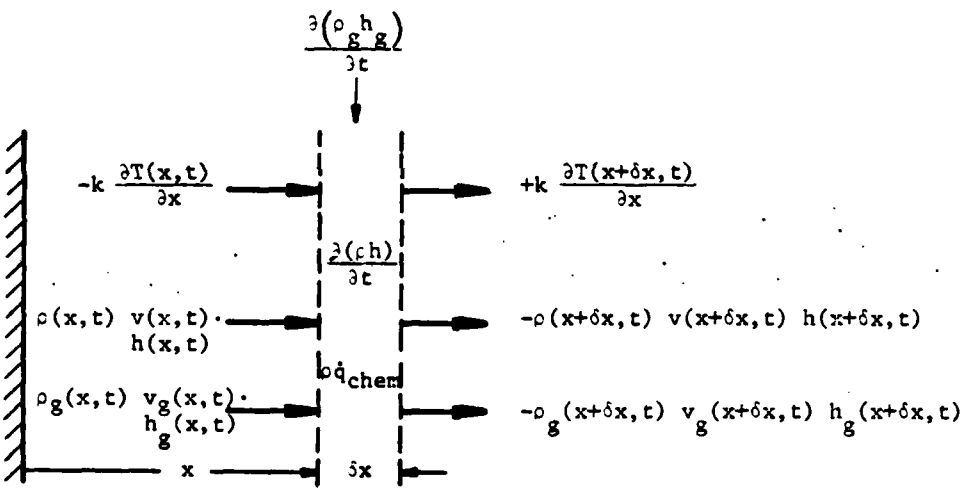

Figure A-2. Energy Conservation

$$\frac{\partial(\rho_g h_g\ \delta x)}{\partial t} + \frac{\partial(\rho h\ \delta x)}{\partial t} + \rho\dot{q}_{chem} = -k\frac{\partial T}{\partial x}\bigg|_{x,t} + \rho vh\bigg|_{x,t} +$$

$$\rho_g vh_g\bigg|_{x,t} + k\frac{\partial T}{\partial x}\bigg|_{x+\delta x,t} - \rho vh\bigg|_{x+\delta x,t} - \rho_g vh_g\bigg|_{x+\delta x,t} \qquad \text{(A-5)}$$

where the cross-sectional area has been divided out of each term. Performing the Taylor series expansion about (x,t), cancelling terms, and letting the infinitesimal thickness δx go to zero results in:

$$\frac{\partial\left(\rho_g h_g\right)}{\partial t} + \frac{\partial(\rho h)}{\partial t} + \rho \dot{q}_{chem} = \frac{\partial}{\partial x} k \frac{\partial T}{\partial x} - \frac{\partial}{\partial x}(\rho v h) - \frac{\partial}{\partial x}\left(\rho_g v h_g\right) \qquad \text{(A-6)}$$

The terms on the left-hand side of Equation (A-6) can be expanded:

$$\frac{\partial\left(\rho_g h_g\right)}{\partial t} + \frac{\partial(\rho h)}{\partial t} = h_g \frac{\partial \rho_g}{\partial t} + \rho_g \frac{\partial h_g}{\partial t} + h \frac{\partial \rho}{\partial t} + \rho \frac{\partial h}{\partial t} \qquad \text{(A-7)}$$

Likewise, the last two terms on the right-hand side can be expanded:

$$\frac{\partial(\rho v h)}{\partial x} = h \frac{\partial(\rho v)}{\partial x} + \rho v \frac{\partial h}{\partial x} \qquad \text{(A-8)}$$

$$\frac{\partial\left(\rho_g v h_g\right)}{\partial x} = h_g \frac{\partial\left(\rho_g v\right)}{\partial x} + \rho_g v \frac{\partial h_g}{\partial x} \qquad \text{(A-9)}$$

Inserting Equations (A-7) through (A-9) into Equation (A-6), and utilizing the mass conservation equations, Equations (A-3) and (A-4), yields:

$$\rho_g \frac{\partial h_g}{\partial t} + \rho \frac{\partial h}{\partial t} =$$

$$\frac{\partial}{\partial x} k \frac{\partial T}{\partial x} - \left(h_g - h\right) \dot{r}_g - v\rho \frac{\partial h}{\partial x} - v\rho_g \frac{\partial h_g}{\partial x} - \rho \dot{q}_{chem} \qquad \text{(A-10)}$$

We now make use of a thermodynamic identity for enthalpy:

$$dh = C_p\, dT + V\cancelto{0}{dP} \qquad \text{(A-11)}$$

where C_p is the specific heat capacity at constant pressure, T is the temperature, V is the specific volume, and P is the pressure. The change in pressure, dP, is negligible in comparison to the changes in temperature in the intumescent system. Also, the gas temperature, T_g, can be taken to be equal approximately to the bulk temperature since (1) phase transitions occur at constant temperature, and (2) if the gas generated in the interior moves "slow enough" to the surface, it will have essentially the same temperature as the bulk material. Thus, Equation (A-10) becomes, after insertion of Equation (A-11),:

$$\left[\rho C_p + \rho_g \left(C_p\right)_g\right] \frac{\partial T}{\partial t} = \frac{\partial}{\partial x} k \frac{\partial T}{\partial x} -$$

$$\left(h_g - h\right) \dot{\Gamma}_g - v \left[\rho C_p + \rho_g \left(C_p\right)_g\right] \frac{\partial T}{\partial x} - \rho \dot{q}_{chem} \qquad \text{(A-12)}$$

This Page Intentionally Left Blank

APPENDIX B

COMPUTATIONAL ALGORITHMS

B.1 Discretizing the Differential Equations

To solve numerically the differential equations which apply at all locations within the intumescent coating, the coating material is divided into increments. Because the model is one-dimensional, each increment can be represented by a grid point. The differential equations are then written as difference equations and applied at each of the grid points. Thus, each of the variables, e.g., T, ρ, and v, is computed at each of the grid points.

The overall approach is to move forward in time by computing all the variables at a new time step in terms of known values from the previous time step, and values already computed at the current time step. This explicit formulation, as it is called, is straightforward, but the time step must be within certain bounds for the numerical procedure to remain stable.

B.2 Logic Flow

The computer program consists of a main program, called PAINT, which controls the flow of the numerical procedure by calling subroutines. Each subroutine generally performs one specific computational procedure. Figure B-1 presents the overall logic flow of PAINT. The subroutines called from PAINT may in turn call a series of subroutines, each performing their own specific computational task. Figure B-2 presents subroutine READ with the list of input values required by the program. This subroutine also performs various initialization procedures.

The subroutine which computes the time step (or increment) is divided into two completely separate portions with their own entry points, TIMSTP (time step) and TIMCHK (time check), Figure B-3. A time step is computed from the requirements for numerical stability for the energy equation. This operation is performed in TIMSTP. The continuity equation also has an associated stability criterion. After computing the velocities and densities, the time step criterion is checked against the time step currently being used. If the

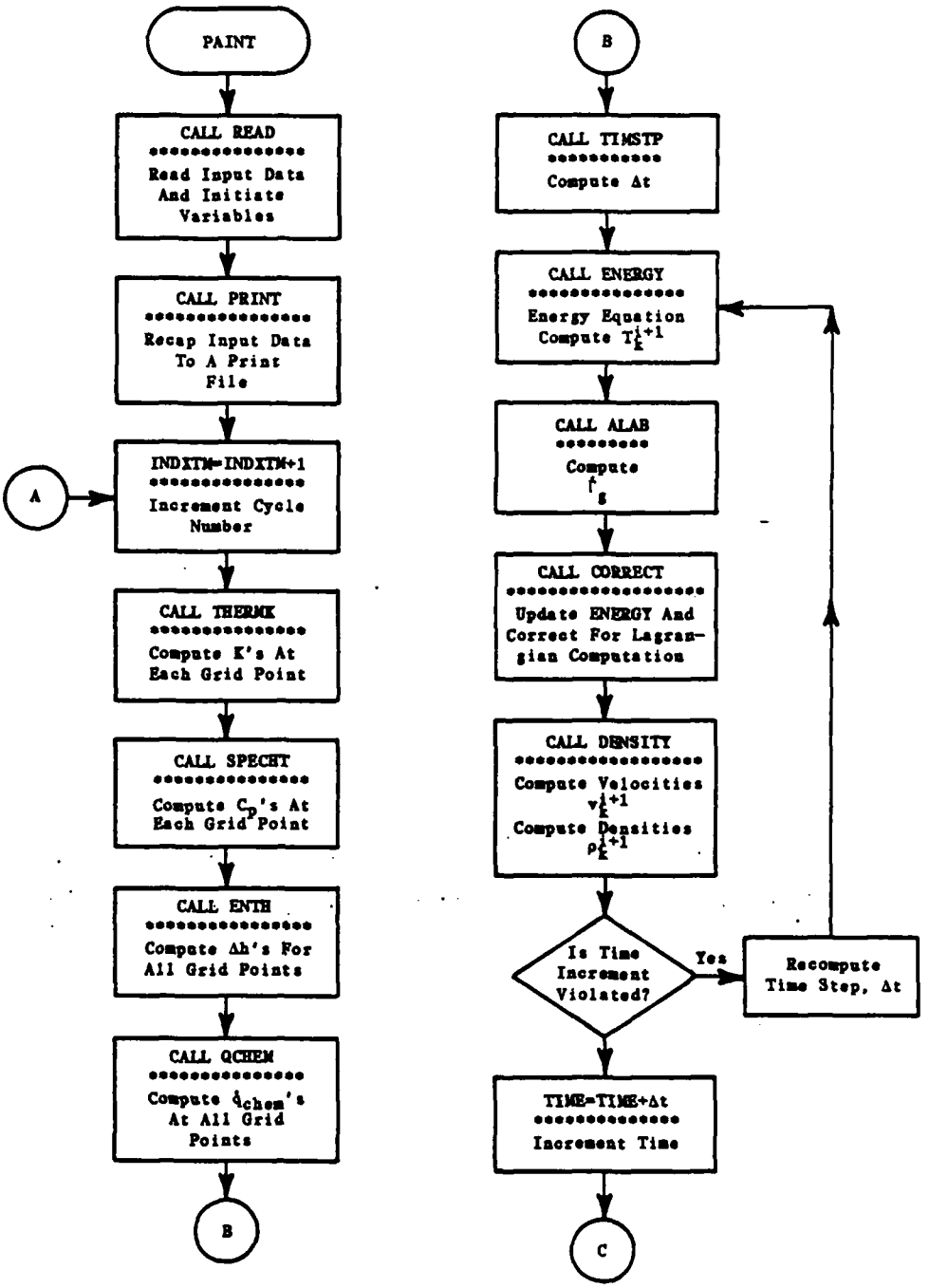

Figure B-1. Flow Diagram for Overall Logic Flow

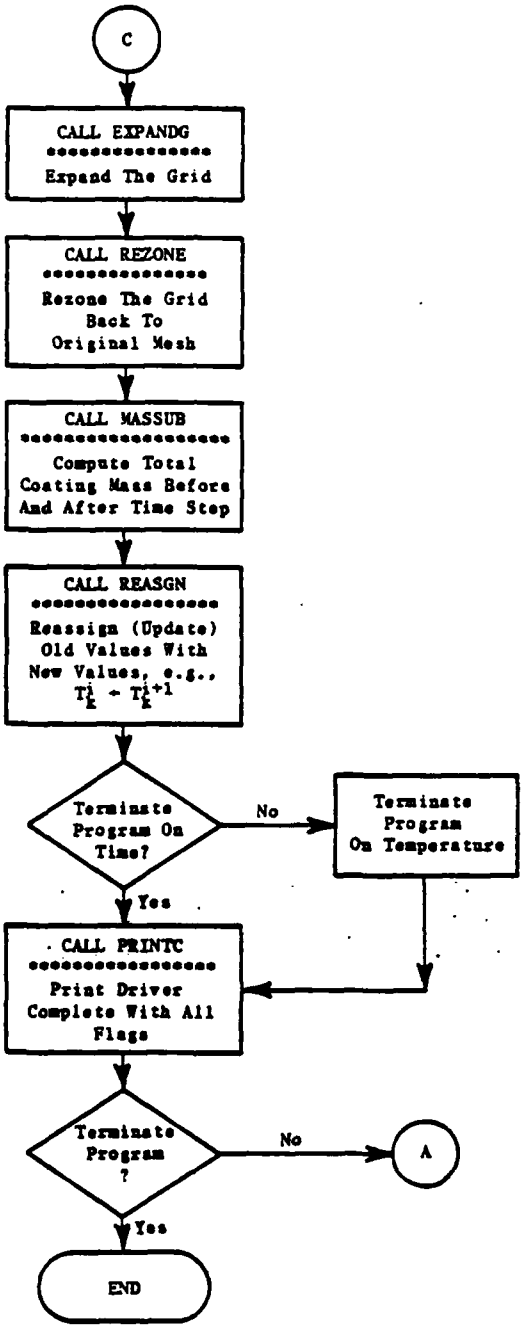

Figure B-1. Flow Diagram for Overall Logic Flow (Continued)

INTRVL		Number Of Computational Zones In The Coating
TSTPF:	t_f	Time Step Factor
TSTPG:	t_g	Growth Rate For Time Step
TSTPI:	t_r	Initial Reduction Of Time Step
EF:	ε_f	Flame Emissivity
ES:	ε_s	Surface Emissivity
TF:	T_f	Fire Temperature (°C)
TINIT:	T_o	Initial Temperature (°C)
RN		Exponent In Expansion Factor
MLOSS0:	m_f/m_o	Ratio Of Final To Initial Mass Of Formulation
THICK		Thickness Of The Paint (cm)
EFMAX:	$(E_f)_{max}$	Maximum Expansion
RHOSTL		Density Of Steel Substrate (gm/cm^3)
THSTL		Thickness Of Steel Substrate (cm)
H		Convective Heat Transfer Coefficient (cal/cm^2-s-°C)
TK(1):	k_o	Thermal Conductivity Of Virgin Coating (cal/cm-s-°C)
TK(2):	k_c	Thermal Conductivity Of Char (cal/cm-s-°C)
ETK:	q	Exponent In Thermal Conductivity Expression
NOMAT		Number Of Materials In Computational Formulation
MATIDX(I), I=1,NOMAT		Material Code (i.e., Designator)
		1 Polysulfide
		2 DMP-30
		3 EPON 828 Resin
		4 Borax
		5 Glass
		6 Part A
		7 Part B
		8 Part A+B
CONC(I), I=1,NOMAT		Material Concentrations (By Mass)

Figure B-2. Input Values for Subroutine READ

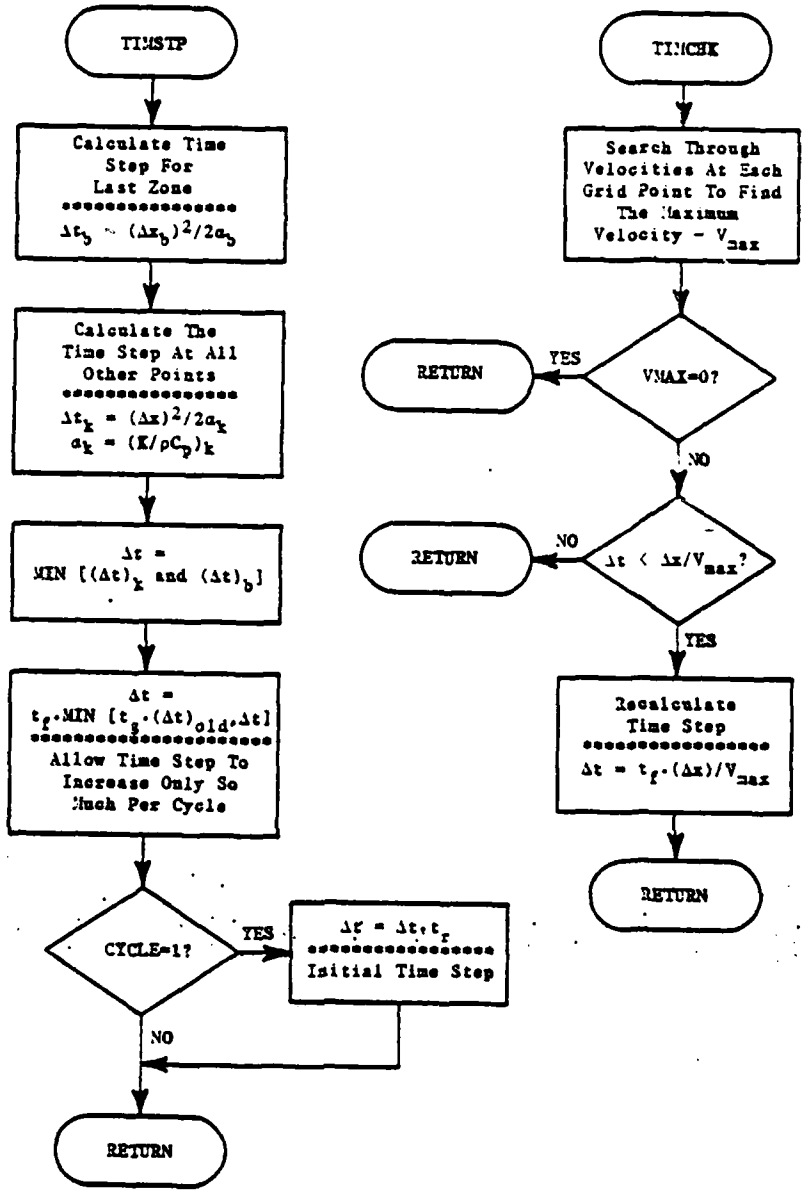

Figure B-3. Flow Diagram for Time Step Determination and Stability Check

stability criterion is violated, the code corrects the time step and recomputes temperatures, etc., with the adjusted time step.

Figure B-4 presents the logic flow of the energy equation for computing the temperatures throughout the computational grid. Also displayed in Figure B-4 is the subroutine CORRECT which is called after the amount of outgassing is computed. This subroutine prepares the energy equation for Lagrangian computation by subtracting out the convective term. Also, the subroutine updates the pyrolysis term with the information for the current time step.

Figure B-5 depicts the logic flow for the continuity equation, which computes the velocities and densities at the grid points. With the velocities known, the expansion of the grid is computed.

After expansion of the grid, it is rezoned back to the original mesh geometry. The logic flow for rezoning is displayed in Figure B-6. Upon completion of rezoning, all variables are updated and the procedure is started over to compute the variables at the next time step.

B.3 Difference Equations and Computational Procedures

B.3.1 Introduction

The difference equations will be presented and briefly discussed since some unique features are present in the numerical formulation. The equations are generally discussed in the order in which they are computed within the program. The following convention will be used: a subscript k will refer to the k^{th} grid point and a superscript i will refer to the time step, e.g., T_k^i is the temperature at the k^{th} grid point at the time, given by t^i, found by summing the time increments from t=0:

$$t^i = \sum_{i=0}^{i} (\Delta t)^i \qquad \text{(B-1)}$$

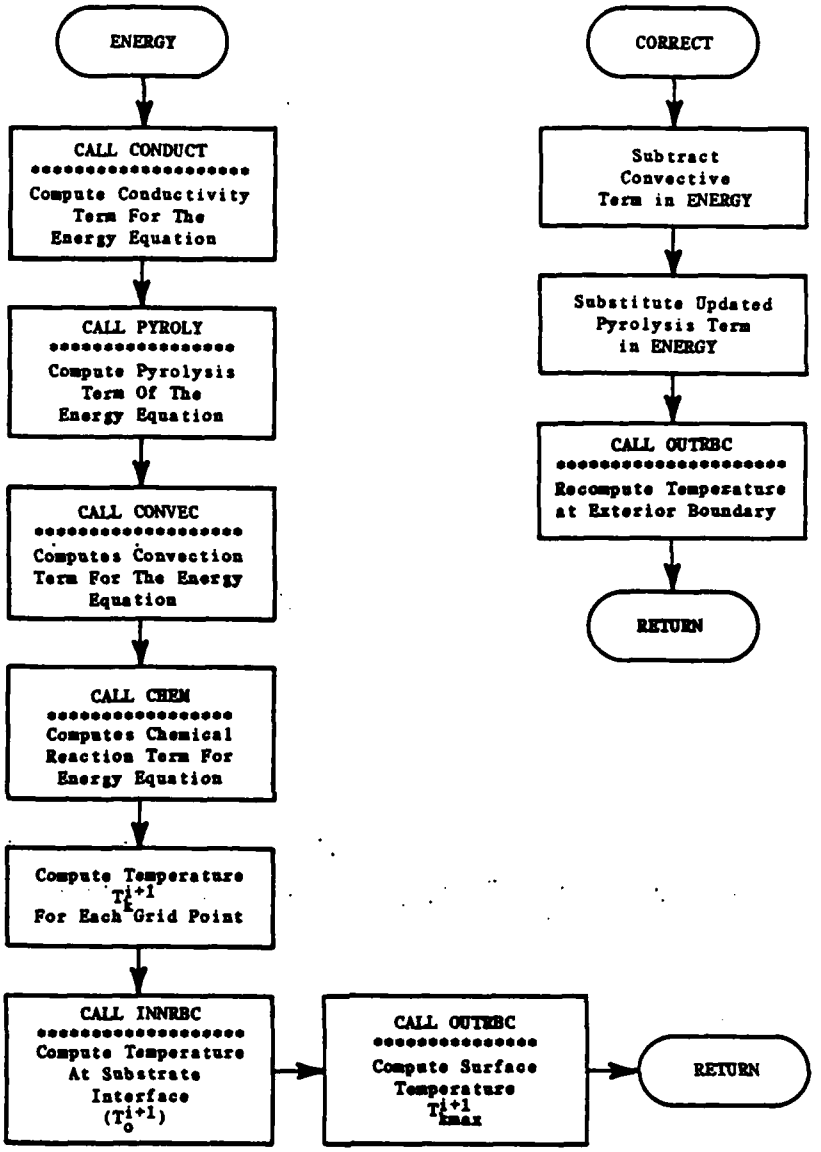

Figure B-4. Flow Diagram for Subroutine ENERGY

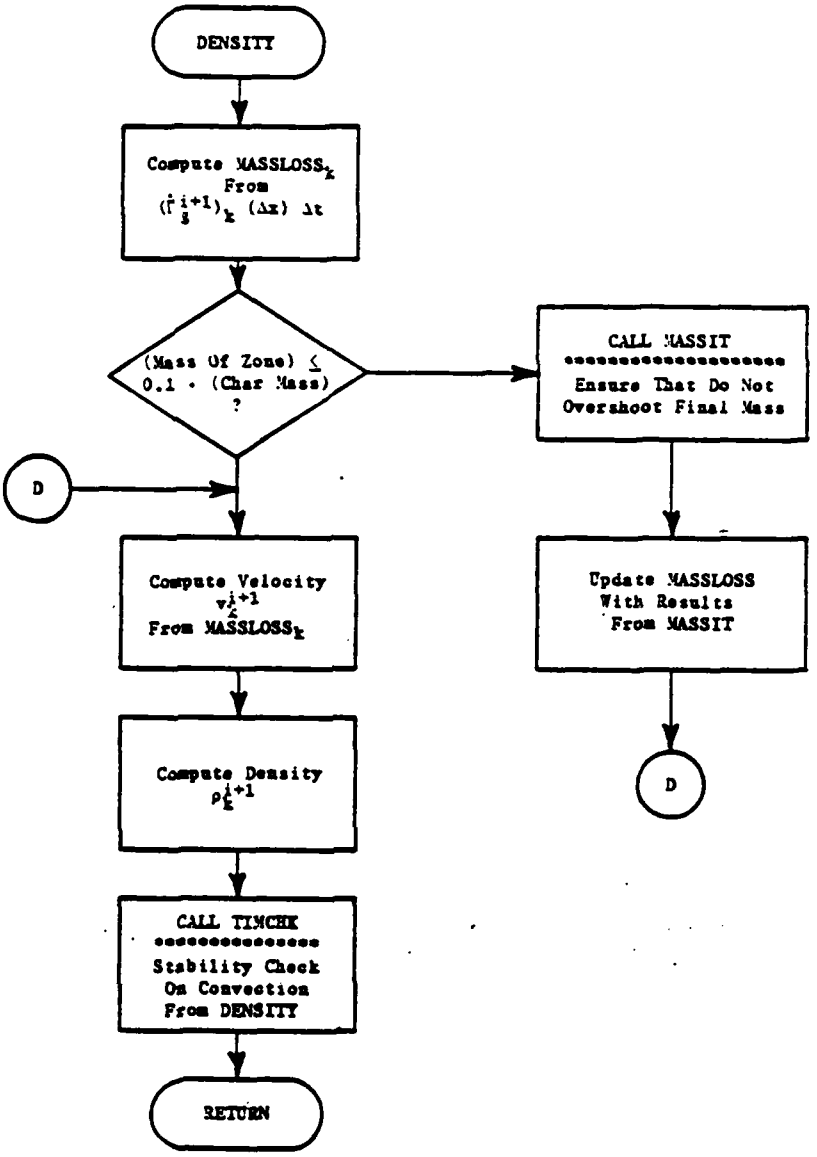

Figure B-5. Flow Diagram for Subroutine DENSITY

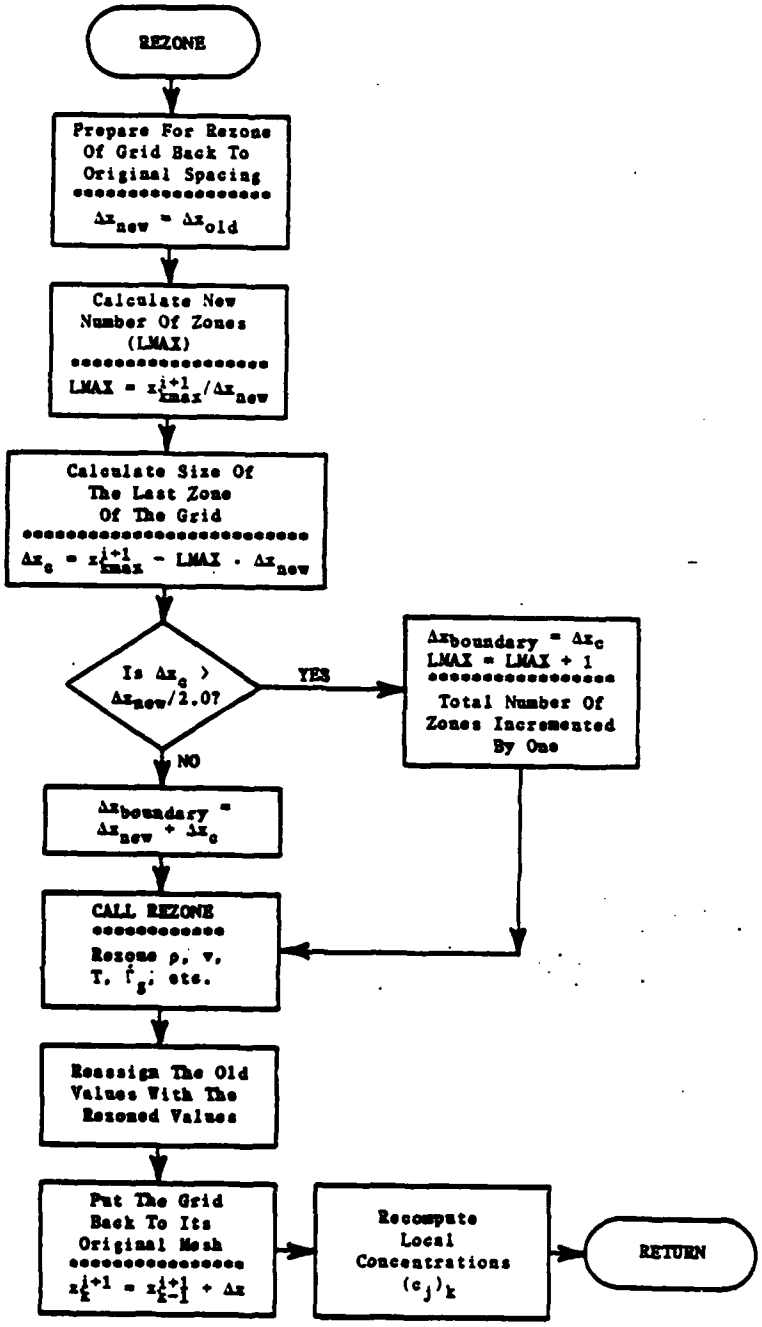

Figure B-6. Flow Diagram for Subroutine REZONE

The derivatives are replaced by differences, e.g.,:

$$\frac{\partial T}{\partial x} \rightarrow \frac{\Delta T}{\Delta x} \tag{B-2}$$

$$\frac{\partial T}{\partial t} \rightarrow \frac{\Delta T}{\Delta t} \tag{B-3}$$

$$\Delta x = x_k - x_{k-1} \tag{B-4}$$

$$\Delta t = t^{i+1} - t^i \tag{B-5}$$

In general, all the zone sizes are equal except for the zone at the boundary which varies in size. This zone, where explicitly necessary, will be designated as $\Delta x_b = x_{kmax} - x_{kmax-1}$.

B.3.2 Energy Equation and Its Boundary Conditions

The energy equation consists of five terms. Each of these terms will be considered separately.

a. Sensible Heat

$$\rho C_p \frac{\partial T}{\partial t} \rightarrow \rho_k^i \left(C_p\right)_k \frac{T_k^{i+1} - T_k^i}{\Delta t} \tag{B-6}$$

b. Conduction

The difference form for the conduction term can best be visualized by referencing Figure 7-1. First, the spatial derivatives between the k+1 and k, and k and k-1 points are considered:

$$K \frac{\partial T}{\partial x}\bigg|_{k+1/2} \rightarrow \frac{\left(K_{k+1} + K_k\right)}{2} \frac{\left(T_{k+1}^i - T_k^i\right)}{(\Delta x)_2} \tag{B-7}$$

$$K \left.\frac{\partial T}{\partial x}\right|_{k-1/2} \rightarrow \frac{\left(K_k + K_{k-1}\right)}{2} \frac{\left(T_k^i - T_{k-1}^i\right)}{(\Delta x)_1} \tag{B-8}$$

Then, the derivative between these two points is taken:

$$\frac{\partial}{\partial x} K \frac{\partial T}{\partial x} \rightarrow \frac{K \left.\frac{\partial T}{\partial x}\right|_{k+1/2} - K \left.\frac{\partial T}{\partial x}\right|_{k-1/2}}{1/2 \left[(\Delta x)_1 + (\Delta x)_2\right]} \tag{B-9}$$

The energy transported by conduction, E_1, is thus given by:

$$E_1 = \left\{ \frac{\left(K_{k+1} + K_k\right)}{2} \frac{T_{k+1}^i}{(\Delta x)_2} + \left[\frac{\left(K_{k+1} + K_k\right)}{2\,(\Delta x)_2} + \frac{\left(K_k + K_{k-1}\right)}{2\,(\Delta x)_1} \right] T_k^i + \frac{\left(K_k + K_{k-1}\right)}{2} \frac{T_{k-1}^i}{(\Delta x)_1} \right\} \Bigg/ \left[\frac{(\Delta x)_1 + (\Delta x)_2}{2} \right] \tag{B-10}$$

Except at the (kmax-1) grid point, $(\Delta x)_1 = (\Delta x)_2 = \Delta x$ which simplifies Equation (B-9). At the (kmax-1) grid point, $(\Delta x)_2 = \Delta x_b$ and $(\Delta x)_1 = \Delta x$.

c. Pyrolysis

$$E_2 = h\,\dot{\Gamma}_g \rightarrow (h)_k \left(\dot{\Gamma}_g\right)_k^i \tag{B-11}$$

d. Convection

$$E_3 = -v\rho C_p \frac{\partial T}{\partial x} \rightarrow -v_k^i\, \rho_k^i \left(C_p\right)_k \frac{\left(T_{k+1}^i - T_k^i\right)}{\Delta x} \tag{B-12}$$

e. Chemical Energy

$$E_4 = -\rho \dot{q}_{chem} \rightarrow -\rho_k^i \left(\dot{q}_{chem}\right)_k \tag{B-13}$$

f. Computation of Temperature

It should be noted that C_p, h, $\dot{q}_{chem}$, and $\dot{\Gamma}_g$ all depend upon the temperature and are found in tables, or in the case of $\dot{\Gamma}_g$, by an analytic expression. The temperature at the new time step can now be determined in terms of quantities from the previous time step:

$$T_k^{i+1} = T_k^i + \frac{\Delta t}{\rho_k^i \left(C_p\right)_k} \left[E_1 + E_2 + E_3 + E_4\right] \tag{B-14}$$

g. Outer Boundary Condition

The condition at the boundary is given by Equation (3-10) but modified to incorporate heat absorption/generation from phase changes, convection, and chemical reactions. Equation (3-10) is the true boundary condition to the differential equation, but we shall account for these other heat terms because of the finite size of the grid. (We shall ignore heat capacity effects in the boundary condition because of its detrimental influence on the computational time step.) Equation (3-10) then becomes:

$$K_{s-1} \frac{\left(T_s - T_{s-1}\right)}{\Delta x_b} - \left(E_2 + E_3 + E_4\right)_{s-1} \Delta x_b = \dot{Q} \tag{B-15}$$

where:

$$T_s = T_{kmax}^{i+1} \tag{B-16}$$

$$T_{s-1} = T_{kmax-1}^{i+1} \tag{B-17}$$

$$\dot{Q} = H\left(T_F - T_s\right) + \varepsilon_s \sigma \left(\varepsilon_F T_F^4 - T_s^4\right) \tag{B-18}$$

Notice that in the limit of $\Delta x_b \to 0$, the second term in Equation (B-15) goes to zero and Equation (B-15) reduces to Equation (3-10).

This is a nonlinear equation in the unknown T_s. The procedure to find T_s is to compute a correction δT_s and then use:

$$T_s^{new} = T_s^{old} + \delta T_s \tag{B-19}$$

to compute a new correction. This procedure is repeated until δT_s reaches some reasonably small value:

$$\delta T_s = \left[\frac{-K_{s-1}}{\Delta x_b} \left(T_s - T_{s-1} \right) + \dot{Q} + \left(E_2 + E_3 + E_4 \right)_{s-1} \Delta x_b \right] \Bigg/ \left[\frac{K_{s-1}}{\Delta x_b} + H + 4 \varepsilon_s \varepsilon_F \sigma T_s^3 \right] \tag{B-20}$$

h. Inner Boundary Condition

The inner boundary condition, Equation (3-13), has a similar modification to account for energy absorption/generation because of the finite width of the zone:

$$\left[\left(\rho C_p \tau \right)_{steel} + \left(\rho C_p \Delta x \right)_{coating} \right] \frac{\Delta T}{\Delta t} = K_0 \frac{\Delta T}{\Delta x} + \left(E_2 + E_3 + E_4 \right)_0 (\Delta x) \tag{B-21}$$

Solving for T_0^{i+1}:

$$T_0^{i+1} = T_0^i + \frac{\Delta t \left[K_0 \left(T_1^i - T_0^i \right) \Big/ \Delta x + \left(E_2 + E_3 + E_4 \right)_0 \Delta x \right]}{\left[\left(\rho C_p \tau \right)_{steel} + \rho_0^i \left(C_p \right)_0 \Delta x \right]} \tag{B-22}$$

Again note that in the limit of $\Delta x \to 0$, Equation (B-22) reduces to Equation (3-13).

B.3.3 Mass Loss

The methodology for computing $d(m/m_o)/dT$ is given by Equation (5-20) where the temperature in Equation (5-20) is given for each zone, T_k^{i+1}. Equation (5-28) is used then to compute $(\dot{\Gamma}_g)_k^{i+1}$. The total mass lost for each constituent is also computed from Equations (5-18) and (5-19) so the local concentrations of each of the constituents, given by Equation (5-22), can be computed.

Because the Fourier series representation can "oscillate," and thus $d(m/m_o)/dT > 0$, a check is put into the algorithm to insure that mass is not added during a time step. The computational technique is general in that it will allow mass addition with a resultant decrease in total thickness (since the resultant boundary velocity will be negative). But this is non-physical. Thus, whenever Equation (5-20) predicts that $d(m/m_o)/dT$ is greater than zero, $d(m/m_o)/dT$ is redefined to be zero, i.e., no mass loss is allowed during that particular time step. However, this procedure could ultimately result in too much mass being subtracted, so another check is put into the code:

$$\frac{d\left(m/m_o\right)}{dT} = 0 \text{ if } \sum_{i=0}^{i} \left(\dot{\Gamma}_g\right)_k^i (\Delta t)^i \, \Delta x < \left[\left(\frac{m}{m_o}\right)_{\substack{\text{lost} \\ 0 \to T}}\right]_k \qquad \text{(B-23)}$$

where the right-hand side of the inequality is given by Equation (5-21).

B.3.4 Correct Energy Equation

Equation (B-14) is used to compute the temperatures at the fixed grid points. These temperatures are then used to compute the amount of outgassing. However, the material expands due to outgassing. Thus, the Eulerian computation for temperature must be corrected back to Lagrangian coordinates. This is easily accomplished since the convective term, Equation (B-12) is basically

the one term that distinguishes the two coordinate systems. In addition, the pyrolysis term is updated for the enthalpy change at the current time step. Hence, the temperature is redefined:

$$T_k^{i+1} \leftarrow T_k^{i+1} - \frac{\Delta t}{\rho_k^i \left(C_p\right)_k} \left[E_2 + E_3 - (h)_k \left(\dot{\Gamma}_g\right)_k^{i+1} \right] \tag{B-24}$$

where E_2 is given by Equation (B-11) and E_3 is given by Equation (B-12).

Equation (B-24) is modified appropriately [see Equation (B-22)] for the temperature of the substrate, T_o^{i+1}. The temperature at the surface is recomputed using the methodology of Section B.2.2(g), but modified to not include the convective term E_2, but using the updated pyrolysis term.

B.3.5 Expansion Factor

The expansion factor, Equation (3-6), is not difficult to calculate. The expansion factor essentially provides the Lagrangian description of the location of a material particle and that location depends upon the past history (i.e., the amount of material outgassed). The original mass in a zone $(m_o)_k$, the final or char mass $(m_c)_k$, and the current zone mass m_k are required for the computation. The mass lost in the k^{th} zone is given by:

$$\left(m_{loss}\right)_k = \left(m_o\right)_k - m_k \tag{B-25}$$

Hence, the expansion factor is given by:

$$\left(E_f\right)_k^{i+1} = 1 + \left[\left(E_f\right)_{max} - 1 \right] \left[\frac{\left(m_{loss}\right)_k^{i+1}}{\left(m_o\right)_k^i - m_c} \right]^n \tag{B-26}$$

Note that the original mass in a fixed zone changes with time $[(m_o)_k^i]$. Because of expansion, the original mass will be partitioned into several zones

at a later time. This tracking of masses is accomplished during the rezoning procedure.

In the local time coordinates, the system has already undergone a certain percentage of its total expansion. The local time step expansion factor is given by the ratio of the expansion factor due to the total mass loss at the current time step to the expansion factor computed from the previous time step:

$$\left[\left(E_f\right)_k^{i+1}\right]_{local} = \frac{\left(E_f\right)_k^{i+1}}{\left(E_f\right)_k^{i}} = \frac{1 + \left[\left(E_f\right)_{max} - 1\right]\left[\frac{\left(m_{loss}\right)_k^{i+1}}{\left(m_o\right)_k^{i} - m_c}\right]^n}{1 + \left[\left(E_f\right)_{max} - 1\right]\left[\frac{\left(m_{loss}\right)_k^{i}}{\left(m_o\right)_k^{i} - m_c}\right]^n} \qquad \text{(B-27)}$$

B.3.6 Continuity Equation

a. Determination of Velocity

The continuity equation, Equation (3-1), is solved in two steps. First, the velocity is computed from the mass loss. The local expansion factor, $[(E_f)_k^{i+1}]_{local}$ is given by Equation (B-27). Using rectangular quadrature for the integral in Equation (3-8), the velocity is calculated from:

$$v_k^{i+1} = \sum_{k=0}^{k} \left\{ \frac{\left\{ \left[\left(E_f\right)_k^{i+1}\right]_{local} - 1 \right\}}{\Delta t} \Delta x \right\} \qquad \text{(B-28)}$$

b. Computation of Density

Once the velocity has been determined, Equation (3-1) can be written as a difference equation:

$$\frac{\rho_k^{i+1} - \rho_k^i}{\Delta t} + \rho_k^{i+1} \frac{\left(v_{k+1}^{i+1} - v_k^{i+1}\right)}{\Delta x} = \left(\dot{\Gamma}_g\right)_k^{i+1} \qquad \text{(B-29)}$$

and thus, the density at the new time step is given by:

$$\rho_k^{i+1} = \left[\rho_k^i + \left(\dot{\Gamma}_g\right)_k^{i+1} \Delta t\right] \Big/ \left[1 + \frac{\Delta t}{\Delta x}\left(v_{k+1}^{i+1} - v_k^{i+1}\right)\right] \qquad \text{(B-30)}$$

Caution must be exercised, however, as the amount of mass in a zone approaches the terminal or char mass. Computationally, if the time step is too large, an excess of mass could be deleted from a zone. The procedure followed is discussed in the next subsection.

c. Mass Iterate

Because of the finite time step, an excess of mass could be deleted from a zone (because of outgassing) which would result in the density falling below the char density. The algorithm developed computes the mass loss necessary for the zone to reach its final or char state, taking into account that the zone will expand during outgassing (whenever the zonal mass is within 10 percent of the char mass):

$$\left(\Delta m_{loss}\right)_k^{i+1} = \rho_k^i \Delta x - \left[\left(E_f\right)_k^{i+1}\right]_{local} \rho_c \Delta x \qquad \text{(B-31)}$$

The mass loss computed from the TGA data is given by:

$$- \left(\dot{\Gamma}_g\right)_k^{i+1} \Delta t \, \Delta x \qquad \text{(B-32)}$$

This quantity is compared against the left-hand side of Equation (B-31). If Expression (B-32) is greater than Δm_{loss}, then $(\dot{\Gamma}_g)_k^{i+1}$ is reduced accordingly:

$$\left(\dot{\Gamma}_g\right)_k^{i+1} \quad \frac{\left(\Delta m_{loss}\right)_k^{i+1}}{(\Delta t)\ (\Delta x)} \text{ if } -\left(\dot{\Gamma}_g\right)_k^{i+1} \Delta t\ \Delta x > \left(\Delta m_{loss}\right)_k^{i+1} \tag{B-33}$$

This is the rate of density change due to outgassing of volatiles which is redefined by Equation (B-33).

To compute $(\Delta m_{loss})_k^{i+1}$, a correction δm is computed from:

$$\delta m_k = \frac{\rho_k^i \Delta x + \left(\Delta m_{loss}\right)_k^{i+1} - \left[\left(E_f\right)_k^{i+1}\right]_{local} \rho_c \Delta x}{-1 - \rho_c \Delta x \left\{\frac{n}{\left(m_{loss}\right)_k^{i+1}} \frac{\left[\left(E_f\right)_k^{i+1} - 1\right]}{\left(E_f\right)_k^i}\right\}} \tag{B-34}$$

where $[(E_f)_k^{i+1}]_{local}$ is given by Equation (B-27). Then $(\Delta m_{loss})_k^{i+1}$ is updated by:

$$\left(\Delta m_{loss}\right)_k^{i+1} \leftarrow \left(\Delta m_{loss}\right)_k^{i+1} + \delta m_k \tag{B-35}$$

This procedure is iterated until δm_k approaches "zero."

B.3.7 Movement of Grid Points

The velocity at each grid point has been computed by Equation (B-28). The material then expands according to the velocity field, and the expanded grid coordinates are given by:

$$x_k^{i+1} = x_k^i + v_k^{i+1} \Delta t \tag{B-36}$$

B.3.8 Rezoning

At the conclusion of the Lagrangian computations, the solution has been advanced in time with appropriate movement of the grid. The next step in the

procedure is to rezone or remesh the computation so that the mesh overlays that present at the start of the cycle. A geometric interpretation is employed coupled with conservation rules.

The first step is to decide whether to add a new zone. Zones are added in order to keep the zones from becoming too large as the system expands due to intumescence. The amount of grid expansion during the present time cycle is simply:

$$(\Delta x)_{expand} = x_{kmax}^{i+1} - (kmax)\cdot(\Delta x) \qquad \text{(B-37)}$$

So long as $(\Delta x)_{expand}$ is less than $\Delta x/2$, the last zone Δx_b is given by:

$$\Delta x_b = \Delta x + (\Delta x)_{expand} \qquad (\Delta x)_{expand} < \Delta x/2 \qquad \text{(B-38)}$$

However, if $(\Delta x)_{expand}$ is greater than or equal to $\Delta x/2$, then a new zone is added to the grid:

$$kmax \leftarrow kmax+1 \text{ if } (\Delta x)_{expand} \geq \Delta x/2 \qquad \text{(B-39)}$$

$$\Delta x_b = (\Delta x)_{expand} \qquad \text{(B-40)}$$

This procedure effectively requires that the last zone be between:

$$\frac{\Delta x}{2} < \Delta x_b < \frac{3\,\Delta x}{2} \qquad \text{(B-41)}$$

Once the number of zones of the new grid have been determined, the rezoning process begins. Referring to Figure B-7, the rezoning procedure defines the variable F_k at x_k (e.g., density, or temperature, etc.) in terms of the G_k's at y_k associated with the expanded grid. From Figure B-7, it can be seen that:

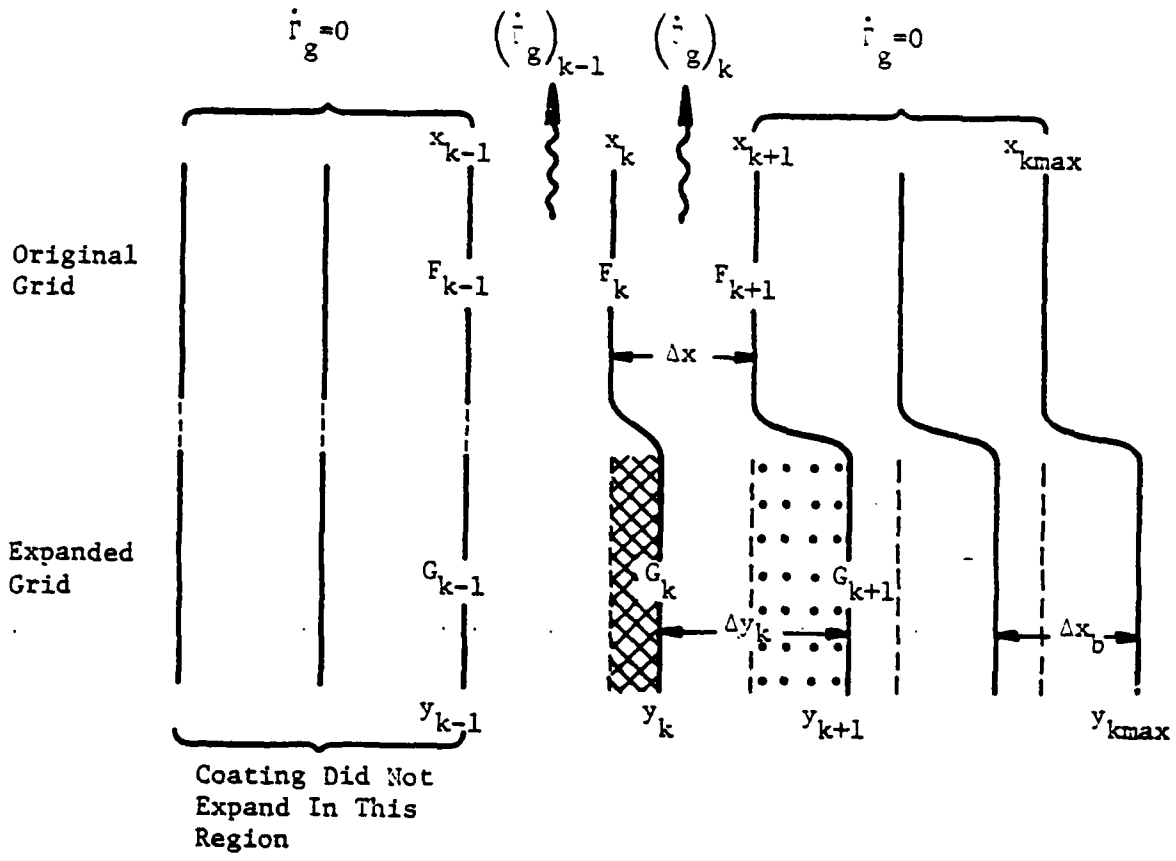

Figure B-7. Schematic of Rezoning Geometry

$$F_k \Delta x = G_k \Delta y_k + (\text{cross-hatch region}) - (\text{dotted region}) \qquad \text{(B-42)}$$

$$F_k = \left[G_k \left(y_{k+1} - y_k\right) + G_{k-1} \left(y_k - x_k\right) - G_k \left(y_{k+1} - x_{k+1}\right)\right] \Big/ \Delta x \qquad \text{(B-43)}$$

Expression (B-43) is representative of the general procedure. Other cases, for example where $x_k = y_k$ but $x_{k+1} < y_{k+1}$, are solved similarly.

Care must be exercised in rezoning some of the variables. Where a grid point variable represents the "condition" of the entire zone, such as density or velocity, the foregoing geometric interpretation is adequate. However, a

mass variable [such as $(m_o)_k$, $(m_c)_k$, etc.] is computed by integrating the density over the width of the zone. To rezone such a variable first requires transformation to a "differential" variable, e.g., $(m_o)_k/(y_{k+1} - y_k)$. After rezoning, the mass associated with the zone is found again by integrating the "differential" variable over the width of the zone: $(m_o)_k \Delta x$. Likewise, instead of rezoning the temperature, the specific energy, $C_p T$, is rezoned, and then the temperature recomputed.

B.3.9 Time Step (Stability Criteria)

The explicit formulation that has been developed is numerically stable so long as the time step, Δt, meets certain criteria. A time step is computed to insure stability of the energy equation. At interior grid points, the condition for stability is:

$$\Delta t_k \leq \frac{(\Delta x)^2}{2\,\alpha_k} \qquad \alpha_k = \left(\frac{K}{\rho\, C_p}\right)_k \tag{B-44}$$

where α_k depends upon the temperature. Thus, the zone with the largest α_k specifies the time step. The boundary zone, because of its different zone size, has a time step Δt_b associated with it:

$$\Delta t_b \leq \frac{\left(\rho\, C_p\right)_k \Delta x\, \Delta x_b}{2\,\bar{K}} \tag{B-45}$$

$$\bar{K} = \frac{\Delta x_b \left(K_{kmax-2} + K_{kmax-1}\right)/2 + \Delta x \left(K_{kmax} + K_{kmax-1}\right)/2}{\Delta x + \Delta x_b} \tag{B-46}$$

The time step is the minimum of these:

$$\Delta t^{i+1} = \text{MIN}\left[\Delta t_k, \Delta t_b\right] \tag{B-47}$$

To catch the sudden jump at t=0 (i.e., the heat flux is suddenly "turned on"), the first cycle time step is reduced by a factor t_r which is generally of the order of 0.01:

$$\Delta t^{o} = t_r \cdot \Delta t \tag{B-48}$$

The time step is then allowed to get larger in succeeding cycles but only at a prescribed growth rate, t_g. Thus, the time step for the computational cycle is taken as:

$$\Delta t^{i+1} = t_f \cdot \text{MIN}\left[t_g \cdot \Delta t^{i}, \Delta t^{i+1}\right] \tag{B-49}$$

where $0 < t_f < 1.0$.

The continuity equation also has a time step stability criteria:

$$\Delta t_c \leq \frac{\text{MIN}\left[\Delta x, \Delta x_b\right]}{v_{max}} \tag{B-50}$$

where v_{max} is the maximum velocity within the grid (i.e., the velocity of the boundary, $v_{max} = v_{kmax}$). After determining the velocities and densities, the program checks for consistency of the current time step [Equation (B-46)] to insure:

$$\Delta t_c \leq \Delta t \tag{B-51}$$

If this relationship is not satisfied, the program computes a new $\Delta t = t_f \cdot \Delta t_c$ and then recycles through the energy equation, etc.

B.3.10 Tabular Entries and Search Subroutines

The data as a function of temperature for enthalpy, specific heat, and chemical heat production have all been entered into the computer program as a subroutine called BLOCK DATA. The values for each of the individual constituents, Part A, Part B, and Part A+B, have been entered. Then each of the three thermodynamic functions are found for the appropriate temperature by a search routine which linearly interpolates between values (where applicable), i.e.,:

$$F = V_i + \left(T - T_i\right) \frac{\theta_{i+1} - \theta_i}{T_{i+1} - T_i} \qquad T_i \leq T < T_{i+1} \tag{B-52}$$

where θ_i and θ_{i+1} are the thermodynamic variables at the respective temperatures T_i and T_{i+1}, and F is the interpolated value ($\theta_i \leq F < \theta_{i+1}$) for the temperature T.

If the coating is assumed to be a composite of the sum of its constituents, then the thermodynamic quantity is $\bar{F}$, computed as a sum of the individual constituent's thermodynamic quantity, F_j, times its respective concentration, c_j, in the mixture:

$$\bar{F} = \sum_{j=1}^{J} c_j F_j \tag{B-53}$$

where there are J total constituents. The c_j's are a function of temperature and are determined by using Equation (5-22).

B.3.11 Thermal Conductivity

There is a thermal conductivity associated with the virgin material, K_o, and another values associated with the char, K_c. The program provides a smooth transition between these two values according to the density change:

$$f = \left[\frac{\rho_c}{\rho_o - \rho_c}\left(\frac{\rho_k}{\rho_c} - 1\right)\right]^q \tag{B-54}$$

$$K = f \cdot K_o + (1 - f) \cdot K_c \tag{B-55}$$

where the exponent q accounts for nonlinearities in the assumed relationship between ρ and k.

DISTRIBUTION LIST (Continued)

REPORT NO. NADC-82211-60

	No. of Copies
U. S. Polymeric, Inc. (D. Beckley), 700 East Dyer Road, Santa Ana, CA 92707	1
University of Dayton Research Institute (I. Salyer), 300 College Park Avenue, Dayton, OH 45469	1
Wright Aeronautical Laboratories (MLBE, MLSA), Wright-Patterson AFB, OH 45433	2

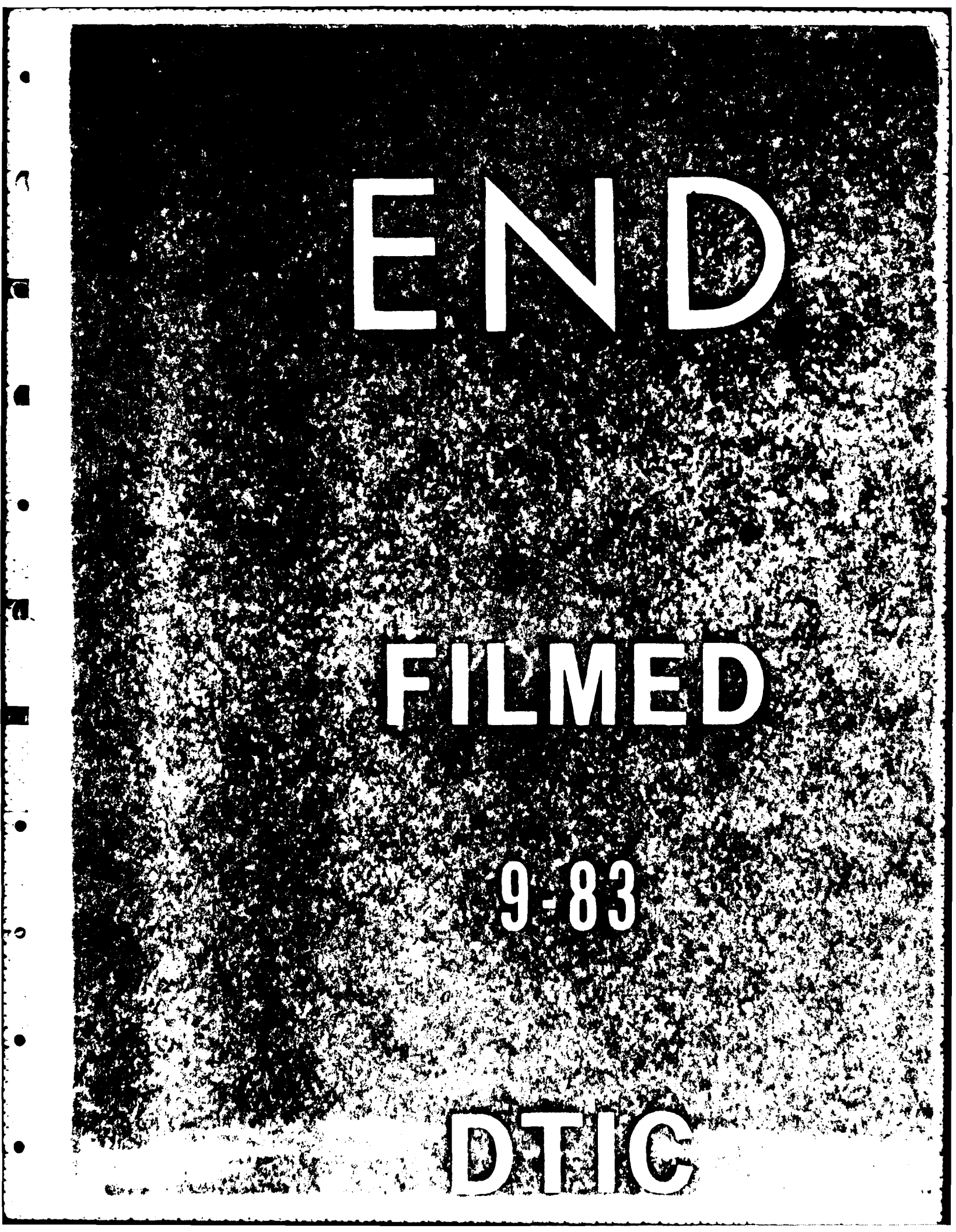
END
FILMED
9-83
DTIC